Centro de Investigación Científica y de Educación Superior de Ensenada, Baja California

Science Postgraduate Program in Electronics and Telecommunications

---

Design of ultra wideband antenna array systems in the environment of 4G mobile wireless communication

Dissertation

Submitted in partial fulfillment of the requirements for the degree of

Doctor in Sciences

Presented by:

Leopoldo Asael Garza Alvarado

Ensenada, Baja California, México

2015

Thesis defended by

Leopoldo Asael Garza Alvarado

and approved by the following committee

Dr. David Hilario Covarrubias Rosales
Thesis Codirector

Dr. Marco Antonio Panduro Mendoza
Thesis Codirector

Dr. Miguel Ángel Alonso Arévalo

Dr. José Luis Medina Monroy

Dr. Carlos Alberto Brizuela Rodríguez

Dr. Hiram Galeana Zapién

Dr. Miguel Ángel Alonso Arévalo
Postgraduate Coordinator
In Electronics and Telecommunications

Dr. Rufina Hernández Martínez
Director of Postgraduate Studies

Resumen de la tesis que presenta **Leopoldo Asael Garza Alvarado** como requisito parcial para la obtención del grado de Doctor en Ciencias en Electrónica y Telecomunicaciones con orientación en Telecomunicaciones.

Diseño de sistemas de agrupamientos de antenas de banda ultra ancha en el entorno de comunicaciones móviles inalámbricas 4G

Resumen aprobado por:

Dr. David Hilario Covarrubias Rosales Codirector de tesis	Dr. Marco Antonio Panduro Mendoza Codirector de tesis

En la actualidad, las redes de comunicaciones móviles inalámbricas están experimentando un enorme crecimiento en la demanda de servicios, y el número de subscriptores de estos. Este aumento ha generado dos problemas principales que deben ser atendidos. El primero es la saturación en el espectro radioeléctrico y el segundo es el incremento en el consumo de energía. Por esta razón, es necesario proponer nuevas estrategias que den solución a estos problemas para los sistemas de comunicaciones móviles inalámbricas de 4G. En este trabajo de investigación, se proponen soluciones dentro del área tecnológica del diseño de agrupamientos de antenas, los cuales son ahora necesarios para los sistemas de 4G, ya que representan una solución para incrementar la eficiencia en diferentes escenarios en aplicaciones de comunicaciones y de radar. En esta tesis, las estrategias de solución propuestas están divididas en dos partes. La primera parte está enfocada en la síntesis de agrupamientos de antenas con características de escasez. Este tipo de síntesis tiene como objetivo reducir el número de elementos de antena, con lo cual se reduce el número de recursos utilizados, el costo, la complejidad y el consumo de energía. En otras palabras, se obtiene un agrupamiento de antenas bajo el enfoque de redes verdes. La segunda parte, se enfoca en la síntesis de agrupamientos de antenas de banda ultra ancha. En este tipo de síntesis, el objetivo es obtener una conformación del haz del diagrama de radiación de manera óptima en todo el espectro de frecuencias asignado para la tecnología de banda ultra ancha (UWB). Esto permite que el agrupamiento de antenas pueda operar de manera eficiente dentro de diferentes bandas de frecuencias. Este trabajo de investigación contribuye al estado del arte en el escenario del diseño de agrupamientos de antenas con nuevas técnicas de síntesis, para los sistemas de comunicaciones móviles inalámbricas de 4G.

Palabras clave: Comunicaciones Móviles Inalámbricas 4G, síntesis de Agrupamientos de Antenas, Banda Ultra Ancha, Escasez en Agrupamientos de Antenas, Conformación de Haz.

Abstract of the thesis presented by **Leopoldo Asael Garza Alvarado** as a partial requirement to obtain the Doctor of Science degree in Electronics and Telecommunications with orientation in Telecommunications.

Design of ultra wideband antenna array systems in the environment of 4G mobile wireless communication

Abstract approved by:

Dr. David Hilario Covarrubias Rosales
Thesis codirector

Dr. Marco Antonio Panduro Mendoza
Thesis codirector

Actually, mobile wireless communications networks are experiencing a tremendous growth in demand for services, and also, the number of subscribers. This increase has generated two main problems that must be addressed. The first is the saturation of the radio spectrum, and the second is the increase in energy consumption. For this reason, it is necessary to propose new strategies that provide solutions to these problems for wireless communications systems 4G. In this research work, solutions strategies within the technological area of the design of antenna array are proposed, which are now required for 4G systems, as they represent a solution to increase the efficiency of different scenarios in communications and radar applications. In this thesis, the proposed solution strategies are divided into two parts. The first part is focused on the synthesis of antenna arrays with sparseness characteristics. This type of synthesis is aimed to reduce the number of antenna elements, whereby the number of resources used, cost, complexity and power consumption is reduced. In other words, an antenna array under green networks approach is obtained. The second part is focused on the synthesis of ultra wideband antenna arrays. In this type of synthesis, the objective is to obtain an optimum beamforming of the radiation pattern across the whole spectrum of frequencies allocated for ultra wideband technology (UWB). This allows antenna array to operate efficiently within different frequency bands. This research work contributes to the state of art of the design of antenna arrays with new synthesis techniques, for wireless communications systems 4G.

Keywords: 4G Mobiles Wireless Communications, Antenna Array Synthesis, Ultra Wideband, Sparse Antenna Arrays, Beamforming.

Dedication

To my parents,
Leopoldo Garza and Josefina Alvarado,
thanks for everything.

Acknowledgments

I would like to express my gratitude to my advisor, **Dr. David Covarrubias** for your guidance, encouragement, and patience over last four years. Your advice was essential for the successful completion of this work. Thank you for sharing with me your knowledge and experience that helped me during the development of my research work. I will always be grateful for the opportunity and confidence given to me to undertake this difficult scientific experience. To you my greatest gratitude and respect.

I would like to thank to my advisor, **Dr. Marco A. Panduro** for your teaching, support and advice on different aspects of my work. Much of my work would have not have been successful completed without your assistance. I will always be grateful with you for all the years you have trusted on me to carry on different research works at different academic levels. Your support has been invaluable, my greatest respect and gratitude to you.

I would also like to thank to every member of my thesis committee, **Dr. Miguel A. Alonso**, **Dr. Carlos A. Brizuela**, **Dr. José Luis Medina** and **Dr. Hiram Galeana**, for their constructive criticism and valuable feedback that helped me to improve my research work. I am grateful for the attention given to my work.

I extend my thanks to all friends, partners and professors, for offered me their friendship and advices during last four years, **Leonardo Yepes**, **Alberto Reyna**, **Guillermo Galaviz**, **Armando Arce**, **Alejandro Galaviz**, **Enrique Guerrero**, **Shiro Kaishi, Manuel Casillas**, **Beatriz Stephens**, **Christian Soto**, **Pedro Valenzuela**, **Edwin Martinez**, **Ramón Muraoka**, **Dr. Ángel Andrade**, **Dr. Salvador Villarreal**, **Dr. Roberto Conte**, **Aldo Pérez**, **Carlos Martinez**, and so many others to list. All of you have made my stay in CICESE a lot easier. To all of you, thanks.

Also, I express my gratitude to the support given to me by the National Council of Science and Technology (**CONACYT**) under the grant number 241163. And thanks to **CICESE Research Center** and the **Department of Electronics and Telecommunications** for the support provided during my research activities.

Thanks to my **parents** and rest of **family** for your support and comprehension during all my years of study. My eternal gratitude to you all.

Table of Content

List of Figures

Figure Page

List of Tables

Table Page

List of Acronyms

3GPP	3rd Generation Partnership Project
4G	4th Generation
5G	5th Generation
ADC	Analog-to-Digital Converter
AF	Array Factor
BCS	Bayesian Compressive Sampling
BER	Bit Error Rate
BW	Beamwidth
CR	Cognitive Radio
DAA	Detection and Avoid algorithms
dB	Decibel
dBm	Decibel-Milliwatt
DE	Differential Evolution
DEMO	Differential Evolution for Multiobjective Optimization
EDGE	Enhanced Data rates for Global Evolution
EIRP	Effective Isotropic Radiated Power
FB-MPM	Forward-Backward Matrix Pencil Method
FCC	Federal Communications Commission
FDE	Frequency-Domain Equalization
FFT	Fast Fourier Transform
GHz	Giga Hertz
GPRS	General Packet Radio Service
GPS	Global Positioning System
GSM	Global System Communication
HSDPA	High-Speed Data Packet Access
HSPA	High-Speed Packet Access
IEEE	Institute of Electrical and Electronics Engineers
IET	Institution of Engineering and Technology
ITU	International Telecommunication Union

LAPC	Loughborough Antennas and Propagation Conference
LTE	Long Term Evolution
LTE-A	Long Term Evolution – Advanced
MATLAB	MATrix LABoratory
MHz	Mega Hertz
MIMO	Multiple-input Multiple-output
mmWave	Millimeter wave
MPM	Matrix Pencil Method
MTC	Machine-Type Communication
MTFSK	Multi-tone Frequency Shift Keying
MTs	Mobile Terminals
OFDM	Orthogonal Frequency-Division Multiplexing
PSD	Power Spectral Density
R&O	Report and Order
SC	Single-Carrier
SLL	Side Lobe Level
SQP	Sequential Quadratic Programming
TD	Time-domain
UWB	Ultra-wideband
WCDMA	Wideband Code Division Multiple Access
WLAN	Wireless Local Area Network
WPAN	Wireless Personal Area Networks
WRC	World Radio Conference

Chapter 1. Introduction

1.1 Technological Framework and Scope of Work

The increasing use of the wireless communication technologies and the enormous opportunities for research development that these technologies provide, highlight the importance of frequency spectrum and the spectrum management process. Additionally, the International Telecommunication Union (ITU) has reported that at the end of 2013 the number of subscribers at mobile cellular networks around the world was of $4{,}100$ millions, and it has been estimated that at the end of 2018 the number of subscribers will increase up to $4{,}900$ millions. Furthermore, this technological progress has constantly opened the door to a diversity of applications that have induced greater interest in, and demand for the limited frequency spectrum resource. This increased demand of applications and subscribers has saturated the spectrum. This technological problem, requires that the spectrum should be used in an efficient way (ITU, 2015).

Wireless communications are densely used in a rising number of services such as: wireless telecommunications, broadcast, business, industrial, navigation and personal communications, aeronautical and maritime radiocommunications, among others. Moreover, the growing demand of applications has caused that the different access technologies have to coexist in a same scenario, such as Global System for Mobile Communications (GSM), General Packet Radio Service (GPRS), Enhanced Data rates for Global Evolution (EDGE), High-Speed Packet Access (HSPA), High-Speed Data Packet Access (HSDPA), Long Term Evolution (LTE) and LTE-Advanced (LTE-A). As shown in Figure 1, the integration of all these access technologies into a coexistence scenario is known as heterogeneous networks (Sierra, A., Choliz, J., Cluzeaud, P., and Slusanschi, E., 2011; Di Benedetto, M. G., Kaiser, T., Molisch, A. F., Politano, C., and Porcino, D., 2006). The spectrum has to be used efficiently in this saturation situation, its use and administration must be regulated in an efficient way.

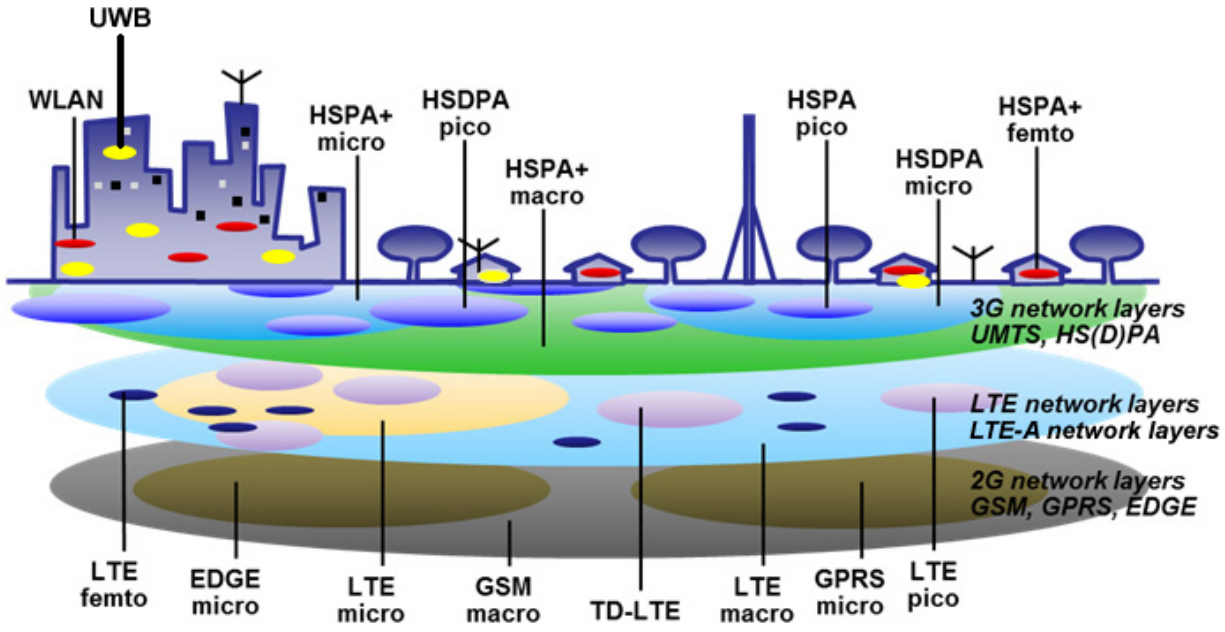

Figure 1. Coexistence of different access technologies which is the main reason of the saturation in the spectrum (SEMAFOUR, 2013).

Different research approaches are being aimed to deal with the lack availability of wireless communication radio spectrum. Two main solutions arise for this saturation problem: cognitive radio (CR) and ultra-wideband technology (UWB).

Cognitive radio is based on cognitive devices (Malanchini, I., Cesana, M., and Gatti, N., 2009). These devices are able to configure their transmission parameters (e.g., frequency band, waveforms, etc.) on the progress, sensing on the surrounding environment by optimizing the identification and access of underutilized spectrum and consequently exploiting under-utilized spectrum portion. This is in order to avoid causing interference to primary users (Lundén, J., Koivunen, V., and Poor, H. V., 2015).

On the other hand, UWB needs no sensing of the spectrum and identify parts of spectrum that are not used at the moment; for avoidance of interference with other systems, UWB transmission are restricted to a maximum radiated power in UWB frequency band of -41.3 dBm/MHz effective isotropic radiated power (EIRP) for indoor applications, as shown in Figure 2.

Based on Federal Communications Commission (FCC) regulation, the allocated frequency range with a bandwidth of 7.5 GHz from 3.1 – 10.6 GHz for UWB applications (FCC, 2002), such as communication and radar systems (Immoreev, I., 2010; Schantz, H. G., 2012).

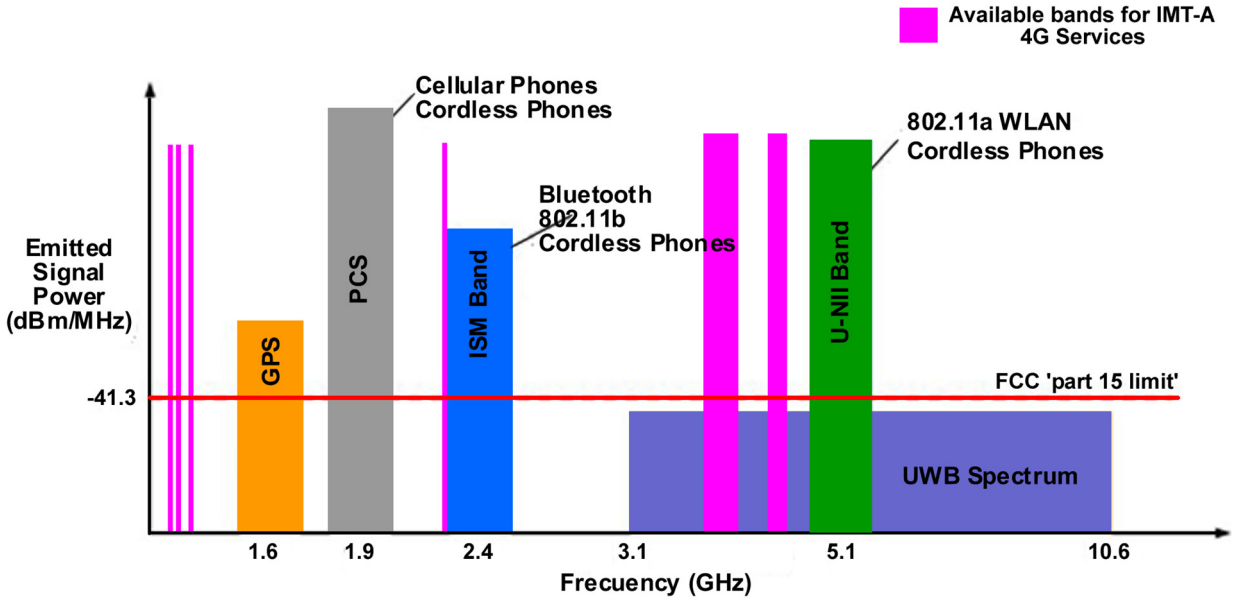

Figure 2. Coexistence of UWB spectrum with other frequency bands.

The coexistence of UWB with other wireless technologies as illustrated in Figure 2, will be integrated into heterogeneous access networks; in addition to the interaction with 5.1 GHz frequency band, the 3rd Generation Partnership Project (3GPP), released new potential frequency bands to be used for IMT-A systems in 4G technology. These bands, identified with pink color in Figure 2, were announced by the 2007 World Radio Conference (WRC): 410– 430 MHz, 450– 470 MHz, 698– 862 MHz, 790– 862 MHz, 2.3– 2.4 GHz, 3.4– 4.2 GHz, and 4.4 – 4.99 GHz. The importance of coexistence of UWB in some frequency bands with other wireless systems is of high interest for research topics.

Different research approaches are being addressed to the design of antenna arrays for UWB communications. A number of proposals, focus on the antenna element and the feeding excitation in order to obtain a more robust data transmission or higher data rates (Adamiuk, G., Zwick, T., and Wiesbeck, W., 2012; Guo, L., Wang, S., Chen, X., and Parini, C., 2010; Ghavami, M., Member, S., Amini, A., and Marvasti, F., 2008; Abbasi, Q. H.,

Khan, M. M., Alomainy, A., and Hao, Y., 2011). The implementation of antenna arrays for applications such as radar and positioning systems is considered in the documents presented by (Adamiuk, G., Heine, C., Wiesbeck, W., and Zwick, T., 2010; Dumoulin, A., John, M., Ammann, M.J., and McEvoy, P., 2009). The UWB antenna arrays, have their application either in directional communications, beamforming, or MIMO techniques. However, the design of antenna arrays have to deal with the enormous bandwidth allocated for UWB technology.

In this area of antenna arrays technology there is a new vision aimed towards strategies that allow to reduce the number of resources in order to support green networks for new wireless communications systems. Particularly, mobile communication networks defined by 3GPP, on the Release 12 and beyond (Astely, D., Dahlman, E., Fodor, G., Parkvall, S., and Sachs, J., 2013), have incorporated the concept of energy efficiency, which could be interpreted either by reducing the energy consumption, or by reducing the number of elements in the array design (e.g., carbon footprint). Another concept incorporated is the mandatory use of Multi-Antenna technology, i.e., the use of antenna arrays, as shown in Figure 3.

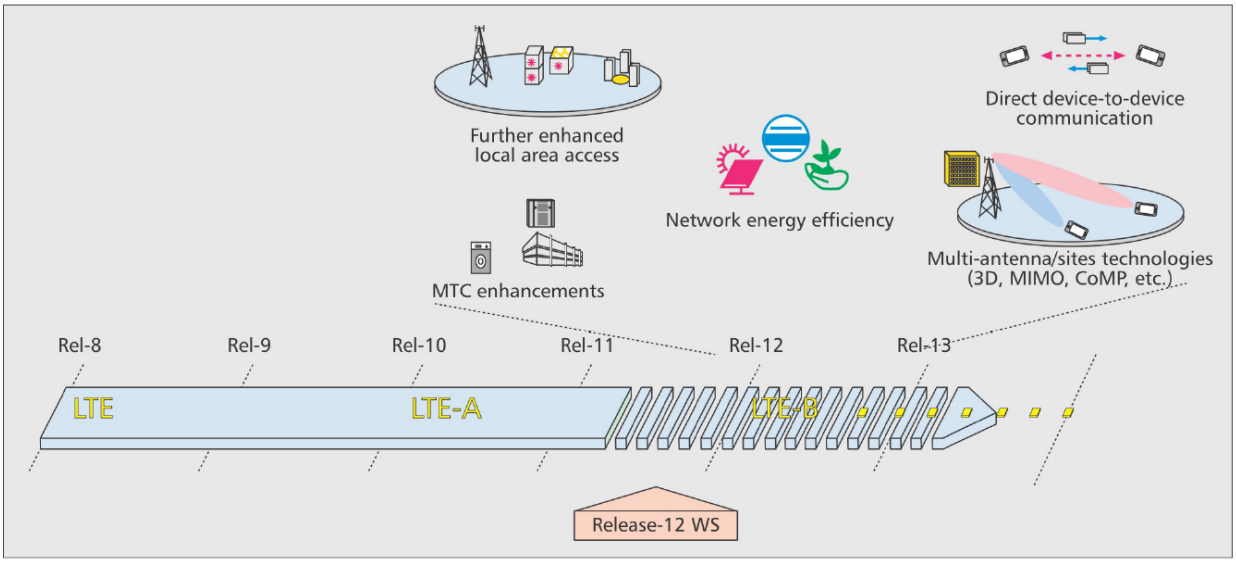

Figure 3. Technological areas considered for LTE – evolution (Asteley, D. et al., 2013).

This thesis is focused on developing new strategies to address two stages of research activities. The first one is focused on reducing the number of antenna array elements from

a reference antenna array with a desired radiation pattern. By this way, it is obtained a reduction of resources. The second one is aimed at designing UWB antenna arrays that are able to generate an optimum radiation pattern in UWB spectrum. Each of these strategies, following their own paths, are focused on one common objective: to fulfill the requirements of future fifth-generation (5G) mobile communication systems (Huawei, 2015).

In addition to above, both aspects, reducing the number of resources and the design for wide bands, are envisioned as requirements for future fifth-generation (5G) wireless communications systems. Both strategies, are focused on a common objective, that is an ultra-low energy consumption, about three orders of magnitude lower energy for green networks (Huawei, 2015). Also, based on the requirements, two major challenges should be addressed for the design of the 5G systems:

- The systems of 5G should be able to have a flexible and efficient use of all available spectrum from low band to high band, of licensed and unlicensed bands, which cover lower part of millimeter wave (mmWave) band.
- The 5G systems should be able to adapt themselves to provide efficiently support for the diverse set of service characteristics, massive connectivity and massive capacity. Flexible network designs are required to improve the spectral efficiency, increase connectivity and reduce latency.

For the next 5G wireless communications, the amount of spectrum that may be utilized will need to increase. New spectrum below 6 GHz is expected to be allocated for mobile communication at the World Radio Conference (WRC) 2015, and the band above 6 GHz is expected to be allocated at WRC 2019, as shown in Figure 4.

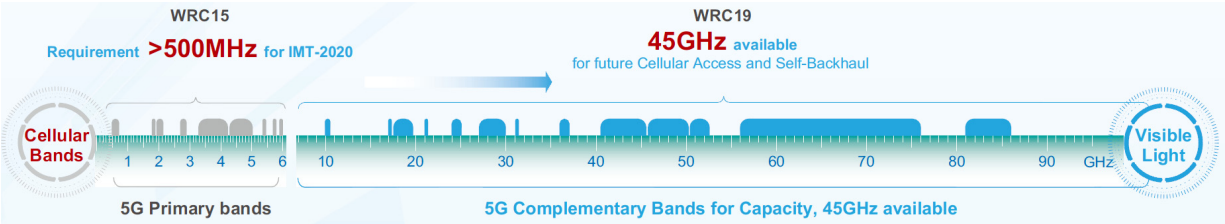

Figure 4. Additional spectrum for 5G wireless communication, Sub 6 GHz and above 6 GHz (Huawei, 2015).

Future 5G networks will be a heterogeneous network which enables the cooperation between lower-frequency wide-area coverage networks and high-frequency networks. Below 6 GHz, will be considered as primary bands, and over 6 GHz will be considered complementary bands.

Another relative aspect in future 5G wireless communications will be the concept of massive MIMO. This concept makes a break with current practice through the use of large-scale antenna systems over networks and devices. This is one of the most promising concepts of the future 5G technology, massive MIMO is a commercial solution since it should represent three orders of magnitude of higher efficiency without installing the same amount of base stations (4G Americas, 2015; Huawei 2015).

The two issues addressed in this thesis, the UWB antenna arrays along with sparse antenna arrays, could be extended in the future to these new 5G concepts of additional spectrum and massive MIMO.

1.2 Problem Statement

The saturation of the frequency spectrum and the requirements for new generation wireless communication systems, have created new challenges in order to develop solutions to those requirements. The systems based on the 3GPP LTE radio access technology, will use reduced number of resources of the entire system.

From the experiences associated within the CICESE Wireless Communication Group, derived by doctoral thesis associated with 3GPP LTE requirements (Galaviz, G., 2012; Arce, A., 2012; Yepes, L., 2014), advised to continue, as a suitable strategy, the problem of reducing the number of antenna elements in order to support the concept of green networks suggested by (Astely, D. et al., 2013).

1.2.1 Synthesis of Antenna Arrays with sparseness characteristics

The approach of reducing the number of antenna elements in arrays provides a reduction of resources, and consequently, reduces cost, power consumption, maintenance, etc. In

this way, in the wide range of possibilities of synthesis techniques, there are proposed deterministic techniques for the reduction of the number of antenna elements in geometry of linear arrays, such as the Matrix Pencil Method (MPM) and its improvement, the Forward-Backward (FB) MPM. In the FB-MPM, a non-iterative procedure based on the singular value decomposition of a Hankel matrix is used to reduce the number of elements (Liu, Y., Nie, Z. and Liu, Q. H., 2008; Liu, Y., Liu, Q. H. and Nie, Z., 2010).

Another approach is the Bayesian Compressive Sampling (BCS) method proposed by (Oliveri, G. and Massa, A., 2011), where a probabilistic formulation of the antenna array synthesis is used to design a maximally sparse array.

A different approach has been presented by (Caratelli, D. and Viganó, M. C., 2011), where an auxiliary array factor function is introduced to provide an optimal array with element density and excitation tapering distribution to imitate a desired pattern. Recently, a new approach has been presented in (Yepes, L. F., Covarrubias, D. H., Alonso, M. A., Ferrus, R., 2014), where a hybrid synthesis is presented based on the adaptation of (Caratelli, D. and Viganó, M. C., 2011), and an iterative optimization method is employed to obtain the complex excitation for phased antenna arrays.

Additionally, there exist different approaches for linear antenna array that are based on density tapering techniques applied over a continue current source for the synthesis of uniform amplitude sparse antenna arrays for narrow and shaped beams (Skolnik, I., 1969; Maffett, A., 1962; Bucci, O. M., D'Urso, M., Isernia, T., Angeletti, P., Toso, G., 2010; Bucci, O. M., Isernia, T., Morabito, A. F., 2013).

For the case of synthesis of two-dimensional antenna arrays, there are proposed techniques over planar arrays such as the extension of MPM (Yang, K., Zhao, Z., Liu, Y., 2011) applied to planar arrays.

Another approach in this scenario considers the synthesis by using independent compression regions (Yepes, L. F., Covarrubias, D. H., Alonso, M. A., Arceo, J. G., 2013).

In addition to these, different approaches based on density tapering techniques have been reported for the synthesis of two-dimensional antenna arrays (Angeletti, P., Toso, G. and Ruggerini, G., 2014; Bucci, O. M., Isernia, T., Morabito, A. F., Perna, S. and Pinchera, D., 2012; Bucci, O. M., Perna, S. and Pinchera, D., 2012; Bucci O. M. and Perna, S., 2011; Milligan, T. A., 2004). Most of them applied over concentric rings antenna arrays. A different approach where a weighting density method is used to search for the optimum radius or rings of a desired array (Jiang, Y. and Zhang, S., 2013).

Another approach is presented that considers the orthogonal method applied to circular antenna arrays to obtain the current excitation (Sahalos, J., 2006; Unz, H., 1966).

However, most of above formulations deal with linear and planar geometries of antenna arrays, and an extension to a circular geometry is not supported because the mathematical formulation of the circular antenna arrays is completely different. This is due to the circumference of the array. Therefore, the above synthesis techniques do not offer a solution to this problem.

Based on the approaches about density tapering techniques, a reference to apply sparse to an antenna array could be achieved by obtaining a continuous current distribution from a desired pattern, but it has not been applied to a circular array. Then, in this thesis, motivated by the feasibility to contribute to the state-of-the-art synthesis of sparse antenna arrays, in a case that has not been widely explored, a synthesis methodology for sparse circular antenna array is formulated using the approach of the orthogonal method applied to circular antenna arrays (Sahalos, J., 2006; Unz, H., 1966). This is in order to obtain a continuous current distribution by an orthogonal analysis, and then, a density/amplitude tapering technique is used over the continuous current distribution to obtain amplitude excitations and angular positions for an antenna array with reduced number of antenna elements.

1.2.2 Synthesis of UWB Antenna Arrays

The case of the design of UWB antenna arrays deals with a particular problem, the large spectral occupancy of UWB wireless signals significantly complicates the design of the

antenna array. By the definition of the FCC, UWB is the simultaneous radiation of an absolute bandwidth over 500 MHz or a relative bandwidth of at least 25%. This definition can be applied to other frequency bands, but in this thesis the design of antenna array is considering the spectrum allowed by the FCC, which is of $3.1 - 10.6$ GHz.

The classical antenna theory is not enough to analyze an antenna array with a large frequency spectrum, especially in applications such as beamforming and directional communications with high rate data transmission and high sensitivity (Barrett, T. W. and Vienna, V. A., 2001; Shlivinski, A., Heyman, E. and Kastner, R., 1997). In such applications, the UWB antenna arrays are required to establish a point-to-point communication with suppression of undesired interferences (Adamiuk et al., 2012). However, the power pattern changes significantly between the lower and upper edges of the UWB frequency band ($3.1 - 10.6$ GHz) defined by FCC (FCC, 2002). This implies a complex design problem due to numerous radiation patterns if the analysis in the frequency domain is used (Sipal, V., Allen, B., Edwards, D. and Honary, B., 2012). An alternative approach is the analysis in the time domain to design UWB antenna arrays. The pattern in the time domain is defined as the energy pattern (Sorgel, W., Sturm, C. and Wiesbeck, W., 2005). The energy pattern of the antenna array is the total response of the power patterns in the frequency domain (Liao, C. H. Hsu, P. and Chang, D. H., 2011). Therefore, by using the energy pattern in the time domain, we avoid the individual beamforming for the power patterns in the frequency domain.

In this sense, time–domain (TD) or pulsed antenna arrays have recently been studied by pondering their advantages of low side lobe levels (*SLL*) and high resolution for applications such as communications, remote sensing and radar (Griffiths H. D. and Cullen, A. L., 2003). The design of TD linear antenna array has been reported in a number of proposals (Chamaani, S., Abrishamian, M. S. and Mirtaheri, S. A., 2010; Leatherwood, D. A., Corey, L. E., Cotton, R. B. and Mitchell, B. S., 2000; Shlivinski, A., Lager, I. E., and Heyman, E., 2013; Wu, X. H., Kishk, A. A. and Chen, Z. N., 2005; Yuan, X. L., Zhang, G. F., Huang, J. J. and Yuan, N. C., 2008), exploiting its features of fixed and scanning beam patterns. The synthesis of linear and circular planar antenna arrays has been reported in (Ciattaglia, M. and Marrocco, G.,2008; Marrocco, M. and Galletta, G., 2010) by modeling

Hermite-Rodriguez waveforms functions to obtain array currents, and the energy pattern by a generalized hypergeometric function. A TD-UWB transverse electromagnetic horn antenna array optimized by a micro genetic algorithm is presented by (Qin, Y., Liao, C. and Wei, T., 2007). Furthermore, a non-uniform UWB linear antenna array optimized by the well-known Differential Evolution algorithm for low side lobe level during beam-scanning is presented in (Panduro, M. A. and Foltz, H., 2013). Moreover, two–dimensional TD arrays with scanning beam pattern by using the Sequential Quadratic Programming (SQP) to find the optimum positions, amplitudes and time delays, are presented in (Reyna, A., Panduro, M. A., and Del-Rio Bocio, C., 2014a, 2014b; Reyna, A. and Panduro, M. A., 2014).

In this thesis, motivated by the feasibility to solve the individual beamforming of a UWB antenna array in a circular geometry, by considering a single ring, our proposed approach is to address the synthesis of TD circular antenna arrays for UWB frequency band. Particularly, our research considers the synthesis of a single-ring circular antenna array with low *SLL* and beam width for a steerable main lobe; and another case for a flat-top main lobe. This UWB circular array considers the optimization of the true-time exciting delays and the amplitude coefficients across the antenna elements to operate with optimal performance in the whole azimuth plane ($360°$). The performance of a UWB circular array could be improved substantially (with respect to the UWB circular array with the conventional progressive delay excitation), if the amplitude and delay excitations are set or optimized in an adequate way. The synthesis process is carried out by Differential Evolution for Multiobjective Optimization (DEMO) (Robic, T. and Filipi, B., 2005) by finding out the optimal true-time exciting delays and amplitude coefficients of pulsed antenna elements. Hence, the novelty of this research is the synthesis of TD antenna array in a circular geometry in order to obtain steerable energy patterns with low *SLL*.

1.3 Objectives

As part of the research process for this thesis, and focused on the two main addressed topics, the synthesis of UWB antenna arrays and the design of antenna arrays with sparseness characteristics, the general and particular objectives are defined as follows:

1.3.1 General Objective

- Establish a synthesis methodology for UWB antenna arrays in order to obtain an optimum radiation pattern in the UWB frequency range ($3.1 - 10.6$ GHz) avoiding individual beamforming.

1.3.2 Particular Objectives

- Identify the adequate parameters necessary for an optimization process, in order to obtain optimum radiation patterns for UWB antenna array.
- Propose a new sparse synthesis methodology to reduce the number of antenna elements for a circular antenna array, in order to obtain low levels of main beamwidth and side lobe.

1.4 Thesis Outline

The main sections of this thesis and their sequence (which are covered in Chapters 2 to 6) are listed in this sub-chapter with a briefly description of the relevant aspects of the synthesis of antenna arrays, focused on the sparse theory to reduce the number of antenna elements of an array. This is in order to present a synthesis methodology to help to contribute to the green networks requirements of release 12 and beyond for LTE-Advanced systems.

Furthermore, the synthesis of UWB antenna arrays to design an antenna array with an optimum radiation pattern in the whole UWB frequency spectrum in order to provide an effective design methodology for antenna arrays wide frequency bands, a requirement that will be mandatory for new 5G communication technologies. It is presented below, in Figure 5, a schematic flow chart that represents the complete thesis structure.

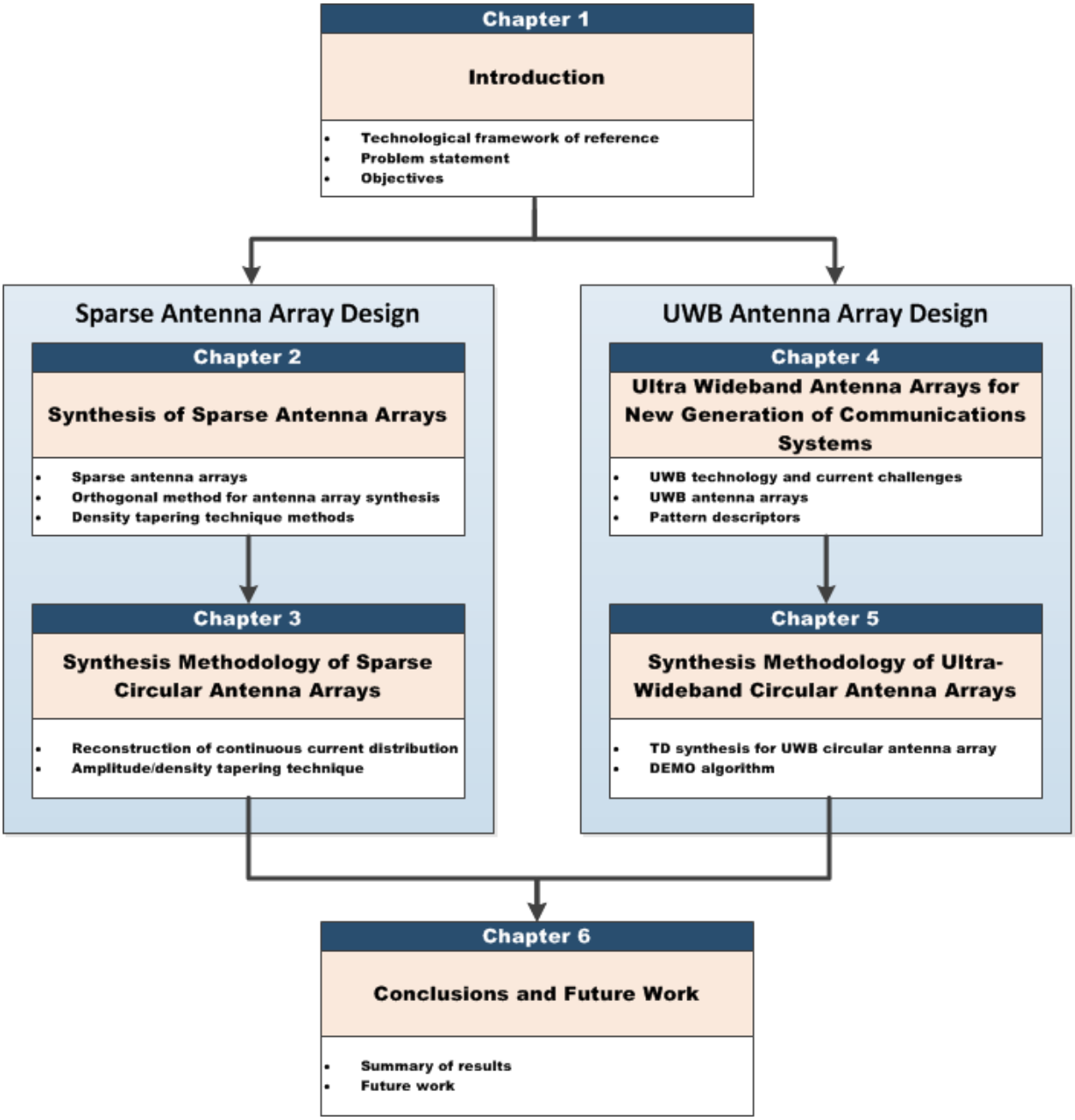

Figure 5. Layout structure and organization of this thesis.

Chapter 2: Synthesis of Sparse Antenna Arrays

Sparse antenna arrays are presented in this chapter, as well as the orthogonal method applied to the synthesis of antenna arrays, which is the most approximate sparse synthesis methodology for circular antenna arrays, geometry that will be addressed in this thesis. Furthermore, the density/amplitude tapering technique for the synthesis of antenna

arrays is also presented, which combined with the orthogonal analysis procedure will be used as reference to develop a new approach of sparse synthesis methodology.

Chapter 3: Synthesis Methodology of Sparse Circular Antenna Arrays

In this chapter, the developed new sparse synthesis methodology is presented in order to reduce the number of antenna elements from a circular antenna array. The methodology presented is based on the expansion of orthogonal basis function to reconstruct a continuous current distribution from a desired radiation pattern and a density/amplitude tapering technique in order to obtain a reduced number of amplitudes and angular positions for antenna elements.

Chapter 4: Ultra-Wideband Antenna Arrays for New Generation of Communications Systems

The UWB technology is presented in this chapter, as well as the participation of this technology in the new communications technologies such as 4G, LTE-Advance and the potential 5G in the future. Besides, the open current challenges for UWB technology and the open research topics, specifically the multiple antenna systems that have to deal with wide frequency band, characteristic of the spectrum assigned to the UWB technology. Also, descriptors for UWB antenna arrays are presented in this chapter.

Chapter 5: Synthesis Methodology of Ultra-Wideband Circular Antenna Arrays

In this chapter a time-domain (TD) synthesis methodology is presented in order to obtain a steerable energy beam pattern and a flat-top beam pattern for a circular antenna array. The methodology presented is based on beam pattern descriptors for a TD analysis, and the amplitudes and time delays are calculated by using the algorithm of Differential Evolution for Multi-objective Optimization (DEMO). By this synthesis procedure, by optimizing in TD, individual beamforming is avoided.

Chapter 6: Conclusions and Future Work.

The most relevant contribution considered to the current research and some potential follow-up research activities are proposed in this final chapter.

1.5 Contributions of this thesis

As a result of the research process followed in this thesis, the main contributions and results were published in the following journals and a conference are:

Journals:

- Leopoldo A. Garza, Marco A. Panduro, David H. Covarrubias, and Alberto Reyna, “Multiobjective Synthesis of Steerable UWB Circular Antenna Array considering Energy Patterns,” International Journal of Antennas and Propagation, vol. 2015, Article ID 789094, 9 pages, 2015. doi:10.1155/2015/789094.

- Garza, L.A., Yepes, L.F., Covarrubias, D.H., Alonso, M.A., and Panduro, M.A., (2015). “Synthesis of Sparse Circular Antenna Arrays applying a Tapering Technique over Reconstructed Continuous Current Distribution,” *IET Microwave Antennas & Propagation* [Currently in press]

Conference:

- Garza, L.A., Panduro, M.A., Covarrubias D.H., (2015). “Time-Domain Synthesis of UWB Circular Antenna Array for Flat-Top Patterns”. *In 2015 Loughborough Antennas and Propagation Conference (LAPC)*, Burleigh Court International Conference Centre, Loughborough University, United Kingdom, November 2-3.

Chapter 2. Synthesis of Sparse Antenna Arrays

2.1 Introduction

The evolution of new generation wireless communication technology, such as LTE-A, requires the use of multiple antenna arrays for communication systems. Furthermore, the design of antenna arrays should consider requirements such energy efficiency and minimizing the number of resources in order to contribute to green networks technology as requested by the 3GPP release 12 and beyond.

This approach of minimizing the number of resources of antenna arrays is defined as one of the problems to address in this research work. In this scenario, in recent literature, sparse antenna arrays are a solution to those requirements. The synthesis of this kind of antenna arrays seeks to obtain an arbitrary beam pattern by using a reduced number of antenna elements. In other words, this represents a minimization of the 'always-on' antenna elements transmission, where the weight, hardware/software complexity, and cost are minimized (Astely et al., 2013). This is of great interest in many applications where the weight and size of arrays are limited, such as radar, satellite communications and mobile cellular technology (Prisco, G. and D'Urso, M., 2011).

Given the above, this Chapter presents the state-of-art proposals of synthesis of antenna arrays, in order to obtain sparseness characteristics, which represents a solution approach to requirements of evolution of LTE-A technology by minimizing the "always-on" antenna elements transmissions (Astely et al., 2013). The methodologies presented in this chapter will be used as references to generate a new proposal focused to address this problem in a circular array geometry, a kind of geometry that has not been explored in the state-of-the-art sparse antenna arrays. This new synthesis proposal will be presented in Chapter 3. The synthesis proposals to be presented are, on the one hand, the Orthogonal Method applied to the synthesis of antenna arrays (Sahalos, J., 2006; Unz, H., 1966), and on the other hand, the sparse synthesis based on density taper techniques (Josefsson, L. and Persson, P., 2006).

2.2 Sparse Antenna Arrays

In antenna arrays, the element spacing represents a different parameter of study, in addition to the current excitations (amplitude and phase excitations), which can be used to control the radiation pattern (Fang, D. G., 2009; Visser, H. J., 2005). In practice, antenna elements cannot be placed much closer than a half wavelength due to mutual coupling problems and because, usually, the size of practical antenna elements are of the order of a half-wavelength dimension, and it would be difficult to make elements much smaller without losing efficiency (Balanis, C. A., 2005; Fang, D. G. 2009).

An array aperture, also known as the length of the array, which contains N elements equally spaced at half-wavelength intervals contains more antenna elements than if the spacing are made unequal or non-uniformly, and if the minimum spacing is half-wavelength. Since the non-uniform spaced antenna array contains fewer elements than the conventional array occupying the same aperture, it is said to be “thinned” if the elements are removed, or it is known as “sparse array”, where the elements are rearranged to different positions into the aperture. The conventional array with half-wavelength spacing is called a “filled” array. Thereby, the terms like “unequally spaced” or “non-uniform” are related to the term “sparse array”.

Sparse antenna arrays may be used to obtain radiation patterns with low peak side lobes levels and a desired main beam pattern. Furthermore, sparse antenna arrays provides an alternative, to permit the array to scan over a wide angle, or to operate over a wide frequency range without the formation of grating lobes that could appear with filled antenna arrays. Moreover, fewer elements result in low cost, easy maintenance, less hardware/software complexity, and an efficient use of resources. By this way, sparse antenna arrays are contributing to the requirements of Release 12 and beyond for LTE-Advanced technology by minimizing the “always-on” antenna elements transmissions (Astely et al., 2013).

In the context of sparse antenna arrays, different approaches have been considered in the literature for different array geometries. For the case of linear antenna arrays, there exist a number of recently proposed deterministic techniques for the reduction of the

number of antenna elements, such as the Matrix Pencil Method (MPM) and its improvement, the Forward-Backward MPM, where a non-iterative procedure on the singular value decomposition of a Hankel matrix is used to reduce the number of elements (Liu et al., 2010; Liu et al., 2008). Another approach is the Bayesian Compressive Sampling (BCS) method proposed in (Oliveri, G. and Massa, A., 2011), where a probabilistic formulation of the antenna array synthesis is used to design a maximally sparse array.

A different approach has been presented by (Caratelli, D. and Viganó, M. C., 2011; Vigano, M. C. and Caratelli, D., 2010), where an auxiliary array factor function is introduced to provide an optimal array element density and excitation tapering distribution to imitate a desired pattern. Recently, a new approach has been presented in (Yepes, et al., 2014), where a hybrid synthesis is presented based on the adaptation of (Caratelli, D. and Viganó, M. C., 2011), and an iterative optimization method is employed to obtain the complex excitation for phased antenna arrays. Other interesting approaches for linear antenna array, are the ones based on density tapering techniques, applied over a continue current source for the synthesis of uniform amplitude sparse antenna arrays for narrow and shaped beams (Bucci et al., 2010; Bucci, O. M., Isernia, T., Morabito, A. F., Perna, S. and Pinchera, D., 2010; Bucci O. M. and Perna, S., 2011; Maffett, A., 1962; Skolnik, I., 1969).

For the case of synthesis of two-dimensional antenna arrays, there are a number of proposed techniques over planar arrays, such as the extension of MPM (Yang et al., 2011); another approach in this scenario has been proposed, where the synthesis focuses on using independent compression regions (Yepes et al., 2013). In addition to these, different approaches based on density tapering techniques have been reported for the synthesis of two-dimensional antenna arrays (Angeletti et al., 2014; Bucci et al., 2012; Bucci, O. M., Perna, S. and Pinchera, D., 2012; Bucci O. M. and Perna, S., 2011; Milligan, T. A., 2004), most of them applied to concentric rings antenna arrays. A different approach has been presented by (Jiang, Y. and Zhang, S., 2013), where a weighting density method is used to search for the optimum radius or rings of a desired array. Another approach is presented by (Sahalos, J., 2006; Unz, H., 1966), where the orthogonal method is applied to circular antenna arrays to obtain the current excitation.

As mentioned in Chapter 1, the case of circular antenna array (arranged on a single ring) with sparseness characteristics has not been widely explored. The main difference can be found by analyzing the array factor of both, linear (1) and circular arrays (2).

The array factor for linear and circular antenna arrays can be determined by the next expressions (Balanis, C. A., 2005):

$$AF_{\text{linear}}(\phi) = \sum_{n=1}^{N} I_n \exp(jkd \sin(\phi)) \tag{1}$$

$$AF_{\text{circular}}(\phi) = \sum_{n=1}^{N} I_n \exp(jkr \cos(\phi - \phi_n)) \tag{2}$$

The array factor of the circular antenna array (2) is found in the slightly more complicated phase expression because of the array curvature. Where I_n is the excitation current, k is the wave number, $k = 2\pi/\lambda$, ϕ is the azimuth angle, d is the position of the antenna element in the linear expression, r is the radius of the array, and ϕ_n the angular position of the antenna element. The phase, or basis function of the expression (2), $\exp(jkr \cos(\phi - \phi_n))$ is not orthogonal, this avoid that the above synthesis methods can deal with this kind of array factor.

Then, motivated by the feasibility of giving an analytical solution, as part of this research work, this section is dedicated to the state-of-art proposals of synthesis of antenna arrays in order to obtain sparseness characteristics. The orthogonal method applied to the synthesis of antenna arrays will be presented in next section.

2.3 Orthogonal Method for Antenna Arrays Synthesis

The orthogonal method applied for the synthesis of antenna array (Sahalos, J., 2006) focuses on the non-uniformly spaced antenna arrays by using an analogous method of the Gram-Schmidt (Abdelmalek, N. N., 1971; Björck, Å., 1994) in order to obtain amplitude

excitations for a desired pattern, for the case of linear and planar antenna arrays. Since the circular geometry will be addressed in this thesis, the orthogonal method designed for a circular antenna array will be described.

Let us consider first a non-uniformly spaced circular antenna array with N elements. The array factor on the plane X–Y is mathematically expressed by (2). For this method the excitations I_n are determined in the case where the desired pattern, array factor $AF(\phi)$ is given. In general, the basis functions (3) in expression (2) are not orthogonal (Sahalos, J., 2006).

$$\varphi_i(\phi) = \exp(jkr\cos(\phi - \phi_n)) \tag{3}$$

By a method analogous to the well-known Gram-Schmidt procedure of orthogonality (Abdelmalek, N. N., 1971; Björck, Å., 1994), an orthogonal basis $\psi_i(\phi)$ can be derived. The procedure has been discussed in detail by (Kantarovich, L. V. and Krylov, V. I., 1964; Unz, H., 1966). Then, the orthogonal set of functions is of the following form (Sahalos, J., 2006):

$$\psi_1(\phi) = \frac{\varphi_1(\phi)}{\langle \varphi_1(\phi), \varphi_1(\phi)\rangle^{\frac{1}{2}}} \tag{4}$$

$$\psi_n(\phi) = \frac{\varphi_n(\phi) - \sum_{j=1}^{n-1}\langle \varphi_n(\phi), \psi_j(\phi)\rangle\, \psi_j(\phi)}{\left\{\int_0^{2\pi}\left[\varphi_n(\phi) - \sum_{j=1}^{n-1}\langle \varphi_n(\phi), \psi_j(\phi)\rangle\, \psi_j(\phi)\right]\right\}^{\frac{1}{2}}} \tag{5}$$

Being $\psi_n(\phi)$ the orthonormalized function expressed as follows (Sahalos, J., 1974; Sahalos, J., 2006):

$$\psi_n(\phi) = \sum_{i=1}^{n} C_1^{(n)}\, \varphi_1(\phi) \tag{6}$$

And the symbol $\langle \varphi_n(\phi), \psi_j(\phi) \rangle$ represents the inner product given by:

$$\langle \varphi_1(\phi), \psi_1(\phi) \rangle = \int_0^{2\pi} \varphi_n(\phi)\, \psi_j^*(\phi)\, d(\phi) \tag{7}$$

The coefficients $C_j^{(n)}$ in expression (6) can be calculated from next group of equations:

$$C_n^{(n)} = \frac{1}{D_n} \tag{8}$$

$$C_k^{(n)} = -\frac{2\pi}{D_n} \sum_{j-k}^{n-1} \sum_{i=1}^{j} C_k^{(j)}\, C_i^{(j)} k_{in} \tag{9}$$

$$D_n = \left\{ 2\pi - 4\pi^2 \sum_{j=1}^{n-1} \left(\sum_{i=1}^{j} C_i^{(j)}\, \hat{k}_{in} \right)^2 \right\}^{1/2} \tag{10}$$

$$\hat{k}_{in} = 2\pi J_0(k) \tag{11}$$

The term J_0 refers to a Bessel function of order zero, and k is the wave number. It is important to mention at this point, that the coefficient $\hat{k}_{in}$ in the above procedure, was corrected, in its original form, as published in (Sahalos, J., 2006), this coefficient has a different expression, but as this synthesis method was validated mathematically in the research process of this thesis, we detected that in its original form the orthogonality cannot be achieved; by what is expressed in (11), the orthogonality was achieved by orthonormal functions $\psi_n(\phi)$. The validation procedure of this is presented in Appendix A.

Now, returning to the procedure, the array factor in (2) can now be written as follows:

$$AF(\phi) = \sum_{n=1}^{N} B_i \, \psi_i(\phi) \tag{12}$$

The term B_i, due to the orthogonality of functions $\psi_i(\phi)$, for a desired pattern, $AF(\phi)$, becomes:

$$B_i = \langle AF(\phi), \psi_i(\phi) \rangle \tag{13}$$

Finally, by associating expressions (2), (6) and (12), the unknown current excitations I_n, can be calculated as follows:

$$I_n = \sum_{n=1}^{N} B_j \, C_i^{(j)} \tag{14}$$

Given the above procedure, one can infer that for a given non-uniformly circular antenna array, the elements current excitations can be achieved by the orthogonal method. The accuracy of the resultant approximated pattern depends on the number and positions of antenna elements.

The complete synthesis process follows the next five steps (Sahalos, J., 2006):

1 Definition of the positions of the antenna elements ϕ_n.

2 Calculations of the coefficients $C_i^{(j)}$.

3 Evaluation of the desired pattern, $AF(\phi)$.

4 Calculation of the quantities of B_i, for a better approximation.

5 Calculation of the excitations, I_n, of the array elements.

Figure 6 shows, as example, the approximation of this orthogonal method as synthesis for a circular antenna array considering an arbitrary pattern, by using $N = 30$ with a radius of $r = 2.2282\lambda$, with $i = 30$.

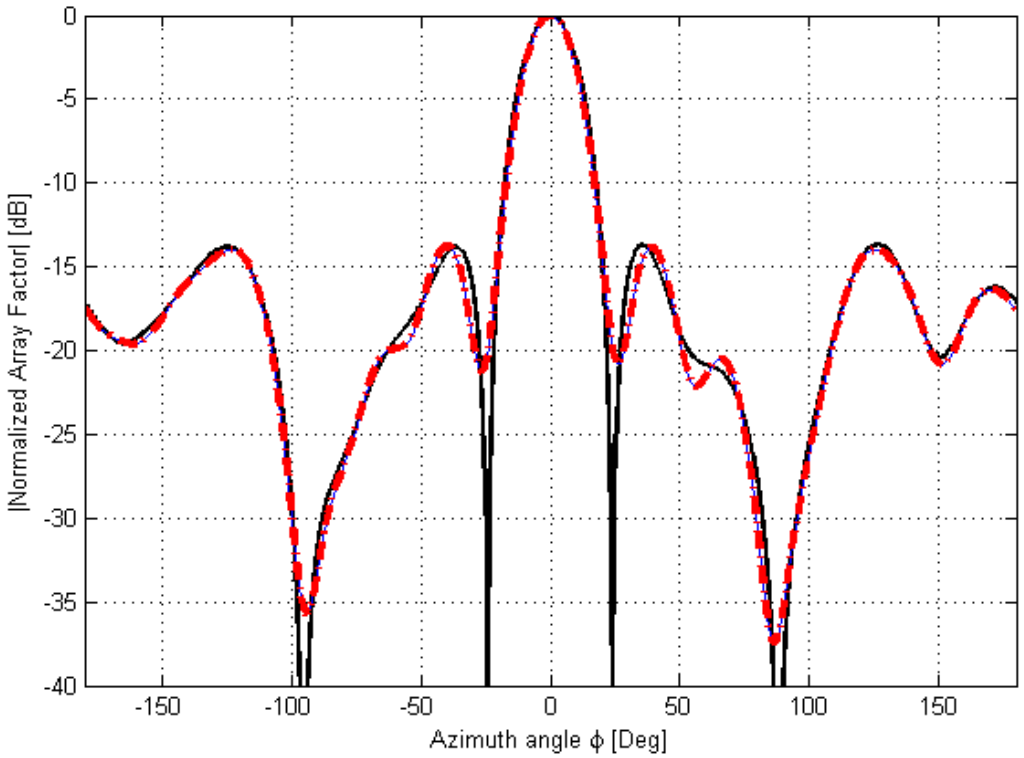

Figure 6. Reconstruction of a desired pattern by 30 non-uniform antenna array elements by the orthogonal method.

As can be seen in Figure 6, the reconstruction of the desired pattern shows a good approximation with slightly drawbacks. These drawbacks are associated to the number of antenna elements and their positions. The orthogonal method as presented here is able to determine the current excitations to find an approximation to the desired pattern, but the optimum element positions is a different problem.

By the orthogonal method as synthesis of antenna arrays, it is viable to obtain an array with sparseness characteristics by knowing the best spatial distribution ϕ_n for the achieved current excitations I_n. But this method can be used as reference to develop different methodology to reconstruct the current excitations for a desired array pattern. One can understand by analyzing expressions (12) and (14), that the desired array pattern (ϕ) and the current excitations I_n, respectively, can be expressed by an extension of orthogonal basis functions; by this way, it is possible to reconstruct a continuous current distribution that could be used to apply it on a tapering procedure as synthesis method to obtain sparseness characteristics.

The next section of this chapter presents, the basic principles of the Doyle-Skolnik approach of density tapering technique for the synthesis of non-uniform antenna arrays (Skolnik, I., 1969).

2.4 Deterministic Density Tapering Technique applied for Synthesis of Linear Antenna Arrays

The synthesis of sparse antenna arrays based on a density tapering is based on the conventional antenna theory (Balanis, C. A., 2005; Visser, H. J., 2005) that describes the type of aperture illumination, i.e. a continuous source acting as reference that is needed to obtain a desired radiation pattern. The theory of synthesis of sparse antenna arrays is developed for continuous source distribution, which can be applied to unequally spaced antenna arrays by arranging the antenna elements, so that the density of elements across the aperture is of the same form as the amplitude of the current density distribution. This is called *density* or *space* taper, and by applying a density tapering on a continuous source, this results in a density taper of the array elements in a way such that the elements of the arrays would be more densely located where the continuous source is higher.

Useful approaches in this context of density tapering have been developed through decades (Ishimaru, A., 1962; Skolnik, I., 1969; Unz, H., 1960; Unz, H., 1966); in particular, the research work of this part of the thesis is based on the Doyle-Skolnik approach (Fang, D. G. 2009; Skolnik, I., 1969) because of the fact that it is the only one which has been proven to be optimal, and because newest developed technologies of sparse antenna arrays (Angeletti et al., 2014; Bucci et al., 2013; Bucci et al., 2012; Milligan, T. A., 2004) are based on this same approach.

The quality of the approximation to the continuous current density function by an antenna array depends on the number of elements. The thinner the array, the poorer the approximation (Skolnik, I., 1969).

On this Doyle-Skolnik density tapering technique, one starts from the idea of approximating a given real and positive continuous source current density denoted by i_0,

serving as reference for a desired pattern F_0 with an array with equal amplitude non-uniformly spaced elements. One criterion for selecting the continuous source i_0 is that, when used, its radiation pattern should be similar to that desired of the density tapered antenna array (Bucci et al., 2010; Fang, D. G., 2009; Skolnik, I., 1969). The continuous source i_0 is shown in Figure 7. To locate the positions of the N antenna elements, the area under the curve is divided into N equal parts and an element is placed at the center of each of the intervals defined by the equal areas, as it is illustrated in Figure 8. The density of the equally excited, unequally spaced discrete currents of Figure 8 shows how it approximates the continuous current density function of Figure 7 (Fang, D. G., 2009; Skolnik, I., 1969).

The antenna element locations in a linear array may be determined with the equal area approximation applied to the cumulative distribution $I_0(x)$ of the continuous source, rather than the current density $i_0(x)$. If the continuous source, i.e. current distribution, $i_0(x)$, and $I_0(x)$ is the cumulative current distribution, then, the relationship between the two variables is given by:

$$I_0(x) = \int_{-a/2}^{x} i_0(x)\, dx \tag{15}$$

The above expression is the integral of the continuous current density $i_0(x)$ taken over the limits $(-a/2\,, x)$, or $(-\infty, x)$, since $i_0(x) = 0$ for $x < -a/2$; variable a represents the aperture of the linear array. The cumulative distribution is illustrated in Figure 9.

The equal areas may be found by dividing the interval $(-a/2\,, a/2)$ into N equal increments, each having the same area $1/N$. This division identifies $N + 1$ boundary points $\{\hat{x}_0, \ldots, \hat{x}_N\}$, with $\hat{x}_N = -\hat{x}_0 = a/2$, such that:

$$I_0(\hat{x}_n) - I_0(\hat{x}_{n-1}) = \frac{1}{N} \tag{16}$$

The elements are located within the center of each interval $(\hat{x}_{n-1}, \hat{x}_n)$ by projecting that point onto the x axis as shown in Figure 9. The procedure is similar to the trapezoidal rule

for approximating an integral (Fang, D. G., 2009). The corresponding projecting point is defined as follows:

$$\frac{[I_0(\hat{x}_{n-1}) + I_0(\hat{x}_n)]}{2} = x_n \tag{17}$$

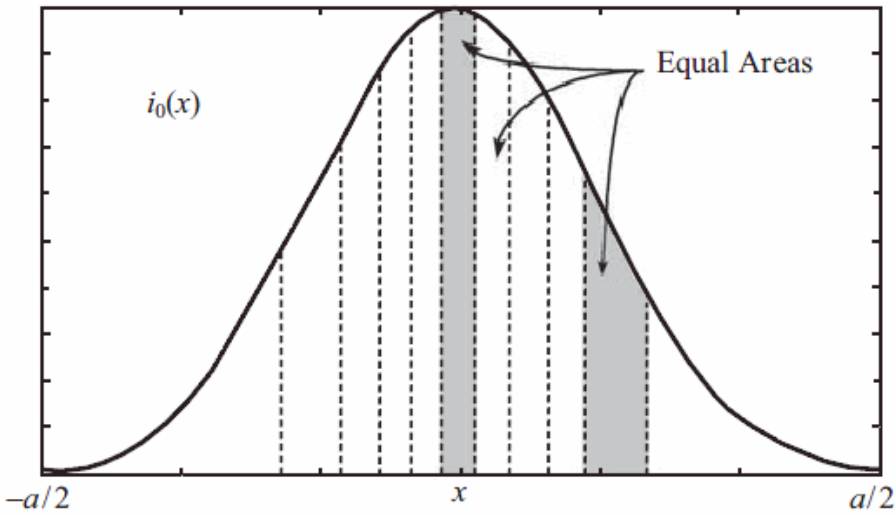

Figure 7. Model of continuous source density function (amplitude taper) divided into 11 equal sub-arrays (Skolnik, I., 1969, Fang, D. G., 2010).

Figure 8. Location of density-tapered elements (Skolnik, I., 1969, Fang, D. G., 2010).

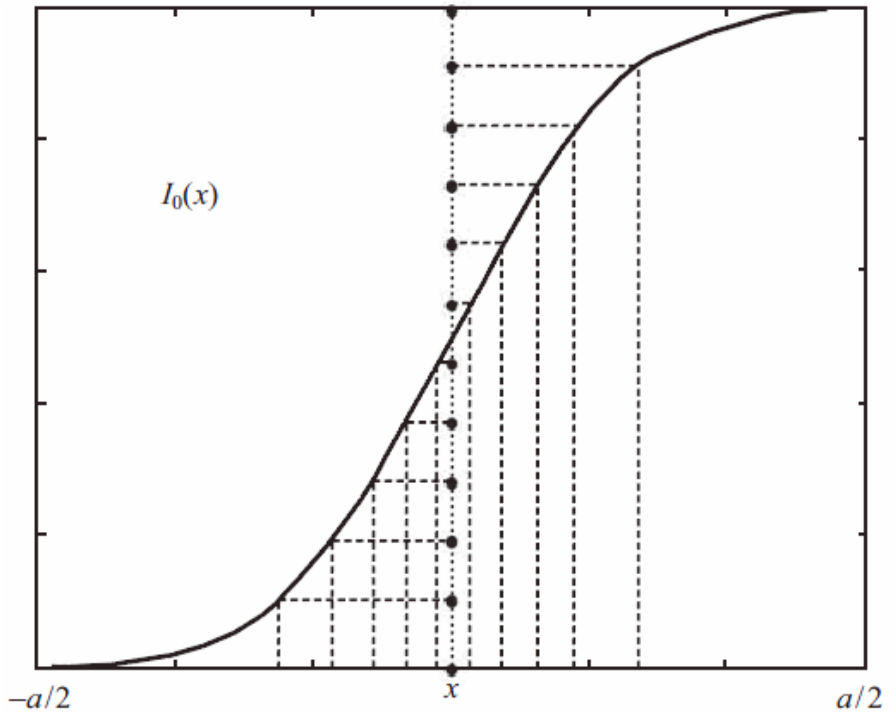

Figure 9. Cumulative current distribution (Skolnik, I., 1969, Fang, D. G., 2010).

The justification for considering the density tapering technique of unequally spaced array design is that the discrete and equally excited currents of the arrays elements approximate to the continuous current distribution amplitude-taper function used as the model. There is no guarantee, however, that the radiation pattern of the density-tapered array will be a suitable approximation to the radiation pattern of the amplitude-tapered model.

In this synthesis procedure, the density-tapered pattern is equivalent to the least-mean-square approximation to the model amplitude-tapered pattern with weighting proportional to the inverse square of the normalized pattern argument. This is shown below as an analysis adapted from (Skolnik, I., 1969).

The antenna far-field pattern produced by an aperture extending from $-a/2$ to $a/2$ with amplitude taper $i_0(x)$ is:

$$F_o(u) = \int_{-a/2}^{a/2} i_0(x) \exp(j2\pi x u)\ dx \tag{18}$$

where $u = \sin(x)$. The function $i_0(x)$ is used as the reference for the density taper. The synthetized unequally spaced array is:

$$F_a(u) = \frac{1}{N} \sum_{n=1}^{N} \exp(j2\pi x_n u) \tag{19}$$

where x_n is the algebraic distance of the $n-$th antenna element, as seen in Figure 10.

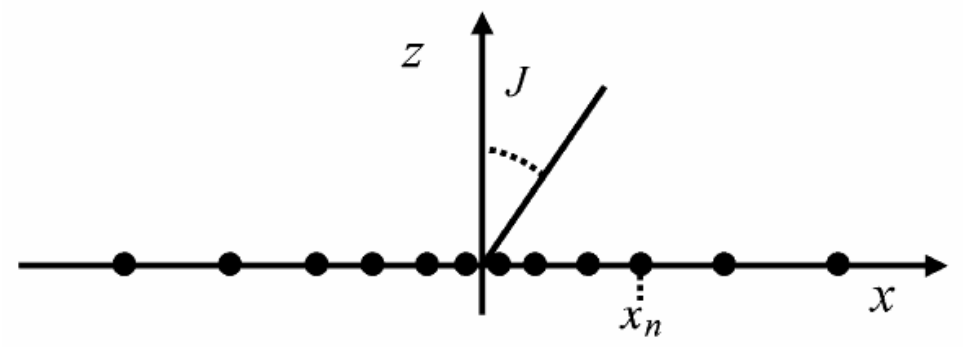

Figure 10. Reference of linear array with unequally spaced arrays (Bucci et al., 2010).

The array continuous current source function can be expressed as a summation of delta functions, as follows:

$$i_a(x) = \delta(x) + \sum_{n=1}^{N} \delta(x \pm d_n) \tag{20}$$

The array pattern may be written similar to the model pattern (18):

$$F_a(u) = \int_{-a/2}^{a/2} i_0(x) \exp(j2\pi xu)\ dx \tag{21}$$

The difference between the model pattern (18) and the array pattern (21) may be expressed in a number of ways. In this analysis, the least-mean-square difference between the two is selected as the criterion for expressing how well the density-tapered pattern approximates that to the model. The difference between the two, or the function error, may be written as follows:

$$\varepsilon = \int_{-\infty}^{\infty} [F_o(u) - F_a(u)]^2\ W(u)\ du \tag{22}$$

where $W(u) = 1\ /\ u^2$ is a weighting function which expresses the relative importance of agreement as function of the angular variable u. The value of $W(u) = 1\ /\ u^2$ is taken, so

that the difference between the two patterns becomes progressively greater with increasing distance from the main beam.

The difference in the radiation patterns is related to the difference in the continuous current densities by a Fourier transform, and that is:

$$F_o(u) - F_a(u) = \int_{-\infty}^{\infty} [i_0(x) - i_a(x)] \ \exp(j2\pi xu) \ du \tag{23}$$

By integrating by parts, introducing the definition of the cumulative distribution function (44), and assuming that the cumulative distributions of the continuous current distributions densities are equal at the end points, i.e., $i_0(-a \ / \ 2) = \ i_a(-a \ / \ 2) = 0$, and $i_0(a \ / \ 2) = \ i_a(a \ / \ 2)$, then:

$$\frac{F_o(u) - F_a(u)}{2\pi xu} = \int_{-a/2}^{a/2} [I_0(x) - I_a(x)] \sin(j2\pi xu) \tag{24}$$

This establishes a Fourier sine transform relationship between the pattern difference and the distribution difference. Applying Parseval's theorem gives:

$$\int_{-\infty}^{\infty} \frac{[F_o(u) - F_a(u)]^2}{u^2} \ du = \ 4\pi^2 \int_{-a/2}^{a/2} [I_0(x) - I_a(x)]^2 \ dx \tag{25}$$

Minimizing the mean-square difference of the patterns on the left side of (25) is thus equivalent to minimizing the mean-square difference between the current distributions on the right side of (25) if the total integrated currents across the intervals in the two cases are equal; i.e., $I_0(a \ / \ 2) = \ I_a(a \ / \ 2)$.

The cumulative function $I_a(x)$ has the form of a sum of steps of equal height. To minimize (25), $I_0(x)$ should pass through each step of $I_a(x)$. If the k-th interval of $I_a(x)$ lying between $(k-1)/N$ and $k \ / \ N$ defines a region on the x axis, $\alpha < x < \beta$ as shown in Figure

11, the problem is to determine x_n within the interval (α, β) so that the mean-square difference between the model distribution and the array distribution is a minimum. Thus it is required to minimize the next expression:

$$\int_{\alpha}^{\beta} [I_0(x) - I_a(x)]^2 \, dx = \int_{\alpha}^{x_k} \left[I_0(x) - \frac{k-1}{N}\right]^2 dx + \int_{x_k}^{\beta} \left[\frac{k}{N} - I_0(x)\right]^2 dx \qquad (26)$$

Differentiating with respect to x_k and solving gives:

$$I_0(x_k) = \frac{2k-1}{2N} \qquad (27)$$

which states that each step of $I_a(x)$ crosses the middle of the step, as seen in Figure 11.

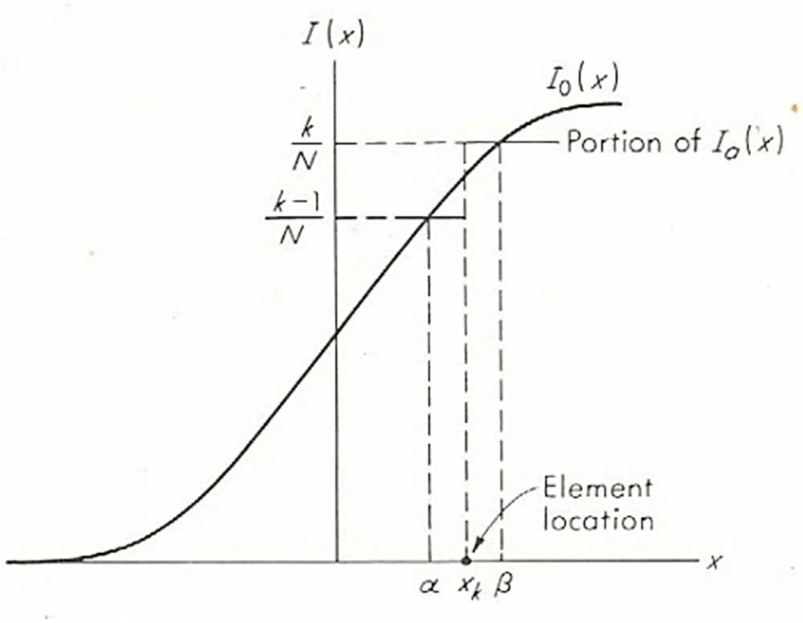

Figure 11. Fitting of $I_a(x)$ to $I_0(x)$ so as to minimize mean-square difference [Eq. (24)] (Skolnik, I., 1969).

Figure 12 shows the density tapered antenna array with 20 elements with equal-amplitude, using a Taylor linear source distribution as an aperture reference (Angeletti, P. and Toso, G., 2009; Taylor, T. T., 1960) with 25dB of target side lobe level (*SLL*) and $n_{bar} = 3$. The resulting tapered sparse array illustrated in Figure 13, shows a good

approximation of the main lobe, but presents some disadvantages since it does not meet the *SLL* requirements, having a peak *SLL* of -18.93dB. This is because it was reduced to 20 elements, and it would requires more antenna elements to upgrade the approximation to the desired *SLL* requirements.

A fixed approach based on this Doyle-Skolnik method was reported in (Angeletti, P. and Toso, G., 2009), where in addition to the density taper method, an amplitude taper is used, by this way, an array with unequally amplitude and positions is presented over the same taper array. The amplitude/density array with 20 antenna elements is presented in Figure 14 with two amplitude excitation levels $(1;\ 1/2)$, both defined by the authors; and this amplitude/density tapered array exceeds the *SLL* requirement being below the reference by having a peak *SLL* of -25.39dB, shown in Figure 15, almost 6dB lower than the equal-amplitude array. This is because the larger minimum inter-element spacing presented by this case; and this was obtained due to the subdivision of areas over $i_0(x)$ that was made proportional to the array amplitude excitations instead of equal areas like in Doyle-Skolnik method.

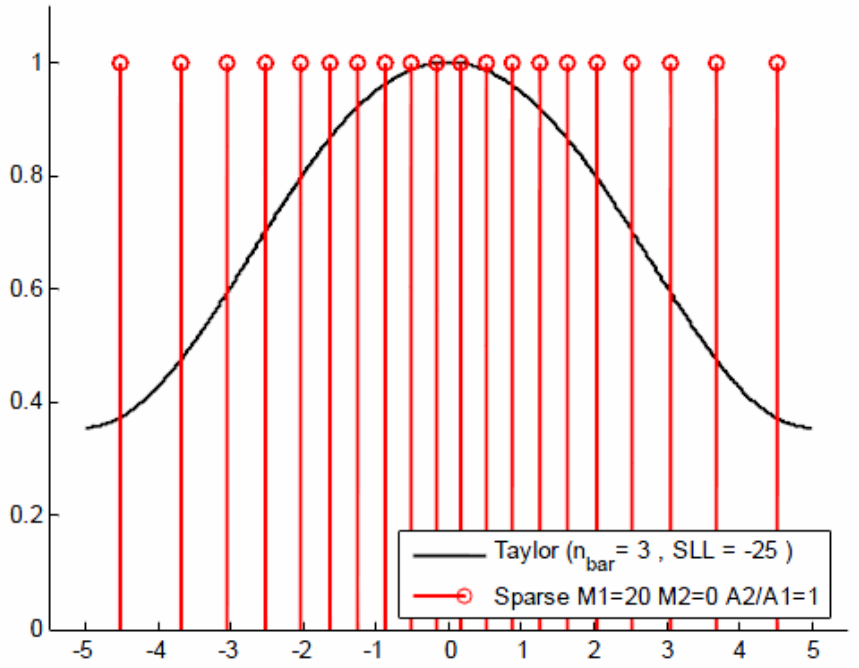

Figure 12. Location of the Density Tapered Array Elements (Angeletti, P. and Toso, G., 2009).

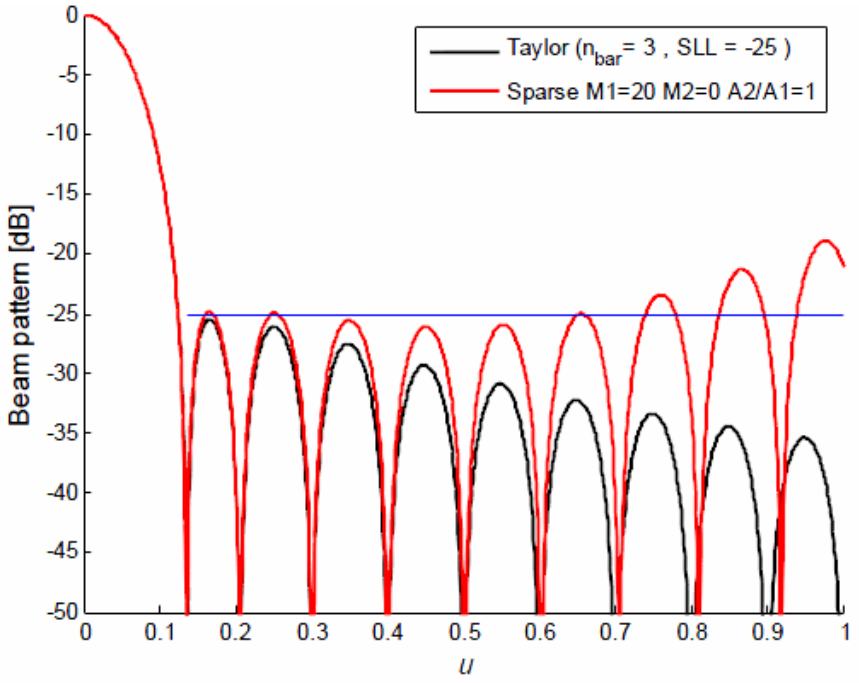

Figure 13. Radiation Pattern of the Density Tapered Array (Angeletti, P. and Toso, G., 2009).

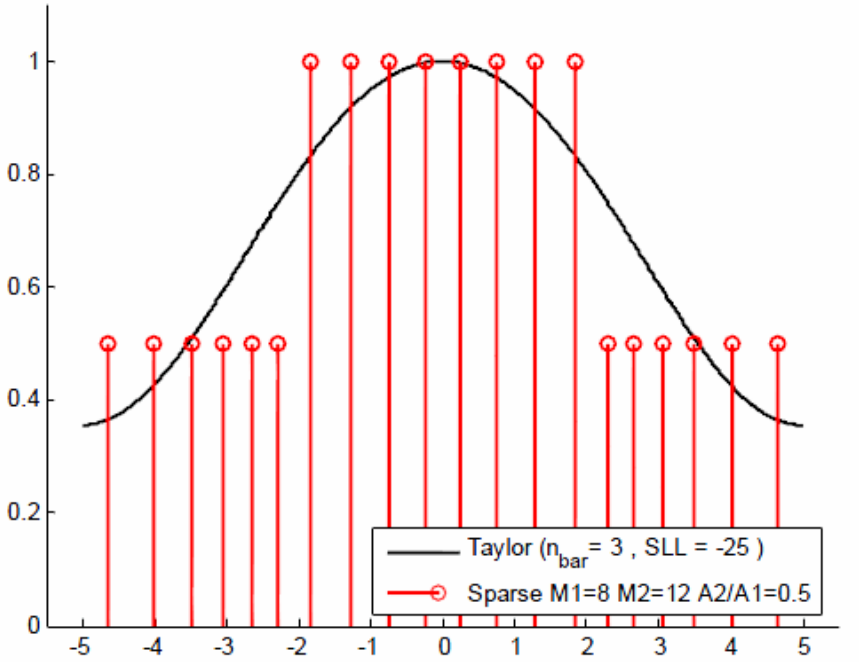

Figure 14. Location and Amplitudes of the Amplitude/Density Tapered Arrays Elements (Angeletti, P. and Toso, G., 2009).

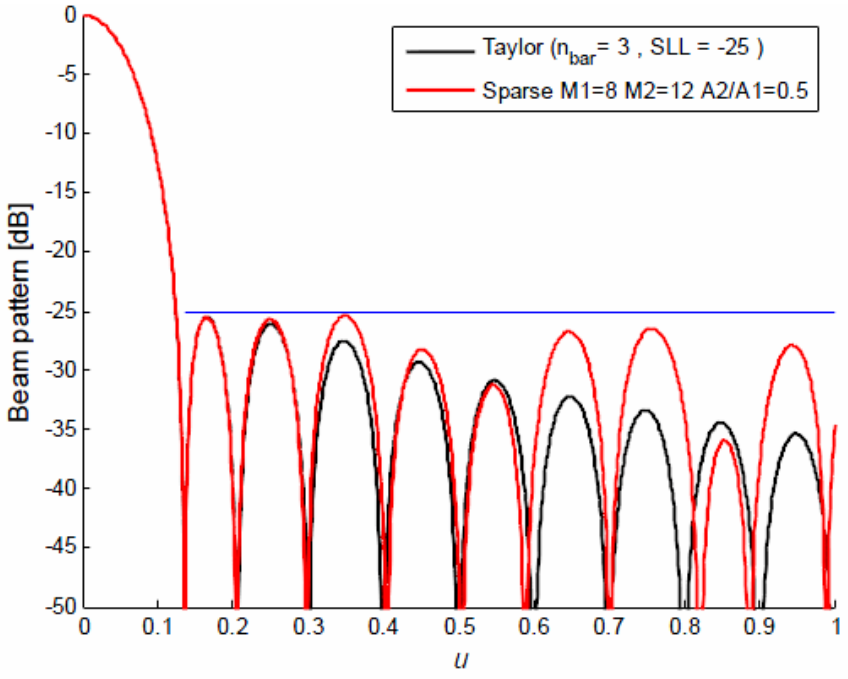

Figure 15. Radiation Pattern of the Amplitude/Density Tapered Array (Angeletti, P. and Toso, G., 2009).

This addition of amplitude/density tapering offers a degree of freedom, where in addition the projection of the x-axis for positions, a projection of current proportional to the array amplitude excitations is also useful for a better approximation in the synthesis of sparse antenna arrays.

2.5 Deterministic Density Tapering Technique applied to the Synthesis of Circular Planar Antenna Arrays

The density tapered linear array, designed to achieve a given continuous current distribution (Skolnik, I., 1969), can be extended to circular planar antenna arrays, i.e., concentric rings antenna arrays. For the linear array, a desired current distribution is picked, such as the Taylor distribution (Taylor, T. T.,1960), and use the uniform-amplitude density tapered array elements to approximate it. The antenna elements are spaced so that the width associated with each element matches the scaled integral of distribution along the same length (24).

For the extension of the density tapering technique to circular planar antenna arrays, as suggested by (Milligan, T. A., 2004), the process starts by finding the continuous current

distribution. While a normalized linear distribution spans $[-a\ /\ 2, a\ /\ 2]$, the normalized circular distribution spans the radius $[0,1]$. The circular Taylor distribution is used because it can be designed for any *SLL*, and it can be expanded its aperture distribution in a finite Fourier-Bessel series (Milligan, T. A., 2004):

$$E(r) = \sum_{m=0}^{n-1} B_m J_0(\pi S_m r) \tag{28}$$

where $r \leq 1$ and the factor πS_m is the mth root of $J_1(x)$.

To sample this distribution, ring arrays are used to contain elements spaced uniformly in angle around the ring. The authors varies the radius of a finite number of rings to sample the circular distribution. Begin the process by integrating the distribution from zero to a series of given radii, and create a table of radius versus the cumulative distribution for this kind of array (Milligan, T. A., 2004):

$$\int_0^r d_e(\rho)\, E(\rho)\, d\rho \tag{29}$$

The term $\rho d\phi$ is eliminated from the integral because the elements are spaced uniformly around the ring. In general, the rings have different element radial spacing $d_e(r)$. The number of antenna elements around each ring is given by:

$$N_p(r) = \frac{2\pi r}{d_e(r)} \tag{30}$$

A table is generated by forming a cubic spline, with the cumulative distribution as the abscissa and the radius as the ordinate. The cumulative distribution is evenly divided by the number of rings, and evaluate the spline in the center of each segment along the distribution to find its radius. Figure 16, taken from (Milligan, T. A., 2004), illustrates this method for a 16-ring circular planar array sampling a 30dB circular Taylor distribution that

spans a 14λ radius for equal spacing $d_e(r)$ in all rings. Table 1 lists the radius of each ring that lies in the center of each region along the abscissa of Figure 16.

Figure 17 illustrates the layout of the 845 antenna elements that formed the 16-rings antenna array for an element spacing of 0.66λ around the rings. The center ring only had three antenna elements. The closest element spacing was 0.51λ in the center.

The pattern for this case, was calculated and produced the radiation pattern showed in Figure 18. Other pattern through other radial planes produced almost exactly the same pattern, and showed that the array achieved the design *SLL* close in to broadside. Similarly to all space-tapered arrays, Figure 18 shows the eventual degradation of the *SLL* as lobes rise above -30dB (Milligan, T. A., 2004), similar to Doyle-Skolnik result in Figure 13 for a linear array.

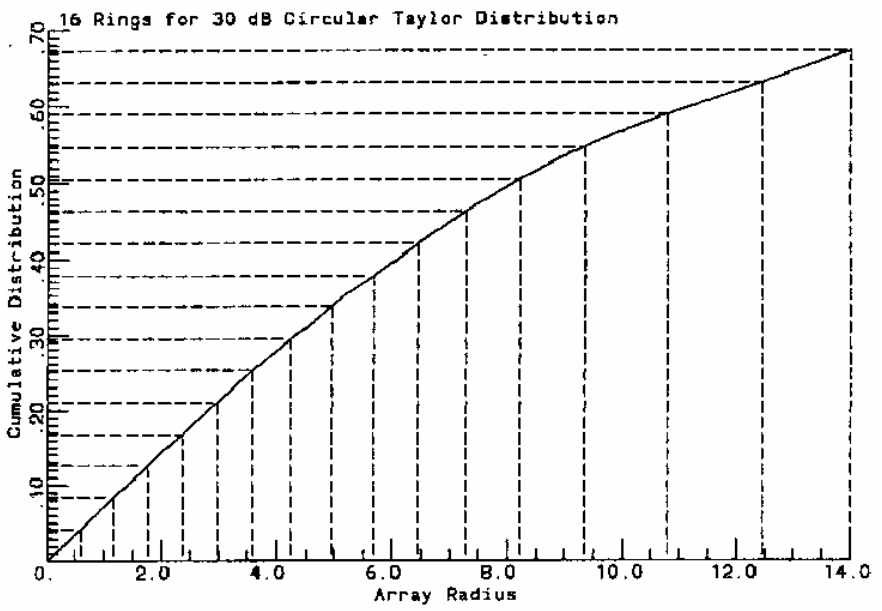

Figure 16. Extension of Doyle-Skolnik tapering method to a circular planar array, where the cumulative distribution was divided into 16 equal-width lines. Projection onto the radius axis finds the ring radii (Milligan, T. A., 2004).

Table 1. The 30dB circular Taylor distribution radii for 16 rings spanning 14λ (Milligan, T. A., 2004).

Ring	*Radius* (λ)
1	0.294
2	0.884
3	1.473
4	2.069
5	2.671
6	3.289
7	3.929
8	4.600
9	5.308
10	6.060
11	6.864
12	7.742
13	8.751
14	10.012
15	11.617
16	13.241

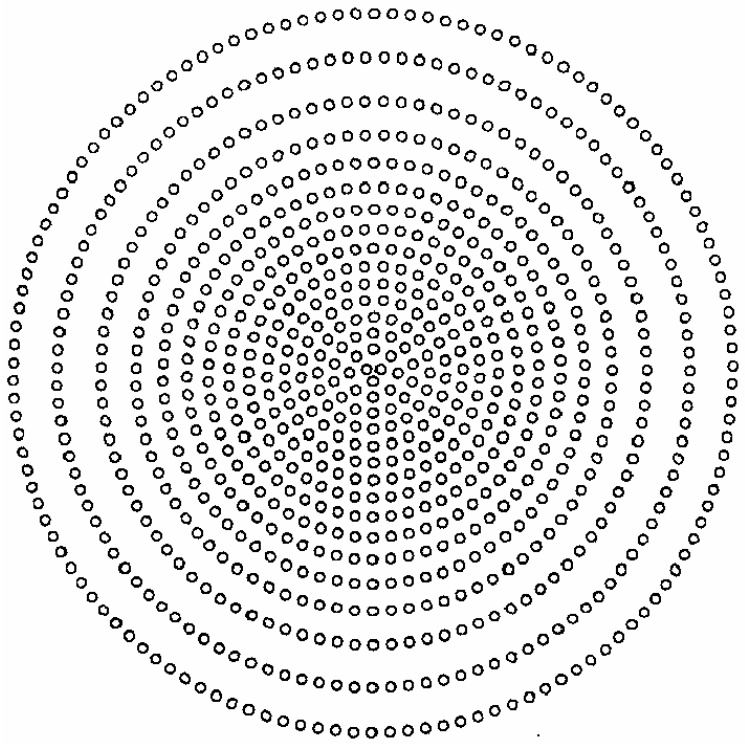

Figure 17. Layout of the 845-element space-tapered ring array with 16 rings for a 30dB circular Taylor distribution spaning a diameter of 28λ (Milligan, T. A., 2004).

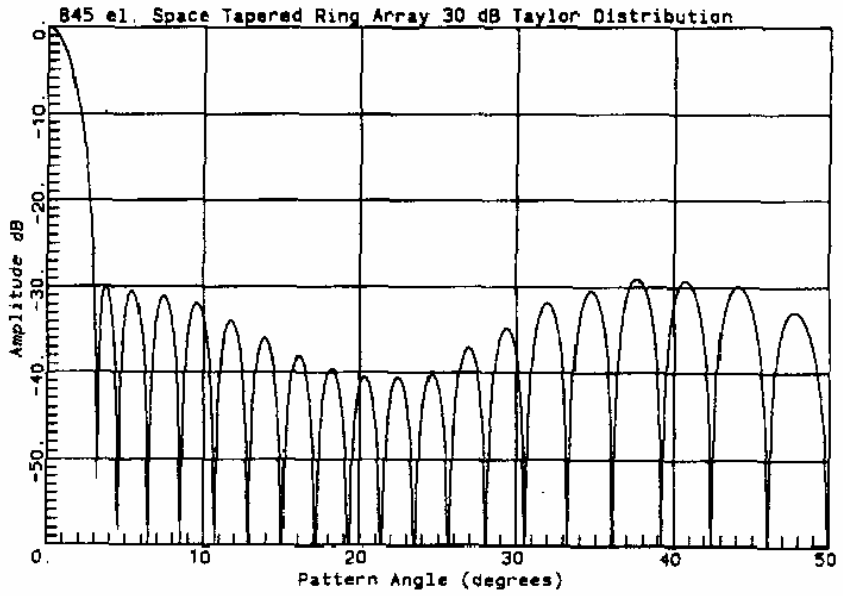

Figure 18. Pattern response of the 845 antenna elements space-tapered for 16 ring antenna array (Milligan, T. A., 2004).

With the above, we have finalized the basic summary of the theory of sparse antenna arrays by density tapering technique for the synthesis of antenna arrays.

2.6 Conclusions

In this chapter, we have presented the relevant approaches for the synthesis of sparse antenna arrays that will be used as reference to develop a new synthesis methodology in next chapter.

The approaches presented in this chapter, such as the orthogonal method applied to the synthesis of antenna arrays, and the density tapered method, offer antenna arrays with sparseness characteristics in order to reduce the number total of antennas, by employing the non-uniformity along the antenna elements by different methodology strategies, which together can be useful to extend to new scenarios.

The orthogonal method applied to the synthesis of antenna arrays, resulted in a good option to operate with the non-orthogonality of the non-uniform circular array mathematical expression, i.e., array factor, in order to obtain amplitude excitations, but, it

is necessary to define a-priory an optimal space distribution so this technique could obtain a good approximation to the desired pattern.

Also, the Doyle-Skolnik density tapered method resulted in a good approach to use as reference a continuous current distribution to obtain a sparse antenna array for geometries such as linear and planar. However, as showed by (Angeletti, P. and Toso, G., 2009), a combination of amplitude/density tapering technique could offer a better synthesis fulfilling the desired pattern requirements.

To further contribute to the state-of-the-art sparse synthesis and detecting the lack of this kind of work over a single ring circular antenna array with the synthesis of sparse antenna arrays, in next chapter, a new synthesis will be introduced, which is focused in working with the non-orthogonality of the circular array in order to obtain a continuous current distribution, by an expansion of orthogonal basis, as (Sahalos, J., 2006) proposes, and obtaining the discrete currents excitations, and non-uniform antenna positions by using the theory of the density tapering method, based on the option presented by (Angeletti, P. and Toso, G., 2009) of modification of the subdivision of intervals over the current, and incorporating the analysis of the current in addition of the positions of antenna elements to obtain a better approximation to a desired pattern.

Chapter 3. Synthesis Methodology of Sparse Circular Antenna Arrays

3.1 Introduction

In this chapter, we present an alternative solution for reducing the resources used in the antenna arrays, and by this way, supporting the requirements of 3GPP for LTE-A systems about green networks. The fact that the case of circular antenna array with sparseness characteristics has not been widely explored in the state-of-art, and encouraged to develop an analytical methodology to give sparseness characteristics to antenna arrays with this particular geometry that find its application in both communications and radar systems.

This synthesis proposal is based on the two analytical procedures presented in Chapter 2, the orthogonal method applied to the synthesis of circular antenna arrays, and a density/amplitude tapering technique. In the first part of the proposed synthesis, inspired by the orthogonal method applied over circular antenna arrays (Sahalos, J., 1974; Sahalos, J., 2006), where the current excitations are represented by a set of orthogonal basis functions, the proposal of this part of the thesis starts from the reconstruction of a continuous current distribution by an expansion of orthogonal basis, for a desired array pattern.

In the second part, in order to obtain the excitations and elements angular positions, the proposal is based on the synthesis procedure suggested by (Josefsson, L. and Persson, P., 2006), in which a continuous current distribution is uniformly sampled to obtain the locations and excitation values; in contrast, in our approach, an adapted density/amplitude tapering procedure is used over the reconstructed continuous distribution to determine the current excitation and elements' angular positions for a circular array with sparseness characteristics.

Also, numerical experiments are presented to evaluate the performance of the proposed method and then it is compared with respect to the synthesis methods presented in Chapter 2, the synthesis procedure with uniform distribution reported by (Josefsson, L.

and Persson, P., 2006) and the orthogonal method applied over circular antenna arrays proposed by (Sahalos, J., 2006).

3.2 Array Factor

To start with our analysis, let us consider a circular array with N identical antenna elements evaluated in broadside as seen in Figure 19.

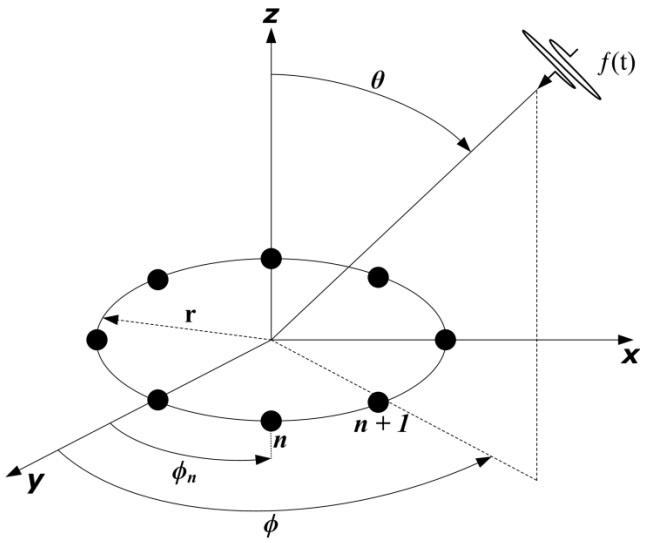

Figure 19. Representation of a circular antenna array.

The array factor for this circular geometry is defined by (Balanis, C. A., 2005):

$$AF(\phi) = \sum_{n=1}^{N} I_n \exp(jkr\cos(\phi - \phi_n)) \tag{31}$$

The variable N is the number of antenna elements, $I_n \in \mathbb{C}$ is the current excitation, $r \in \mathbb{R}$ is the circular array radius, ϕ is the azimuth plane, ϕ_n is the *n*th element's azimuth position, j is the imaginary unit, and $k = 2\pi/\lambda$ represents the free-space wavenumber, where λ is the wavelength.

As can be seen, the expression in (31) is composed of basis functions $\exp(jkr\cos(\phi - \phi_n))$ that are non-orthogonal. The issue in the calculation of the current excitations I_n comes from the fact that the array factor is expanded in a non-orthogonal set of functions (Sahalos, J., 1974). This drawback has been previously discussed in (Sahalos, J., 1974;

Sahalos, J., 2006), by using the classical procedure of the orthogonal method to derive a set of orthogonal functions in order to obtain the current excitations I_n of the antenna elements with a pre-defined non-uniform distribution, and then generate a desired pattern $F(\phi)$, but, knowing the pre-defined non-uniform distribution it's a problem by itself, since mostly of time, the optimum distribution is not known. Then, inspired on this technique, we propose to reconstruct a continuous current distribution, for a desired pattern by an extension in orthogonal basis functions, later, a tapering technique is applied to find the non-uniform distribution and current excitations to give sparseness to the circular array.

3.3 Reconstruction of Continuous Current Distribution

Since we want to reconstruct a continuous current distribution, the continuous representation of the array factor for a circular antenna array evaluated in broadside is defined by (Balanis, C. A., 2005; Josefsson, L. and Persson, P., 2006):

$$F(\phi) = \frac{1}{2\pi} \int_{-\pi}^{\pi} I(\varphi) \exp(jkr \cos(\phi - \varphi))\, d\varphi \tag{32}$$

The variable $I(\varphi)$ is the continuous current distribution that we need to reconstruct in the continuous azimuth angle φ, in order to apply a tapering technique, as it can be seen in expression (32), that it is a periodic function over 2π, so it can be expanded in orthogonal basis functions as Fourier series. For this, the complex Fourier series defined by (Ersoy, O. K., 1994) were used, and they are defined as following:

$$f(t) = \sum_{-\infty}^{\infty} X(m/T) \exp(2\pi jmt/T) \tag{33}$$

$$X(m/T) = X_m = \frac{1}{T} \int_{-T/2}^{T/2} f(t) \exp(2\pi jmt/T)\, dt \tag{34}$$

Applying these complex Fourier series definitions to the circular antenna array with current distribution $I(\varphi)$ and period $T = 2\pi$, the next expressions are obtained:

$$I(\varphi) = \sum_{-\infty}^{\infty} \hat{C}_m \exp(jm\varphi) \tag{35}$$

$$\hat{C}_m = \frac{1}{2\pi} \int_{-\pi}^{\pi} I(\varphi) \exp(-jm\varphi)\, d\varphi \tag{36}$$

The function $\exp(jm\varphi)$ is an orthogonal basis function of order m, with $\varphi = \in [-\pi, \pi]$ and the variable $\hat{C}_m$ represents the coefficients of the series expansion. Substituting the expression (35) into expression (32), and reversing the order of integration and summation yields (Josefsson, L. and Persson, P., 2006):

$$F(\phi) = \sum_{-\infty}^{\infty} \frac{\hat{C}_m}{2\pi} \int_{-\pi}^{\pi} \exp(jm\varphi) \exp(jkr\cos(\phi - \varphi))\, d\varphi \tag{37}$$

On the other hand, the representation of the desired pattern must also be a periodic function over 2π (Josefsson, L. and Persson, P., 2006), by this way, we can also expand the desired pattern in orthogonal basis function as Fourier series:

$$F(\phi) = \sum_{-\infty}^{\infty} \hat{A}_m \exp(jm\phi) \tag{38}$$

Being $F(\phi)$ the representation of the desired pattern of a circular antenna array defined in the continuous, its Fourier coefficients $\hat{A}_m$ can be derived by the next expression:

$$\hat{A}_m = \frac{1}{2\pi} \int_{-\pi}^{\pi} F(\phi) \exp(-jm\phi) \tag{39}$$

Observing the expressions (38) and (39), we find that the coefficients $\hat{A}_m$ are related to the coefficients $\hat{C}_m$. Then, the reconstruction is the continuous current distribution has been reduced to calculating the coefficients $\hat{C}_m$. By substituting (39) in (37), we obtain the next expression:

$$\hat{A}_m = \frac{\hat{C}_m}{2\pi} \int_{-\pi}^{\pi} \exp\big(jm(\varphi - \phi)\big) \exp(jkr\cos(\phi - \varphi))\, d\varphi \tag{40}$$

The above expression can be treated as a Bessel function of order m (Balanis, C. A., 2005; Josefsson, L. and Persson, P., 2006). Then (40) can also be written as:

$$\hat{A}_m = j^m\, \hat{C}_m\, J_m(kr) \tag{41}$$

Finally, it is possible to calculate the coefficients $\hat{C}_m$, as shown in the following:

$$\hat{C}_m = \frac{\hat{A}_m}{j^m J_m(kr)} \tag{42}$$

Now, the desired pattern in (37) can be rewritten by summarizing all basis function given the total pattern:

$$F(\phi) = j^m\, \hat{C}_m\, J_m(kr) \exp(jm\phi) \tag{43}$$

After this point, the reconstructed continuous current distribution $I(\varphi)$ for the desired radiation pattern can be evaluated through (35). A good reconstruction of the continuous current distribution in (35) will depend on the number of harmonics m used; the authors in (Josefsson, L. and Persson, P., 2006) recommend that the number of harmonics must be less than the number of antenna elements, high values of m could lead to the presence of oscillations and distortions in the reconstructed current distribution becoming unsuitable for our sparseness proposal. Furthermore, in our experiments, we found that each desired pattern requires a different number of harmonics for a good approximation of a desired pattern $F(\phi)$. Then, the value of m is determined through an iterative process where the initial value of m is set to the unit and the iterative process increases the value of m until obtaining the best approximation of $F(\phi)$ through (38), without the presence of oscillations in $I(\varphi)$. By this iterative process, we ensure to reconstruct a suitable current distribution for the sparseness procedure by applying a tapering technique.

3.4 Tapering Technique over Reconstructed Current

In order to obtain the desired sparseness characteristics for the circular antenna array, it is required to use a tapering technique over the reconstructed continuous current distribution to obtain the discrete current excitations and angular positions of the antenna elements. In this sparse synthesis proposal, we use a general tapering technique based to determine the position of the N antenna elements.

The proposed procedure is defined in the following steps:

1. The cumulative current distribution $I_C(\phi)$ of the reconstructed current distribution for the circular array geometry is evaluated by the next line integral:

$$I_C(\phi) = \int_{-\phi}^{\phi} |I(\varphi)|\, r d\varphi \tag{44}$$

   where 2π is the total continuous source dimension and r is the radius of the circular array. Although $I(\varphi) \in \mathbb{C}$, in our experiments, the antenna element positions can be determined by considering only the real part of $I(\varphi)$. This consideration has been used by other approaches in the case of linear arrays (Caratelli, D. and Viganó, M. C., 2011; Vigano, M. C. and Caratelli, D., 2010), and, as will be presented later in this chapter, it has shown good results in our proposal.

2. The interval $(-\pi, \pi)$ of the continuous source dimension is divided into N sub-intervals of equal lengths, with $N+1$ boundary points $\hat{\phi}_n$. Hence, the intervals boundaries are defined as $\left(\hat{\phi}_{n-1}, \hat{\phi}_n\right)$.

3. The antenna position ϕ_n is determined in each sub-interval by next expression:

$$I_C(\phi_n) = \frac{I_C\left(\hat{\phi}_n\right) - I_C\left(\hat{\phi}_{n-1}\right)}{2} \tag{45}$$

The projection of $I_C(\phi_n)$ onto the ϕ determines the antenna element position ϕ_n as seen in Figure 20. Representation of the tapering technique over the cumulative current distribution.

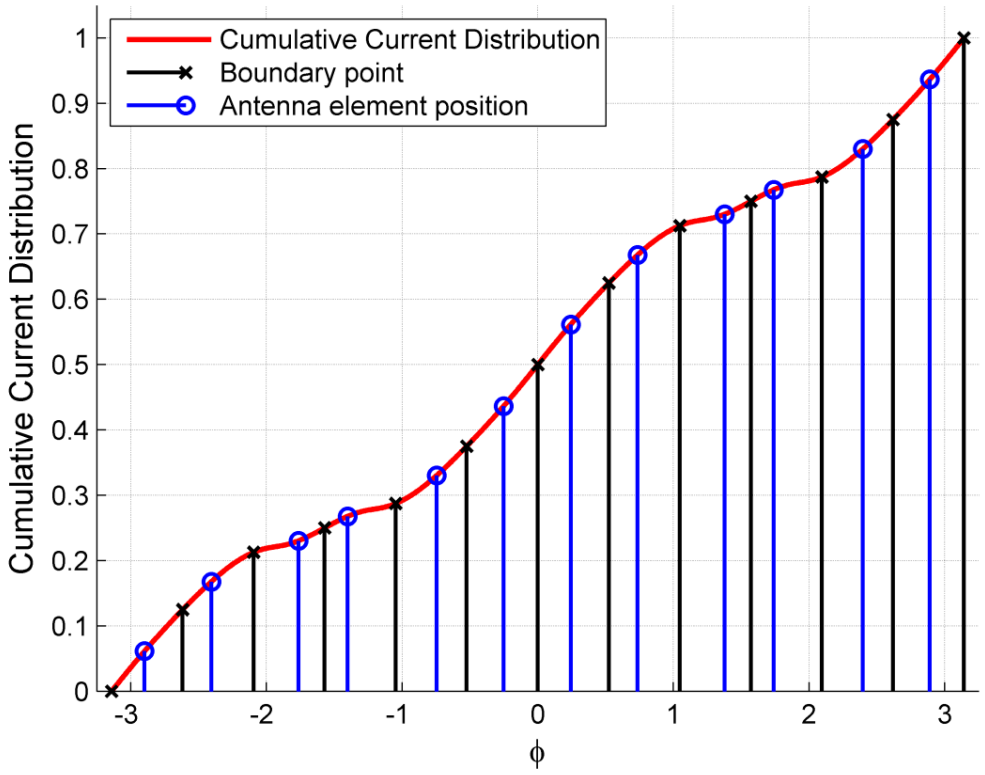

Figure 20. Representation of the tapering technique over the cumulative current distribution.

As seen in Figure 20, the antenna element is placed in the numeric center (blue lines with circles) of each sub-interval (black lines with cross) over the cumulative function $I_C(\phi)$ (red line), as indicated by expression (45).

4. The complex excitation current I_n in each interval is determined by taking the value of $I(\varphi)$ at the position ϕ_n. For excitation of amplitude, we take the value of $|I(\phi_n)|$, and $\mathrm{Arg}(\phi_n)$ for the phase excitation, as seen in Figure 21.

With the above, the process is equivalent to a density/amplitude tapering technique, but also, the phase considered in order to complete the current excitation with its real and complex part.

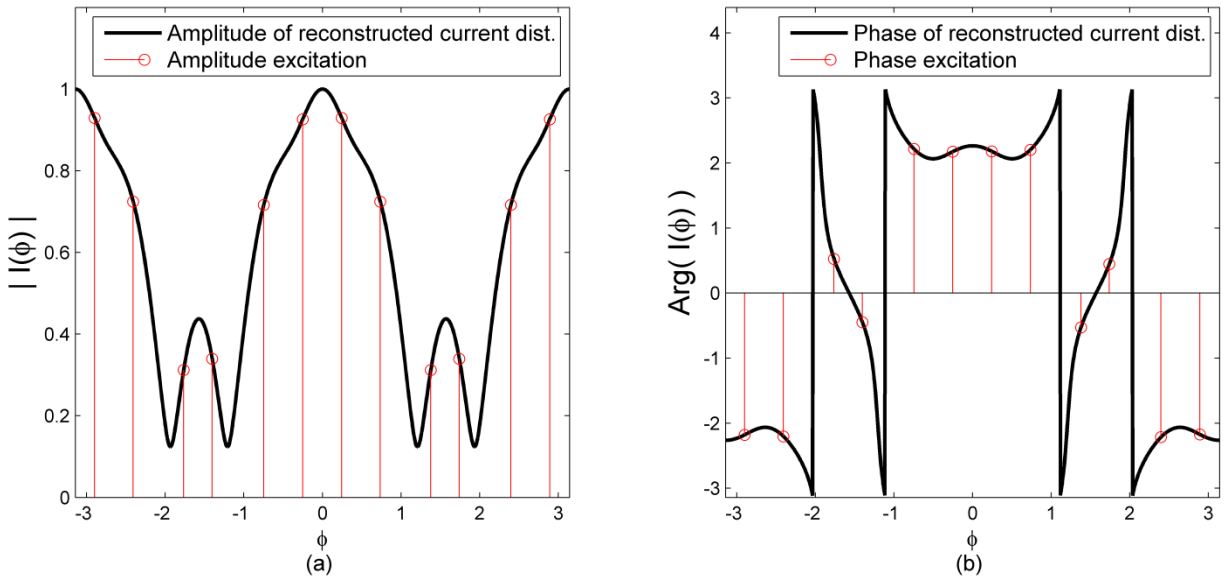

Figure 21. Projection of the antenna element positions ϕ_n to (a) amplitude and (b) phase of reconstructed current distribution to determine the amplitude and phase values of excitation current I_n.

3.5 Iterative Method to obtain Optimums Circular Array Radius

Finding the excitation currents I_n and the angular positions ϕ_n does not completely solve the problem; it is necessary to determine a suitable radius r for the circular antenna array. A suitable radius r is a critical parameter for the synthesis of a circular antenna array since the coefficients $\hat{C}_m$ used to calculate $I(\varphi)$, are too sensitive to small variations of values of r, this behavior is influenced by the Bessel function in the denominator (42). This problem has been treated by (Rahim, 1980), where the value of a harmonic is used to determine the radius of the array. For our sparse synthesis proposal, r is determined by an iterative procedure, where the reconstruction of the continuous current distribution and the tapering procedure to find ϕ_n and I_n are obtained by evaluating a range of values of radii by analyzing the error in the beamwidth and the maximum side lobe level resultants with respect to the desired pattern $F(\phi)$. Then, the r which presents a minor error from $F(\phi)$, or fulfills the requirements of side lobe level and beamwidth after being evaluated under the proposed approach as it is illustrated in Figure 22, will be selected as the optimum radius.

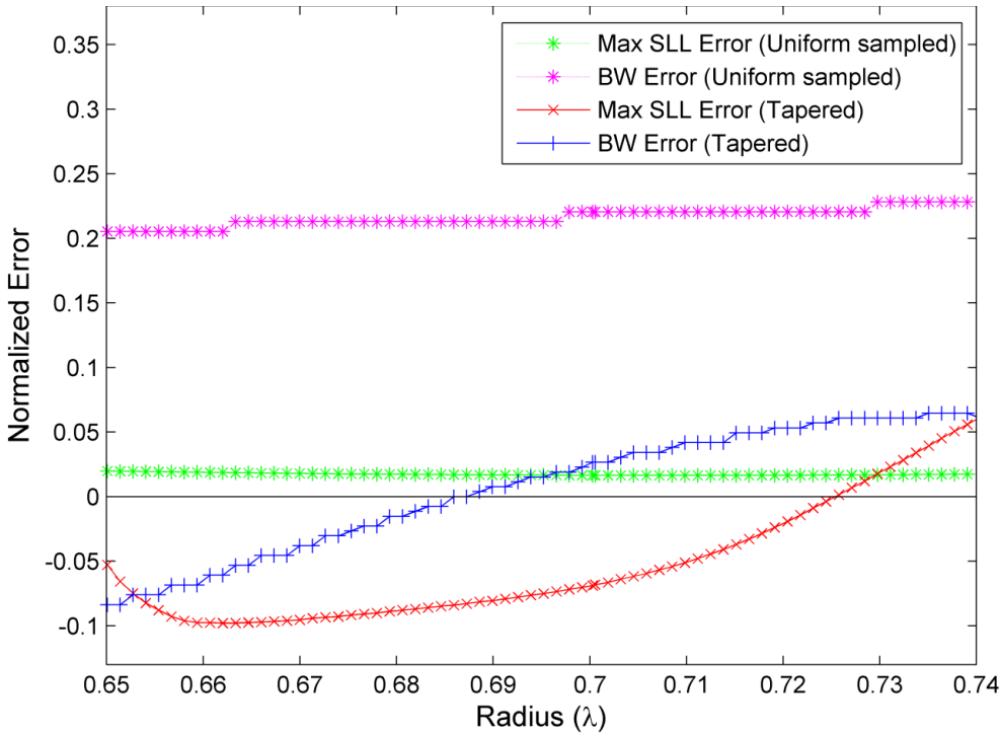

Figure 22. Graphical representation of the iterative process to evaluate beamwidth and side lobe level error for the uniform sampled approach and the proposal approach to find a suitable value of r.

The evaluation of different values of r through the described iterative process is shown in Figure 22 along with the uniform sampled method presented by (Josefsson, L. and Persson, P., 2006). It is clearly shown that the iterative process finds a suitable value of r for the proposal, which presents a minimized error that fulfills the requirements of the beamwidth and the maximum side lobe level for a desired pattern $F(\phi)$. According to the Figure 22, the numerical value of r for this case is 0.6859λ, in which the beamwidth has an almost 0 of error with respect to a reference value of beamwidth, and the value of side lobe levels are below the reference, which is a desirable behavior, in order to have the lower interference values.

3.6 Numerical Analysis and Assessment

In this section, we present the results of three numerical cases to synthesize circular antenna arrays: narrowbeam, flat-top and square-cosecant beam patterns. We assess the performance of our proposed approach, and it is compared to uniform sampled approach (Josefsson, L. and Persson, P., 2006) and the orthogonal method synthesis for

circular antenna arrays (Sahalos, J., 1974; Sahalos, J., 2006). These two synthesis methods have been implemented and validated with our computational tool built under the MATLAB programming platform. For each case, we evaluated our proposal with different number of antenna elements N. For sparseness characteristics, we minimized the number of N to find the best result with a minimum N.

In order to have a fair comparison among our proposal and the mentioned synthesis methods, the number of antenna elements N and the value of the radius r, calculated by applying the procedure described in Section 3.5, were used for each synthesis method to have the same conditions of evaluation. Also, it is important to clarify that for the uniform sampled method, the excitation currents I_n are found by just sampling uniformly the reconstructed current distribution $I(\varphi)$ at the antenna element positions ϕ_n (Josefsson, L. and Persson, P., 2006); for the following test cases $I(\varphi)$ was used by our proposal and for uniform sampled method. For the orthogonal method synthesis, it is necessary to propose a-priori non-uniform antenna positions to determine the excitation currents by using the orthogonal method (Sahalos, J., 1974; Sahalos, J., 2006). Since this spatial distribution needs to be proposed, we used the same non-uniform distribution obtained by our tapering procedure, by this way, we keep a fair comparison with the same conditions.

3.6.1 Narrow-Beam Pattern

As a first test case, we consider the synthesis of a narrow-beam pattern with a $BW = 95°$ and a $SLL = -20\,dB$. After a comprehensive analysis of the proposal procedure, we minimized the number of antennas to $N = 12$ to observe the compromise between the approaches and the reference narrow-beam pattern as shown in Figure 23.

In this test case, our proposal obtained a narrow beamwidth of $94.3°$, just a difference of $0.7°$ with respect to narrowbeam reference pattern, while the other synthesis methods have differences of $24°$ for the uniform sampled method and $17°$ for the orthogonal method. In terms of side lobe levels, our proposal is below the reference with $SLL = -21.62dB$, while a slight increment of the side lobe level is presented in the uniform

sampled method with $SLL = -19.6dB$, and the orthogonal method achieved a $SLL = -20.88dB$.

As it can be seen in Figure 23, our proposed sparse synthesis technique fulfills both requirements, beamwidth and side lobe level, while the uniform sampled method presented some drawbacks in both requirements. Both techniques used the same reconstructed current distribution $I(\varphi)$, but were sampled by different criteria, the non-uniformity obtained by the tapering procedure achieved a better reduction of the beamwidth and side lobe level. The same non-uniformity distribution of antenna positions was used for the orthogonal method synthesis, and it contributes to obtain low side lobe levels, but not to obtaining a narrow beam pattern; our proposal found a closer response to the reference pattern requirements for this test case.

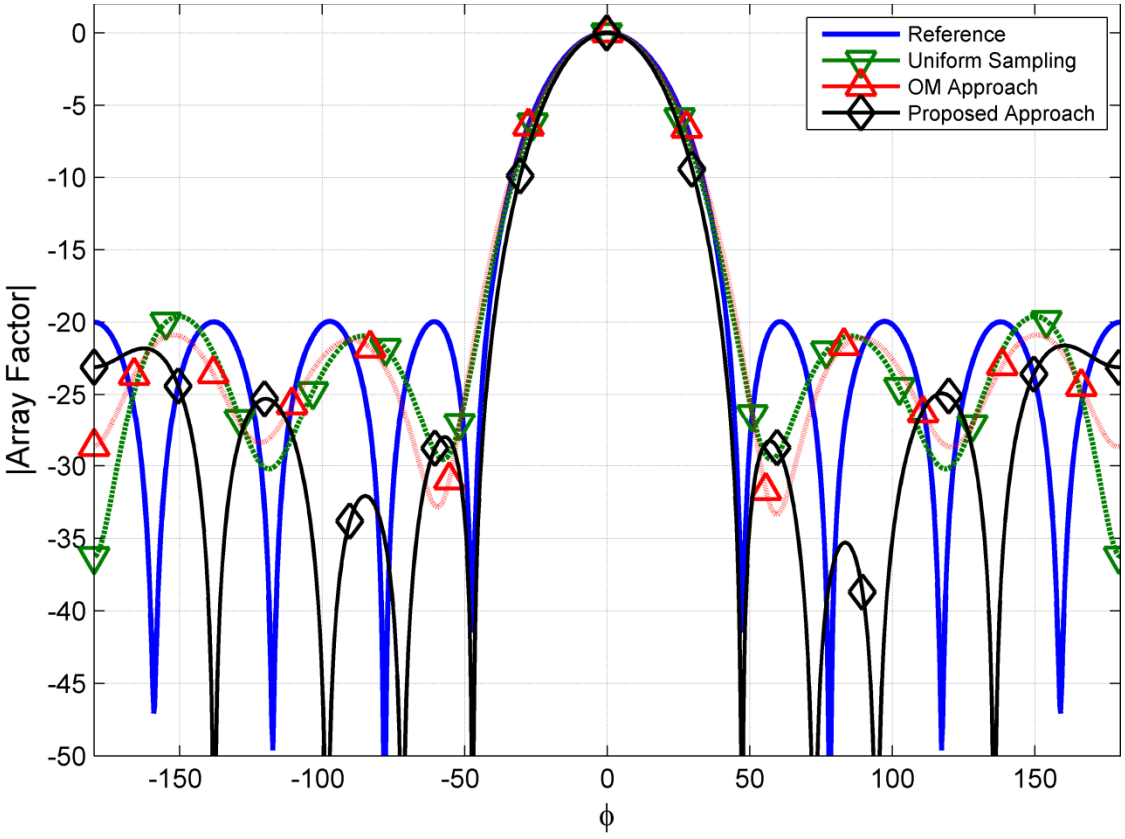

Figure 23. Narrow-Beam pattern with 12 antenna elements for each synthesis technique.

This is due to the combination of positions and excitation currents obtained by the reconstructed current distribution $I(\varphi)$. It is important to mention that as we use a minimum number of antenna elements (for sparseness characteristics) for this case, the

beamwidth and side lobe level of each synthesis approach pattern presents slightly variations with respect the reference pattern.

The number of harmonics used to reconstruct the continuous current distribution has been found to be $M = 7$ by the iterative procedure, and we found that for this value of m, the value of the radius which fulfill the requirements for this case was $r = 0.6859\lambda$, we used this value of r for the other approaches to keep the fair comparison. In addition to this result, Table 2 shows the positions, amplitude and phase excitations of antenna elements obtained by our proposal in this case.

Table 2. Numerical values of positions and current excitations of antenna elements for Narrow-Beam case.

n	ϕ_n	$\lvert I(\phi_n)\rvert$	$\mathrm{Arg}(\phi_n)$
1	-2.8981	1	-2.1787
2	-2.4065	0.7793	-2.2030
3	-1.7633	0.3357	0.5270
4	-1.4019	0.3651	-0.4474
5	-0.7457	0.7708	2.2157
6	-0.2517	0.9960	2.1737
7	0.2435	0.9999	2.1787
8	0.7351	0.7793	2.2030
9	1.3783	0.3357	-0.5270
10	1.7397	0.3651	0.4474
11	2.3959	0.7708	-2.2157
12	2.8899	0.9960	-2.1737

3.6.2 Flat-Top Beam Pattern

In order to show the versatility of the proposed sparse synthesis approach, we have considered a flat-top pattern as the objective reference for the second case test. The considered flat-top pattern has a $95°$ beamwidth and $-20\,dB$ peak sidelobe level. The number of antenna elements has been minimized to $N = 40$ for each approach to maintain the fair comparison. More antenna elements are required, compared to the previous case, to fulfill the requirements of the shaped beam.

In Figure 24, it can be seen that the three approaches fulfill the requirements of the flat-top beam, but our proposal and the uniform sampled approach have a lower side-lobe level than that of the orthogonal method, which exhibits a slight drawback at $\phi = 147°$.

Even though this method has the same condition of non-uniformity that our proposal, the excitation currents obtained by this method were unable to avoid these slight drawbacks for this test case. In terms of beamwidth, the three synthesis methods have a difference in the range of of $8°$ and $10°$. The behavior of the reconstructed current distribution $I(\varphi)$ achieved a beam pattern that fulfills the requirements of the desired pattern in terms of not exceeding the side lobe levels for a reduced number of antenna elements.

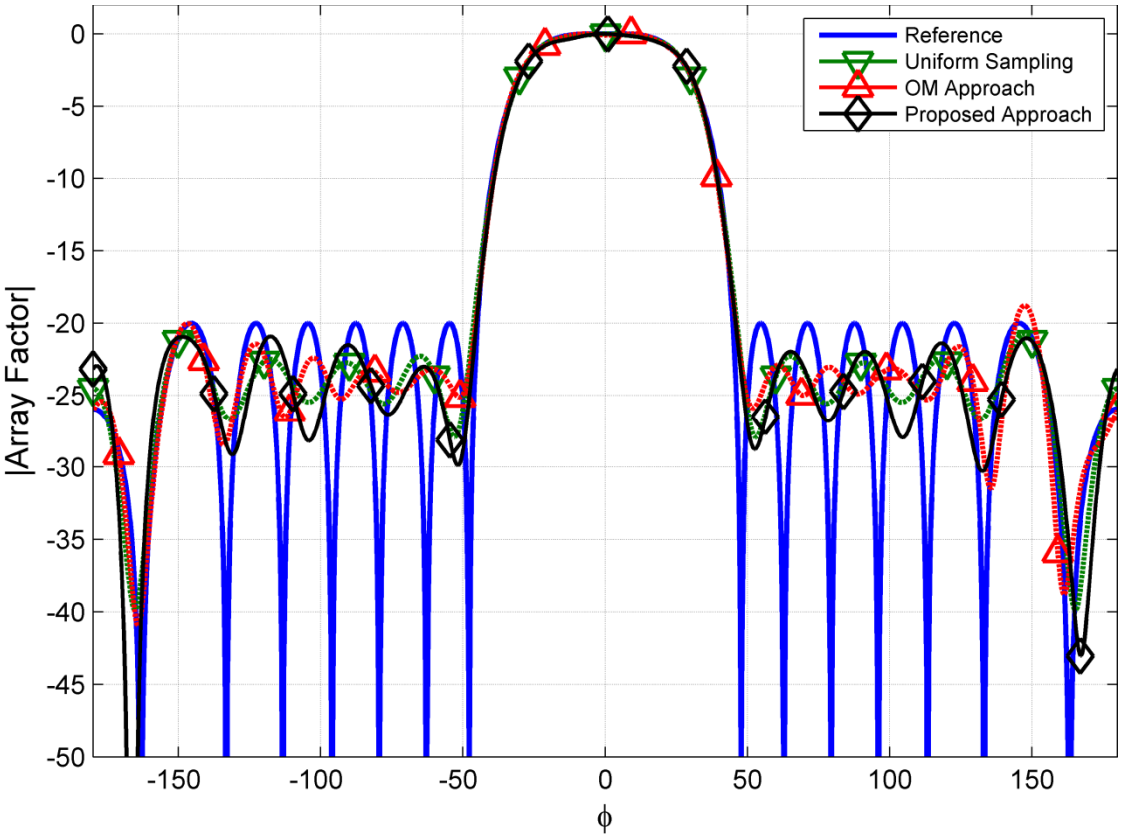

Figure 24. Flat-Top beam pattern with 40 antenna elements for each synthesis technique.

After a comprehensive analysis to obtain a suitable reconstructed current distribution for a good reconstruction of this particular case of shaped beam, it was found that the number of harmonics was $M = 13$, and the radius of the array which showed a lower error after the minimization of the number of antenna elements was found to be $r = 2.9748\lambda$, to continue with a fair comparison with the other approaches the same value of r was used for each approach. To get further insight of this obtained values, notice that values of the number of harmonics M and radius r are higher compared to the previous case, this is because the flat-top beam represents a more complicated beam pattern and it was necessary to increase the value of M in (38) to get a better approximation to the flat-top

beam pattern, and the value of r had to be increased to find a suitable solution for $I(\varphi)$. Furthermore, the positions, amplitude and phase excitations of antenna elements obtained by our proposal in this case, are shown in Table 3.

Table 3. Numerical values of positions and current excitations of antenna elements for Flat-Top case.

n	ϕ_n	$\lvert I(\phi_n)\rvert$	$\mathrm{Arg}(\phi_n)$	n	ϕ_n	$\lvert I(\phi_n)\rvert$	$\mathrm{Arg}(\phi_n)$
1	-3.0666	0.9999	-0.8470	21	0.0750	1	0.8470
2	-2.9118	0.9094	-0.6427	22	0.2298	0.9094	0.6427
3	-2.7586	0.7331	-0.4222	23	0.3829	0.7331	0.4222
4	-2.6055	0.5027	-0.3243	24	0.5360	0.5027	0.3243
5	-2.4498	0.3317	-0.4052	25	0.6917	0.3317	0.4052
6	-2.2976	0.2329	-0.5097	26	0.8440	0.2329	0.5097
7	-2.1463	0.1429	-0.2517	27	0.9953	0.1429	0.2517
8	-1.9766	0.1419	0.5484	28	1.1649	0.1419	-0.5484
9	-1.8271	0.1576	-0.6958	29	1.3144	0.1576	0.6958
10	-1.6837	0.1115	0.5338	30	1.4579	0.1115	-0.5338
11	-1.5094	0.0930	-0.3493	31	1.6322	0.0930	0.3493
12	1.3482	0.1509	-0.6848	32	1.7934	0.1509	0.6848
13	-1.2006	0.1510	-0.6251	33	1.9409	0.1510	0.6251
14	-1.0339	0.1293	0.0646	34	2.1076	0.1293	-0.0646
15	-0.8671	0.2186	0.5065	35	2.2745	0.2186	-0.5065
16	-0.7078	0.3195	0.4204	36	2.4338	0.3195	-0.4204
17	-0.5465	0.4881	0.3241	37	2.5951	0.4881	-0.3241
18	-0.3901	0.7227	0.4142	38	2.7514	0.7227	-0.4142
19	-0.2354	0.9045	0.6336	39	2.9061	0.9045	-0.6336
20	-0.0801	0.9983	0.8428	40	3.0615	0.9983	-0.8428

3.6.3 Square-Cosecant Beam Pattern

In this last test case, we have used a square-cosecant beam pattern with a ripple of ± 0.5 dB from $\phi = 20°$ to $\phi = 95°$, with a side-lobe level of -20 dB, and a region of -30 dB from $\phi = -46°$ to $\phi = -1°$. Figure 25 shows the square-cosecant pattern synthesized with 40 antenna elements for each synthesis approach.

The result obtained by our approach fulfills the requirements of the shaped beam, and the levels in both side lobe regions as well as the orthogonal method approach, except for a slight drawback presented at $\phi = -163°$ and $\phi = 120°$ with a difference of $3°$ in the beamwidth; in general, our proposal presents a good fulfillment of the desired pattern.

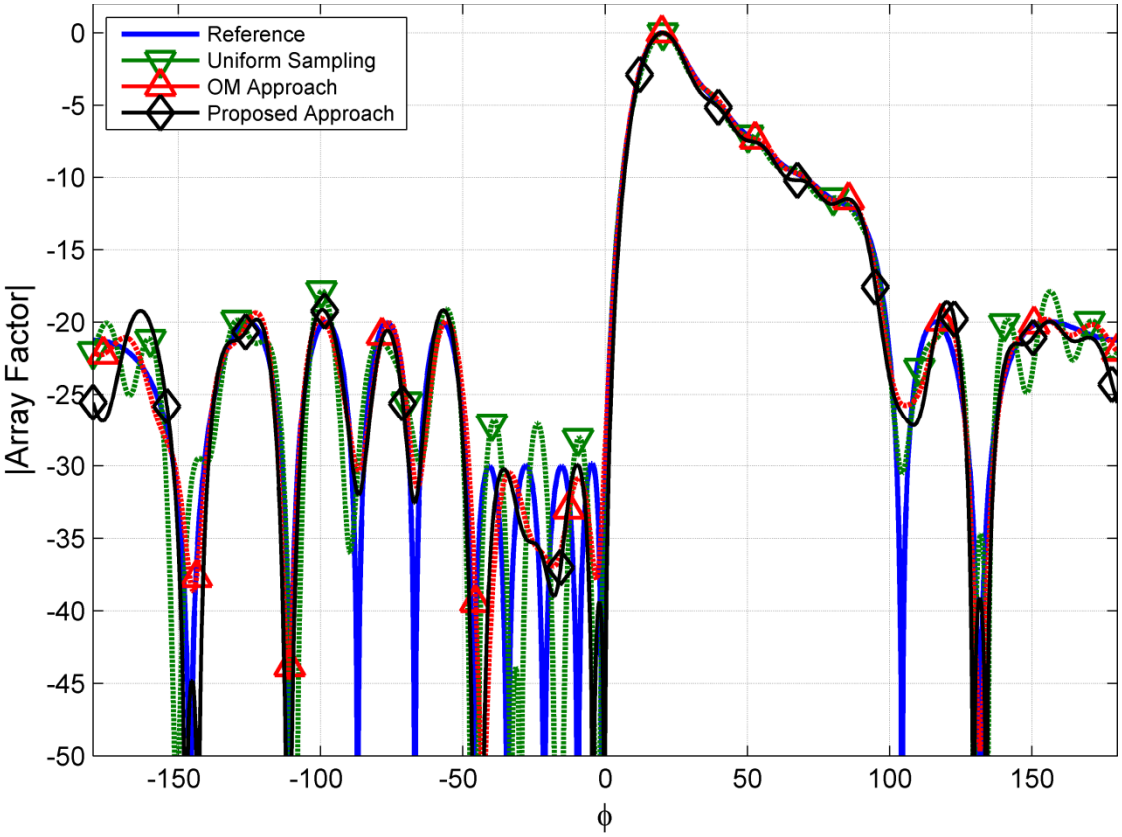

Figure 25. Square-Cosecant beam pattern synthesized with 40 antenna elements for each synthesis technique.

The orthogonal method approach has presented minor drawbacks with the side-lobe level with a difference of $3°$ in the beamwidth, regarding the uniform sampled approach, presents a difference of $2°$, but it has a slight drawback over the $-20\ \mathrm{dB}$ side-lobe level region, and fails over the $-30\ \mathrm{dB}$ side lobe level region. The non-uniformity in the positions of the antenna elements obtained by the tapering procedure in our proposal and also used by the orthogonal method approach has improved the resulting beam pattern compared with the uniform sampled approach, because the resultant beam pattern in our proposal and the orthogonal method fulfills to a greater extent the requirements of the desired array pattern in both regions of side lobe.

Since the square-cosecant pattern represents a more complicated beam to approximate by (38), more harmonics M were needed to obtain a good approximation. Then, the number of harmonics was found to be $M = 22$ after the comprehensive iterative procedure to find a suitable reconstructed current distribution, and the radius used for

each synthesis approach was $r = 3.3804\lambda$. Numerical values of positions, amplitudes and phase excitations achieved by our proposal for this case are presented in Table 4.

Table 4. Numerical values of positions and current excitation of antenna elements for Square-Cosecant case.

n	ϕ_n	$\lvert I(\phi_n)\rvert$	$\mathrm{Arg}(\phi_n)$	n	ϕ_n	$\lvert I(\phi_n)\rvert$	$\mathrm{Arg}(\phi_n)$
1	-3.0665	0.8658	3.1182	21	0.0751	0.8658	-3.1182
2	-2.9100	0.9562	3.0984	22	0.2316	0.9562	-3.0984
3	-2.7536	0.9841	3.0809	23	0.3879	0.9841	-3.0809
4	-2.5965	1	3.0794	24	0.5450	1	-3.0794
5	-2.4408	0.9813	3.1010	25	0.7007	0.9813	-3.1010
6	-2.2834	0.9340	3.1310	26	0.8582	0.9340	-3.1310
7	-2.1267	0.9244	3.1391	27	1.0149	0.9244	-3.1391
8	-1.9708	0.8586	3.1149	28	1.1707	0.8586	-3.1149
9	-1.8131	0.8149	3.0994	29	1.3284	0.8149	-3.0994
10	-1.6571	0.7799	3.1144	30	1.4845	0.7799	-3.1144
11	-1.5001	0.7285	-3.1325	31	1.6415	0.7285	3.1325
12	-1.3435	0.6963	-3.1148	32	1.7981	0.6963	3.1148
13	-1.1865	0.6495	3.1334	33	1.9550	0.6495	-3.1334
14	-1.0280	0.6564	3.1195	34	2.1135	0.6564	-3.1195
15	-0.8728	0.6493	3.1276	35	2.2688	0.6493	-3.1276
16	-0.7143	0.6251	-3.1345	36	2.4273	0.6251	3.1345
17	-0.5558	0.6698	-3.1089	37	2.5857	0.6698	3.1089
18	-0.3992	0.7019	3.1266	38	2.7423	0.7019	-3.1266
19	-0.2410	0.7353	3.1033	39	2.9005	0.7353	-3.1033
20	-0.0835	0.7876	3.1340	40	3.0581	0.7876	-3.1340

Additionally, Table 5 shows a comparison of each synthesis method in terms of SLL and beamwidth obtained for each test case, it can be observed that the proposed method have lower SLL in most of test cases, and also, the beamwidth error is lower for the proposed method in shaped beams cases.

Table 5. Numerical values of SLL and BW of the comparison of each synthesis method for each test case

	Test cases					
	Narrow-beam		Flat-top beam		Square-Cosecant beam	
	SLL [dB]	**BW** [°]	**SLL**	**BW**	**SLL**	**BW**
Reference	-20	95	-20	95	-20	106
Proposed Approach	-21.62	95	-20.91	104	-18.64	108
Uniform sampled approach	-19.6	115	-20.75	106	-17.84	107
Orthogonal method approach	-20.88	119	-18.91	103	-19.93	108

3.7 Conclusions

In this chapter, the synthesis of sparse circular antenna arrays using a tapering technique over a reconstructed continuous current distribution based on an expansion in orthogonal basis functions has been presented. It was shown in our proposal that the reconstruction of the current distribution for a desired pattern and the iterative procedure used achieves to find an optimum radius is able to synthesize an approximation of a desired array pattern with sparseness characteristics over the number of antennas, by obtaining antenna positions and excitation currents.

Also it has been proven with three different array patterns that the non-uniformity achieved by the tapering procedure in our proposed approach yields a better fulfillment of the requirements with respect to a uniform sampled technique, for a desired pattern for circular antenna arrays, in terms of side lobe level and beamwidth with a maximum error of 3 dB in a test case and $8°$ of beamwidth between the first nulls. The best behavior has presented in the case of the narrow-beam pattern, where our proposal does not exceed side lobe levels nor beamwidth.

This proposed synthesis method is an alternative for sparse antenna array in a geometry that has not been widely explored, by this way; we contributed to an option for green networks relatives to new requirements of LTE-Advanced systems in 4G.

Chapter 4. Ultra-Wideband Antenna Arrays for New Generation of Communications Systems

4.1 Introduction

This chapter represents the background of the second part of this research work dedicated to the antenna arrays for the Ultra-wideband (UWB) technology. UWB arises as a potential access technology to participate in the re-use of the saturated frequency spectrum, providing high data rate access in short-range broadband communications for either LTE-A and future 5G wireless communications systems (Adamiuk et al., 2012; Chen, Z. N., 2007; Chong, C. C., Watanabe, F. and Inamura, H. 2006; Di Benedetto et al., 2006). In this chapter, the role and advantages of UWB technology in the LTE environment is presented, in line with the vision of the convergence of these wireless technologies into heterogeneous networks, along with opportunity areas (in this technology) considered for LTE Evolution, and how UWB systems can complement them. Then in order to expand the concept to UWB, it is also presented an overview of the basic characteristics of UWB in order to be integrated to complement 4G wireless systems.

Furthermore, a general overview of the current challenges for this technology is also presented followed by the open research topics to solve these challenges, ending with issues associated for the antenna array for UWB technology and the ways to describe the antenna array in a suitable way for an extreme bandwidth of UWB spectrum and its requirements that laid the groundwork for the design of UWB antenna arrays for this research work.

4.2 UWB Technology in the LTE Environment

Nowadays, short-range wireless applications and ad-hoc networking have become increasingly important to the 4G mobile broadband systems, in line with the integration of heterogeneous networks in the evolution of LTE and LTE-Advanced. So that the 3GPP has gradually moving its focus toward the step in the evolution of LTE systems, concluding with the workshop “Release 12 and Beyond”, in June 2012 (Astely et al., 2013). In that workshop, it was covenanted that in addition of increasing capacity, enhancing end-user experience, improving energy efficiency, and the support for diverse data applications,

reducing cost, and backhaul enhancements for LTE systems, it is necessary to embrace new machine type and short-range communication scenarios that lead to new traffic type (Adamiuk et al., 2012; Chen, Z. N., 2007; Chong et al., 2006; Di Benedetto et al., 2006). New major technology areas were identified:

- Enhanced local areas access.
- Multi-antennas enhancements.
- Improved support for machine-type communication (MTC)
- Direct device-to-device communication.

Due to the convergence of wireless connectivity, the 4G wireless systems will most likely be an integration of heterogeneous networks including wireless regional area networks, wireless wide area networks, wireless macro area networks, wireless local area networks (WLAN), and wireless personal area networks (WPAN) (Chong et al., 2006), UWB technology is foreseen as one of the most promising technologies for such scenarios. These wireless technologies may be combined on a common platform as shown in Figure 26. The UWB technology can complement other wireless technologies and has the potential to perform seamless connectivity with other communication infrastructure, such as providing users with their desired information on any device anywhere and at any time. These advantages of UWB technology are important even to cellular operators, with the potential, as technology, to play a key role in the 4G network solution, by providing enhancement and add-on functionality to LTE and LTE-A mobile terminals (MTs), such as high data rate applications (i.e., audio/video multimedia data exchange, file sharing, etc.) and low-data rate applications with localization capabilities (i.e., sensor networks, radar services, information services, tracking, etc.).

Moreover, with the frequency expansion expected for 5G wireless communications systems, the above features will be enhanced and their study are necessary in order to improve the approaches solutions for new frequencies bands.

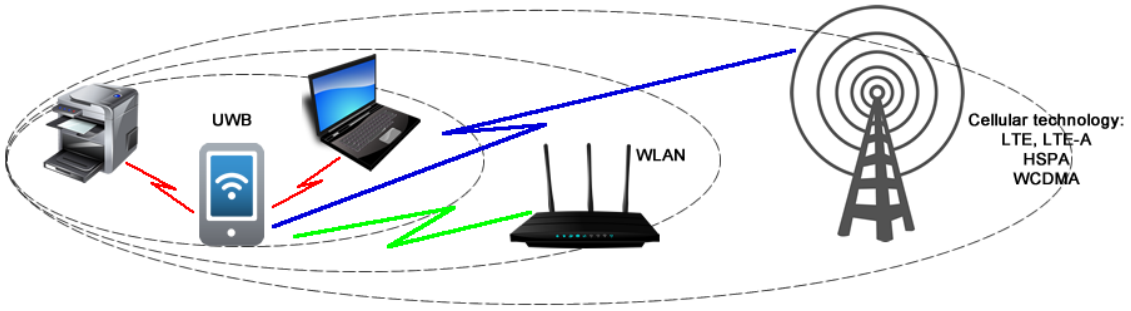

Figure 26. Example of a common platform of various wireless technologies.

One of the biggest advantage of UWB technology is the reduction of the fading, which is a typical narrowband characteristic. In UWB radio cannel, the wide bandwidth reduces the influence of fading and results in a flat propagation loss, even for multipath propagation. This implies a possibility of successful application of UWB system in complex environments.

4.3 UWB Regulation

The US Federal Communications Commission (FCC) issued the First Report and Order (R&O) in February 2002 (FCC, 2002), which gave the authorization to unlicensed UWB operation and commercial deployment of UWB devices. There are three classes of devices defined in the R&O document:

1. Imaging systems: ground penetrating radar systems, wall imaging systems, through-wall imaging systems, surveillance systems, and medical systems.
2. Vehicular radar systems.
3. Communications and measurement systems.

The FCC allocated a block of unlicensed radio spectrum from $3.1 - 10.6$ GHz for the above applications, where each category were allocated a spectral mask as shown in Figure 27.

The FCC only specified a spectral mask, and the bandwidth limitations of a UWB device, but not the type of signal and modulation scheme. The FCC agreed that a UWB signal is defined as an absolute bandwidth of at least 500 MHz to 7.5 GHz (FCC, 2002). In other

words, the spectral mask shown in Figure 27 was designed to protect other spectrum users from undesirable levels of interference caused by UWB transmissions. The FCC limited the power level at -41.3 dBm/MHz, which allows UWB technology to overlay with available services such GPS, IEEE 802.11 WLAN, and services in the frequency bands released for 4G at 3.5 GHz and above.

It is important to mention, that there exist different regulations for the UWB spectrum in Europe, Japan and Korea; but in this research, the design of UWB antenna arrays (Chapter 5) was based on the UWB spectrum issued by R&O in indoor environments.

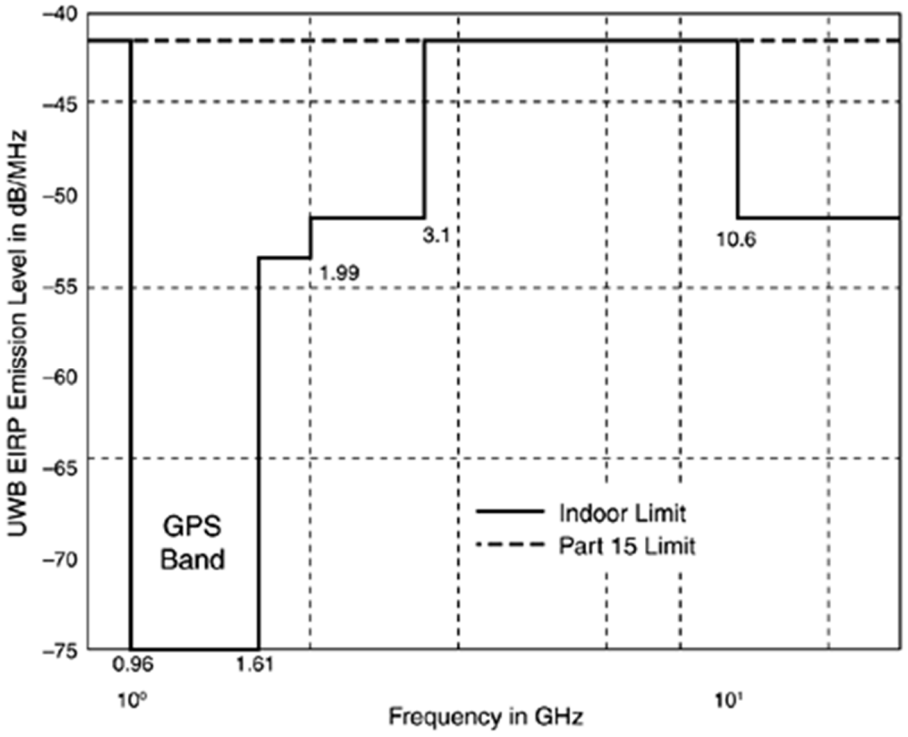

Figure 27. UWB Spectral Mask for indoor environments (FCC, 2002).

4.4 Currents challenges for UWB

UWB technology has many advantages, as above mentioned, that makes it one of the most promising for 4G wireless communication and other applications. But despite these advantages for UWB technology, there are still challenges to resolve in order to achieve a practical performance for wireless communication systems in the market.

In terms of data rate, the reliability and range of UWB are issues standard for most of wireless communications systems. Standards support different data rates ranging from 53.3 to 480 Mbps, but initial expectations for UWB were in the area of Gbps. Therefore, ways to increase these data rates are being explored (Sipal et al., 2012).

The range of UWB systems is strictly limited by the regulated EIRP of -41.3 dBm/MHz, which represents a very strict framework but it allows range estimation for a chosen modulation scheme using a link budget analysis. However, in the same way that data rate, consumers are always ravenous to expand the range (Sipal et al., 2012).

Another current challenge is the chip complexity, this have been one of the main reasons for the delay in introducing UWB devices to the market. Even though the chip cost decreases as the technology matures simply with the production volume, it must be noted that complexity reduction is still a topic that needs to be considered especially as it increases in relation to improvements in reliability, in other words, a more complex coding; to improve the range, signal processing in MIMO systems is considered; for higher data rates it is required faster clocks.

Another issue is the attached challenge of frequency re-use. This includes robustness against the presence of a narrowband interferer, especially for the cases of strong interference from narrow band systems that might overload the communication of the UWB systems.

4.5 Open research topics to solve UWB challenges

In this section, a brief overview of the current research topics are presented, emphasizing at the end of the section with multiple antenna systems as in line with the vision of this research work.

4.5.1 Chip Complexity of OFDM systems

The chip complexity and cost of OFDM systems is caused mainly by the complexity of the fast Fourier transform (FFT) employed by OFDM. The FFT implementation with least

computational demand reported by (Johnson, S. G., and Frigo, M., 2007) does not fulfills the full load of the chip as it also needs to perform other operations besides the FLOP counts for FFT (Sipal et al., 2012). Ideally, all the arithmetic operations should be performed by a chip suitable for handheld devices. For comparison, this FFT computational complexity is approximately 25 times higher than required by chips for 802.11 a/g/n WiFi. This complexity translates into chip cost (Sipal et al., 2012).

To increase in data rate by scaling the OFDM represents an additional challenge in terms of chip complexity and should enter consideration about for future systems such as the next generation of WiMedia systems (WiMedia Alliance) with OFDM symbol bandwidth of 1056 MHz providing data rates in magnitude of 1 Gbps (Heidari, G., 2008).

Then, one of the main research topics in the current UWB landscape is chip optimization and low complexity chip design for WiMedia OFDM that would enable commercially viable operation (Sipal et al., 2012).

4.5.2 Coding and Modulation

The coding and modulation is an alternative to improve UWB system capacity. Choosing an appropriate coding and modulation schemes, a number of aspects have to be considered, such as the trade-off between implementation complexity and system performance (Chong et al., 2006). In terms of reliability, OFDM without channel coding and frequency diversity schemes does not provide the most reliable implementation of UWB system as it capitulates on the exploitation of frequency diversity of UWB systems. To be more specific, individual narrowband subcarriers in the OFDM symbols suffer from frequency-selective fading in the wireless channel (Sipal et al., 2012). However, other modulation implementations have been presented, were using wideband carriers such a single-carrier (SC) UWB with frequency-domain equalization (FDE) or multi-tone frequency shift keying (MTFSK) (Sipal, V., Gelabert, J., Allen, B., Stevens, C. and Edwards, D., 2011).

4.5.3 Interference from Narrowband Systems

A problem present in the rise of the frequency re-use by UWB systems is the interference between primary narrowband (such LTE and LTE-Advance) users and the UWB users. The interference to narrowband users by UWB systems should be negligible because of the low EIRP spectral densities allowed by regulatory authorities. The situation of a narrowband interferer to UWB systems is different.

The strong narrowband interference near of a UWB receiver represents a more serious challenge and means to reduce this problem enable to obtain lower BER or higher data rates. The biggest challenge is the dynamic range of the receiver that is chosen appropriately to the expected power levels of UWB signals. A strong narrowband interferer in proximity may well be outside of this dynamic range and overload the front end of the receiver. Since UWB systems must be capable of operation even under such circumstances, various solutions are considered. The use of Detection and Avoid algorithms (DAA) in UWB systems is of high interest as DAAs are key to switchable band notch systems at the receiver as well as at the transceiver (Sipal et al., 2012). An alternative is the use of band notch antennas that of suppress the typical narrowband interferers while efficiently covering the remainder of the UWB band (Li, W. T., Shi, X. W. and Hei, Y. Q., 2009; Weng, Y. F., Cheung, S. W. and Yuk, T. I., 2010). This approach blindly suppresses the interferer without being aware of its presence. Band notch antennas can also be used in transmitters to reduce interference to narrowband users.

An alternative to blind suppression is the use of switchable band notch filters or antennas that switch the interferer band of only when a presence of a strong interferer is detected (Athukorala et al., 2010). This can be used to suppress the interferer by using a null-steering at a multiple antenna receiver. The challenges and issues of multiple antenna systems for UWB are discussed in the next subsection.

4.5.4 Multiple Antennas Systems for UWB

In wireless communication, multiple antenna systems or antenna arrays are an attractive research topic, as the concept allows more efficient use of the channel resources, interferer suppression or increased security (Chen, C., and Jensen, M. A., 2011; Jensen,

M. A., & Wallace, J. W., 2004). The use of multiple antenna techniques in UWB offers the same benefits as in standard narrowband wireless and it helps to tackle some of the big challenges fulfill actual practical achievements of UWB. For example, it enables higher data rates, and/or better suppression of interferences (Kaiser, T., Zheng, F., and Dimitrov, E., 2009; Vithanage, C. M., Sandell, M., Coon, J. P., Wang, Y., and Toshiba Research Europe Ltd., 2009).

In UWB communications, the antenna arrays might find their application either in directional communication, beamforming, or MIMO technique. In all these applications, the arrays are used to establish a point-to-point connection with suppression of undesired interferences and destructive multipath components, which may cause intersymbol interference. In a simple case, beamforming can be applied to follow the beam during transmission if one of the nodes is mobile.

4.6 UWB Antenna Arrays

The large UWB spectrum significantly complicates the design of antenna arrays for this technology. The UWB interval bandwidth is very large compared to conventional narrowband, ranging from 500 MHz up to 7.5 GHz. This extreme bandwidth available for UWB technology can be seen as a blessing and a curse at the same time. It offers many advantages such inherent frequency diversity, which increases robustness against narrowband interference and frequency selective fading; also, it offers a huge available data rate, and availability of precise ranging (Allen, B., Dohler, M., Okon, E., Malik, W., Brown, A., and Edwards, D., 2006).

However, antenna arrays are associated with many challenges as well, for example, the design of antennas with frequency-independent input impedance and radiation pattern, and requirement of fast ADCs to process the large bandwidth (Allen et al., 2006; Heidari, G., 2008). It is also an issue for a design of antenna arrays. In other words, as S. Rise declares in his work; “UWB antenna array it’s a different world” (Ries, S., and Kaiser, T., 2006).

According to the literature, there are two basic ways to describe UWB antenna arrays (Adamiuk et al., 2012; Allen et al., 2006; Heidari, G., 2008): the standard description as in narrowband systems does, is by the expression of an array factor and antenna patterns or using the beam patterns that are summarized in (Kaiser et al., 2009).

4.6.1 Array Factor as Descriptor for UWB Antenna Arrays

It is well known from basic antenna theory that the array factor, AF, for a circular array along the plane $\mathrm{X}-\mathrm{Y}$ can be calculated by using the following expression (Balanis, C. A., 2005):

$$AF(\theta,\phi) = \sum_{n=1}^{N} I_n e^{j\frac{2\pi}{\lambda} r \sin\theta \cos(\phi-\phi_n)} \tag{46}$$

Where N represents the number of antenna elements in the array, the variable θ represents the elevation angle, and ϕ represents the azimuth angle, λ is the free space wavelength (considering a plane wave), r is the radius of the circular array, I_n is the amplitude excitation and ϕ_n is the angular position of the antenna element.

As seen in the expression (46), AF strongly depends on the relation r/λ which varies significantly between the lower and upper boundaries of the FCC UWB band (3.1 GHz to 10.6 GHz). As a result of this extreme bandwidth, the array factor AF, can change significantly over the frequency band.

As an example of the above, by using the data of Table 6 for a $N = 8$ and $r = 0.7151\,\lambda$, the separations between the antenna elements, or Euclidean distance, showed in third column, are expressed in λ, if we consider the UWB frequency spectrum, its central frequency is 6.85 GHz. At this frequency, then the separation between elements expressed in mm are represented in fourth column, and the radius have a value of $r = 0.0313$ mm

In Figure 28, it is illustrated the array factor considering a frequency of $f = 6.85$ GHz. If the frequency is varied to the UWB spectrum boundaries 3.1 and 10.6 GHz, the resultant array factor changes drastically between its frequency boundary, by preserving the separation in mm. The array factor at $f = 3.1$ GHz increase its beamwidth considerably and also the side lobe level. By the other hand, the array factor at $f = 10.6$ GHz presents grating lobes, an undesirable condition, which is present with by considering a plane wave.

In this case, the issues associated with the large bandwidth are the element spacing between the antenna elements and the different wavelength involved in the UWB spectrum. Moreover, the need of an individual beamforming for each frequency in the UWB spectrum is also a problem.

Table 6. Numerical values of an arbitrary circular antenna array

n	I_n	$d_n\ [\lambda]$	$d_n\ [mm],\ f = 6.85$ GHz
1	0.7765	0.3590	0.0157
2	0.3928	0.5756	0.0252
3	0.6069	0.2494	0.0109
4	0.8446	0.7638	0.0335
5	1.0000	0.6025	0.0264
6	0.7015	0.8311	0.0364
7	0.9321	0.7809	0.0342
8	0.3583	0.3308	0.0145

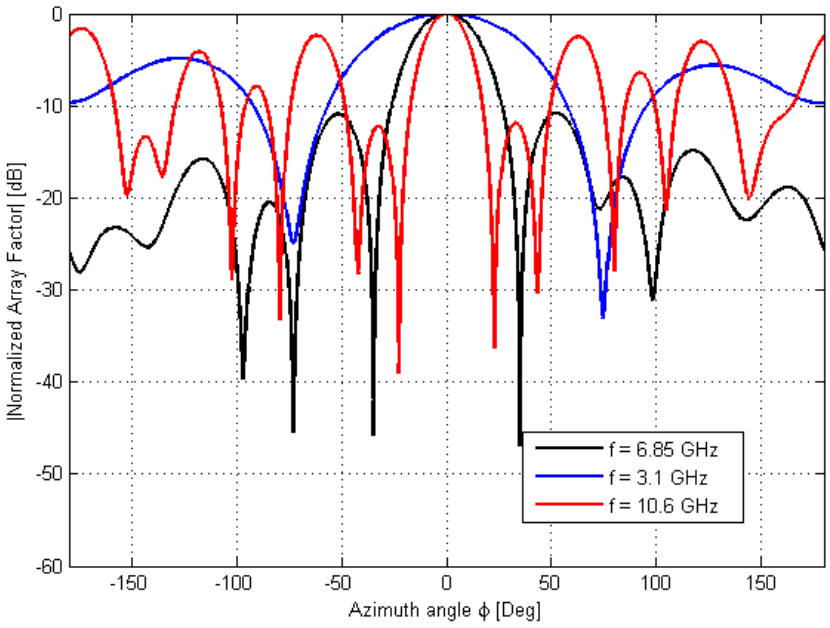

Figure 28. Array Factor for different frequencies in UWB spectrum considering a plane wave.

4.6.2 Beam Pattern as Descriptor for UWB Antenna Arrays

For narrowband systems, the beamforming is performed by varying the phase between the adjacent element and/or the amplitude coefficients. However, in the practice, the realization of a phase corresponds to a time delay. For UWB impulses, the phase shift becomes ambiguous while the time delay is precise and specific.

Therefore, new descriptor for UWB antenna arrays in time domain perspective has been developed (McLean, J. S., Foltz, H., and Sutton, R., 2005) by considering the phase shift as a time delay. For example, the expression for an energy pattern of an antenna array based in these descriptors is defined as follows:

$$P_{energy}(\theta,\phi) = \int_{0}^{t} |s(t,\theta,\phi)|^2 dt \tag{47}$$

Where $s(t,\theta,\phi)$ is the far-field wave form for the antenna array, t is the time of the signal wave, and $P_{energy}(\theta,\phi)$ represents the total response of the power patterns in the frequency domain. By this way, it is possible to evaluate the array factor without the problem of individual beamforming for each frequency in the UWB spectrum.

Nevertheless, it is necessary to consider signal wave different from the plane wave, for the same variations present in the pattern responses, as shown in Figure 28. Moreover, it is necessary to satisfy the FCC UWB mask. Then, the next subsection is dedicated to present the pulse shape as a signal wave to be considered by UWB antenna arrays.

4.7 Pulse shape for UWB antenna arrays

In the time domain, the higher order derivatives of the Gaussian pulse resemble sinusoids modulated by a Gaussian pulse-shaped envelope (Sheng, H., Orlik, P., Haimovich, A. M., Cimini Jr., L. J., and Zhang, J., 2003). This lead to considering high-order derivatives of the Gaussian pulse as candidates for UWB transmission. Specifically, by choosing the order of the derivative and a suitable pulse width to satisfy the FCC UWB mask.

In the work presented in (Sheng et al., 2003), the authors evaluates different high-order derivatives of the Gaussian pulse for UWB indoor systems as shown in Figure 29. The objective of this (Sheng et al., 2003) is to obtain a pulse that matches the FCC's PSD mask as closely as possible, but which also maximizes the bandwidth for a better use under the mask.

In this case, it is clear in Figure 29 that the fifth-order Gaussian pulse should be used to satisfy the FCC's PSD mask for UWB spectrum, because this pulse does not violate the strict limits and also maintain the bandwidth as wide as possible.

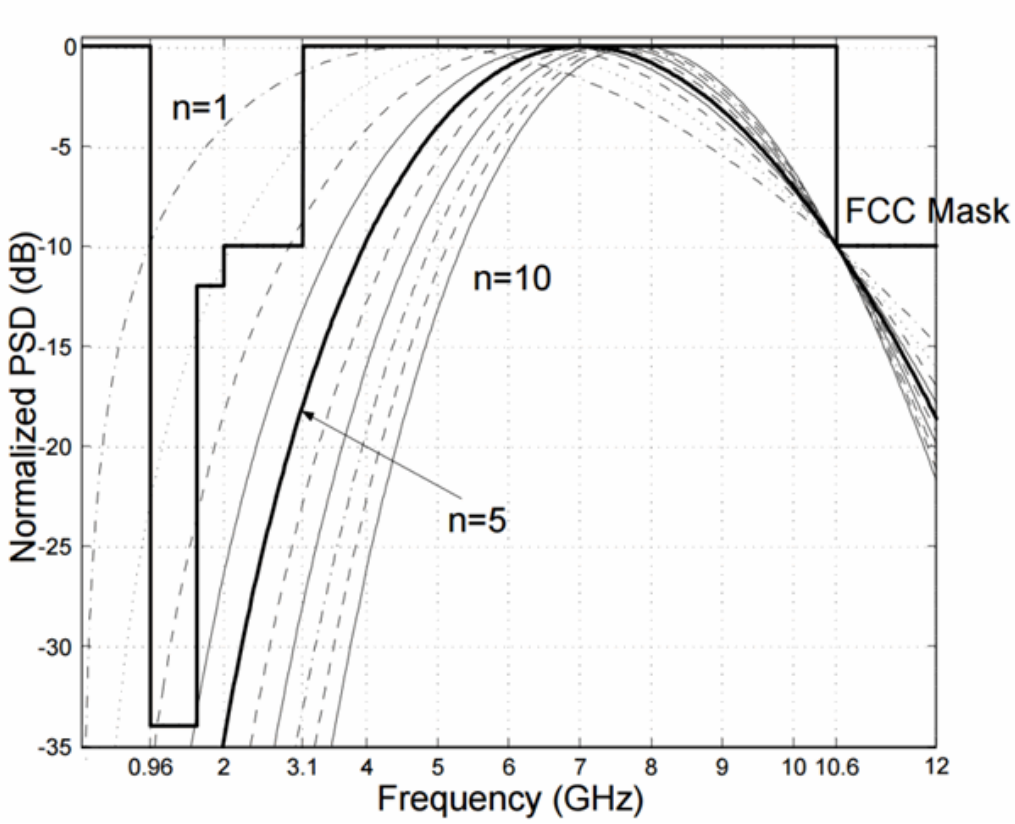

Figure 29. Power spectral density of different derivatives of the Gaussian pulse (Sheng et.al., 2003)

This represents the main justification why the fifth-order Gaussian pulse will be used in order to design UWB antenna arrays in next Chapter.

4.8 Conclusions

A general overview of the UWB technology and its participation and coexistence with LTE Evolution systems have been presented, as a background for the second phase of this

thesis focused on the design of UWB antenna arrays and the challenges associated with this topic. Besides of the basic characteristics of UWB to fulfill the requirements of the FCC, some current challenges of this technology such as the chip complexity, coding and modulation, the interference from narrowbeam systems and multiple antenna systems. Open research topics are also presented, in order to improve the UWB systems to upgrade the coexistence with 4G wireless communication.

The case of the antenna array for UWB technology is also addressed, the considerations needed to evaluate and to design the antenna array will be presented in the next chapter.

This applied to the design of UWB antenna array, in order to avoid the issues associated with the large frequency spectrum of UWB, which complicates the design and modeling of these arrays, such as the pulse signal and the difference between the frequency domain modeling by using the array factor as descriptor of the antenna array and the time domain modeling by using the descriptor patterns to avoid individual beamforming for each frequency, and also the grating lobes.

Chapter 5. Synthesis Methodology of Ultra-Wideband Circular Antenna Arrays

5.1 Introduction

The design of antenna arrays has gained an increased attention in UWB applications such directional communications and radar systems. Therefore, this chapter presents a design methodology in order to avoid the individual beamforming problem, presented in the previous chapter. The proposed methodology to synthetize UWB antenna arrays is based on the evaluation of the array factor equivalent as beam pattern descriptor for the UWB antenna array. In basic antenna theory, the evaluation of the performance of the array is carried out by considering its power pattern in the frequency domain, but due the power pattern varies with each frequency throughout the entire UWB frequency spectrum, the synthesis of UWB antenna arrays becomes a complicate problem. Hence, in the presented methodology, the synthesis is accomplished in the time-domain (TD) perspective as an alternative way to design the UWB antenna array by just evaluating the energy pattern as the total response of the power patterns in the frequency domain (Liao et al., 2011). Furthermore, this synthesis methodology for the design of UWB antenna arrays uses the DEMO algorithm (Robic, T. and Filipi, B., 2005) to compute the optimum amplitude coefficients and time delay excitations. This proposal is proven valid to two different beams patterns (steerable narrow-beam, and flat-top beam) for a UWB circular antenna array.

5.2 Time-domain antenna array model

First, let us consider a TD circular antenna array of N antenna elements grouped in a circular geometry located in the plane $\mathrm{X}-\mathrm{Y}$ as shown in Figure 30. Each antenna receives a short pulse $f(t)$ with different time delays and amplitude coefficients. The short pulses are added in the space by resulting in far–field waveform. Then, the far–field waveform will depend basically on four parameters referred as the waveform of feeding short pulse, the antenna element positions ϕ_n, the time delays among the short pulses and the amplitude coefficients (Barrett, T. W., and Vienna, V. A., 2001).

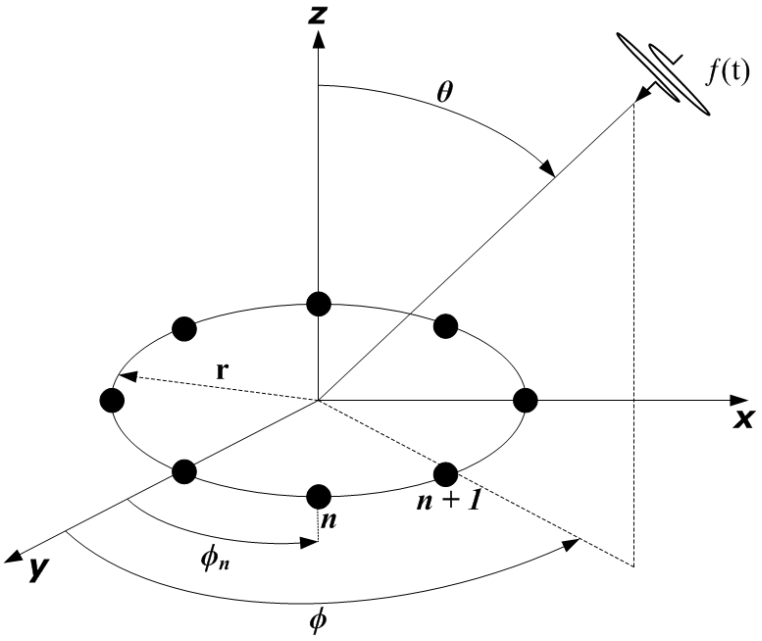

Figure 30. Time domain circular antenna array model

Then, the far–field waveform for the TD circular antenna array shown in Figure 30 is defined as follows (Foo, S. and Kashyap, S., 2003):

$$s(t,\theta,\phi) = \sum_{n=1}^{N} a_n f_n\big(t - \Delta t_n + \tau_p - \tau_n, \theta, \phi\big), \tag{48}$$

where N is the total number of antenna elements; a_n is the amplitude coefficient of the antenna element n, and $f_n\big(t - \Delta t + \tau_p - \tau_n, \theta, \phi\big)$ is the short pulse received at the antenna element n, where θ represents the elevation angle, and ϕ represents the azimuth angle. The variable t is the time of the pulse, Δt_n is the delay of the antenna element n, τ_p is the progressive delay and τ_n is the delay excitation of the element n. These delay variables are defined as follow:

$$\Delta t = \frac{r}{c}\sin\theta\cos(\phi_n - \phi) \tag{49}$$

$$\tau_p = \frac{r}{c}\sin\theta_0\cos(\phi_n - \phi_0) \tag{50}$$

The variable r represents the radius of the circular array, and c is the propagation speed ($3 \times 10^8\ m/s$). The angles (θ_0, ϕ_0) provide the desired maximum direction. The term ϕ_n is the angular position of element n. These spatial variables are defined as follows:

$$r = \sum_{n=1}^{N} \frac{d_n}{2\pi} \tag{51}$$

$$\phi_n = \sum_{n=1}^{N} \frac{2\pi n}{N} \tag{52}$$

Now in order to evaluate the far-field waveform by the expression in (48), it is necessary to define the short pulse that will be used. The 5th derivative Gaussian pulse is known for having the most effective pulse shape with the power spectrum under the FCC limitation floor, and this pulse can be transmitted without additional filtering (Sheng et al., 2003) as it was shown in previous chapter.

For this reason, the 5th derivative Gaussian pulse as the wave form of the receiving short pulses to each antenna element, and this pulse is defined as follows (Kim, Y. and Joo, Y., 2005; Sheng et al., 2003):

$$f_n(t) = A\left(-\frac{t^5}{\sqrt{2\pi}\sigma^{11}} + \frac{10t^3}{\sqrt{2\pi}\sigma^9} - \frac{15t}{\sqrt{2\pi}\sigma^7}\right)\exp\left(-\frac{t^2}{2\sigma^2}\right) \tag{53}$$

In the above expression, the variable A is the amplitude of the pulse, σ is a time constant and t is the duration of the pulse. In order to satisfy the FCC regulations, these parameters are chosen to be $A = 1$, $\sigma = 51ps$ and $t = 250ps$ (Chen, Z. N., Wu, X. H., Li, H. F., Yang, N. and Chia, M. Y. W., 2004; Kim, Y. and Joo, Y., 2005; Sheng et al., 2003). Now, the radiation properties of the TD circular array can be modeled to obtain radiation patterns to describe the antenna array behavior.

In the frequency-domain perspective, the power patterns can be obtained by a Fourier transform of the far-field waveform $s(t, \theta, \phi)$ as follows (McLean et al., 2005):

$$P(f,\theta,\phi) = \left| \int_{-\infty}^{\infty} s(t,\theta,\phi) e^{-j2\pi f t} dt \right| \quad (54)$$

The variable f is the frequency, for the UWB antenna array, the value of f belongs to the interval of 3.1 GHz to 10.6 GHz defined by the FCC regulations for UWB systems (Chen et al., 2004; Kim, Y. and Joo, Y., 2005; Sheng et al., 2003). The total of power patterns is also known as the spectrum in frequency.

On the other hand, in the time-domain the energy pattern is defined as follows (McLean et al., 2005):

$$P_{energy}(\theta,\phi) = \int_{0}^{t} |s(t,\theta,\phi)|^2 dt \quad (55)$$

As it can be seen in (54), in order to apply an optimization process to obtain amplitude and time delay excitations, it would be necessary to evaluate a power pattern for each frequency in the UWB frequency interval; this would complicate the analysis process by increasing the dimensions of the optimization process. On the other hand, by taking into account the energy pattern in (55) in the time-domain, which is defined as the total response of the power patterns in the frequency domain, just one pattern would be evaluated in an optimization process.

5.3 Differential Evolution for Multiobjective Optimization algorithm

In this design of UWB antenna arrays, the optimization process is carried out by the DEMO algorithm for the effectiveness in antenna arrays design (Panduro, M. A., Brizuela, C. A., Garza, J., Hinojosa, S. and Reyna, A., 2013). DEMO is an optimization approach based on the classical method of Differential Evolution (DE) (Storn, R. and Price, K., 1997) combined with the mechanisms of Pareto-based ranking and crowding distance sorting, employed in the literature of evolutionary algorithms for multiobjective optimization.

There are three variants to implement DEMO: DEMO/parent, DEMO/closest/dec and DEMO/closest/obj. In a performance comparison of these three DEMO variants applied to design concentric ring antenna arrays presented by (Panduro et al., 2013), it was shown that the DEMO/parent version finds a better set of nondominated solutions as an approximation to the Pareto set. Based in these presented comparisons, DEMO/parent was chosen in this simulation process, to be implemented into the design of UWB circular antenna arrays.

The procedure used for DEMO/parent is described as follows (Robic, T. and Filipi, B., 2005; Storn, R. and Price, K.,1997):

1. Evaluate the initial population $\mathcal{P}$ of random individuals.
2. While stopping criterion not met, do:
    a) For each individual P_i $(i = 1, \cdots, popSize)$ from $\mathcal{P}$ repeat:
        i. Create candidate C from P_i.
        ii. Evaluate candidate.
        iii. If the candidate dominates the parent, the candidate replaces the parent.

        If the parent dominates the candidate, the candidate is discarded. Otherwise, the candidate is added into the population.
    b) If the population has more than $popSize$ individuals, truncate it by sorting the individuals with nondominated sorting and then evaluating the individuals of the same front with the crowding distance metric.
    c) Randomly enumerate the individuals in $\mathcal{P}$.

For the candidate creation, the DE scheme DE/rand/1/bin (Robic, T. and Filipi, B., 2005; Storn & Price, 1997) is used, and the procedure for this scheme is described as follows:

1. Randomly select three individuals P_{i_1}, P_{i_2}, P_{i_3} from $\mathcal{P}$, where i, i_1, i_2 and i_3 are pairwise different.
2. Calculate candidate C as $C = P_{i_1} + F \times (P_{i_2} - P_{i_3})$, where F is a scaling factor.

3. Modify the candidate by binary crossover with the parent using crossover probability p_c.

The immediate replacement of the parent individual with the candidate that dominates it, emphasizes elitism within reproduction, which helps achieving the convergence to the true Pareto front. Furthermore, the use of nondominated sorting and crowding distance metric in truncation of the extended population, stimulates the uniform spread of solutions, finding as diverse nondominated solutions as possible (Robic, T. and Filipi, B., 2005).

Therefore, the procedure of the DEMO/parent algorithm for our design problem is described in Figure 31. The individuals are encoded in a vector of real numbers that represents the amplitudes excitations on the range $(0, a_{max})$, and a vector of real numbers restrained on the range $(0, \tau_{max})$ that represents the time delay excitations. The stopping criterion to meet is that the total number of iterations reaches $total\_ITE$.

5.4 Test Cases and Simulation Results

In this section, two test cases proposed for the design process of UWB circular array antennas are presented: a steering narrow-beam pattern and a flat-top beam pattern.

5.4.1 Steerable Narrow-Beam Pattern

In this test case, the proposed synthesis procedure is to obtain an steerable narrow beam pattern by optimizing the amplitude excitations and the disturbing exciting time delay of a circular antenna array for a maximum performance in terms of the side lobe level and a desired main beamwidth in a scanning range of [-180°,180°]. The design of a steerable UWB circular antenna array could be achieved by considering the rotation properties of monochromatic circular arrays, i.e., the rotation properties of circular arrays (for just one frequency) could be extended to design steerable UWB circular arrays considering energy patterns.

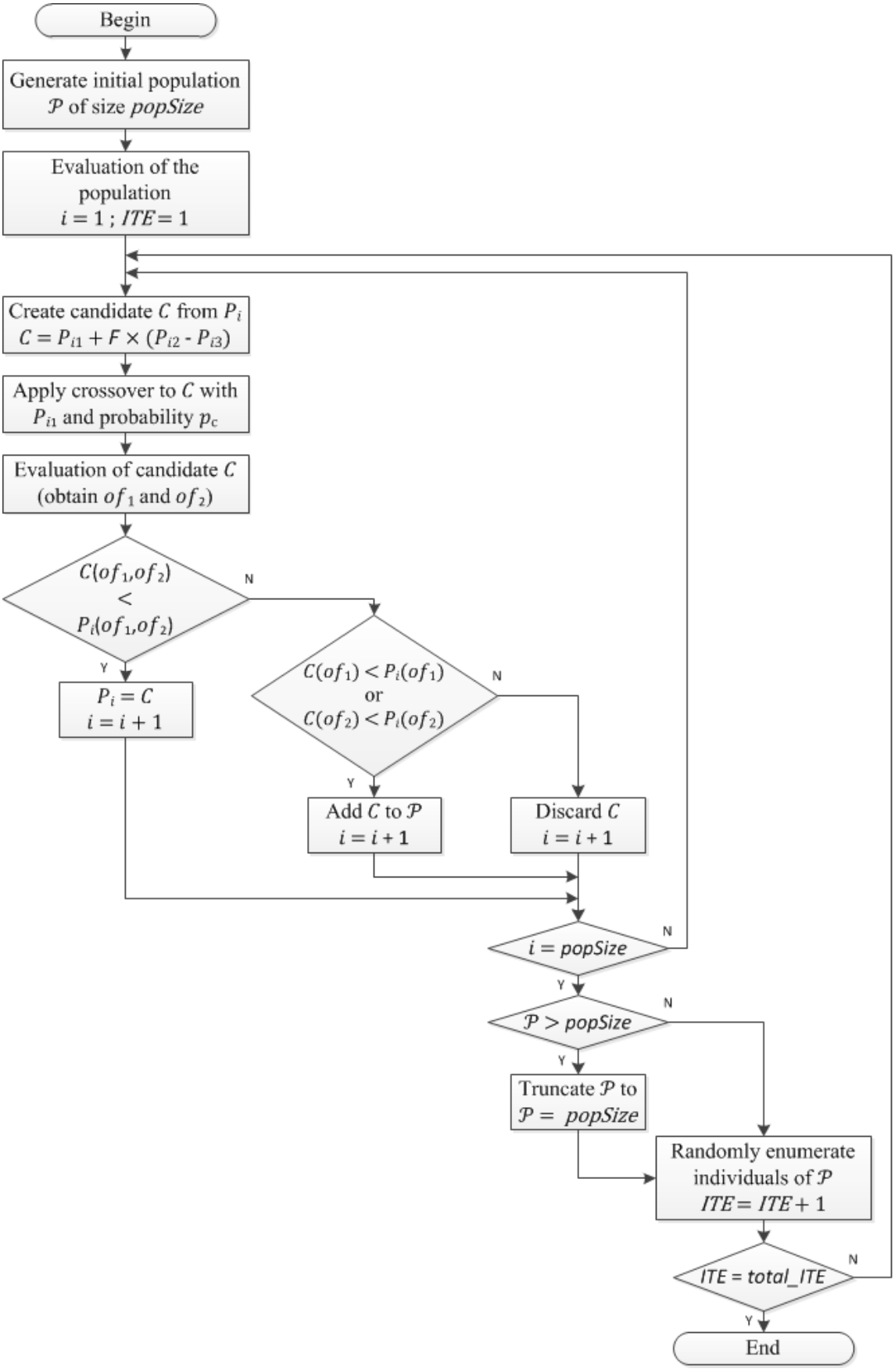

Figure 31. Flow chart for the implemented DEMO/parent algorithm.

This design rule is very simple. Let us consider a circular array of N elements to illustrate this point. In this case, it is considered the behavior of the array factor for the scanning range of $-180° \leq \phi_n \leq 180°$ (with ϕ_0 as the beam direction in azimuth plane). If the number of antennas is $N = 8$ and there is an uniform angular separation of $45°$ between different beam steering angles, the optimal excitation solution (amplitudes and time delays) for a particular beam steering angle should also apply to other beam steering angles by substituting (a_n, τ_n) into (a_{n+1}, τ_{n+1}) when the beam steering is increased $(\phi_0 + 45°)$ (Panduro, M. A., Brizuela, C. A., Balderas, L. I. and Acosta, D. A., 2009; Reyna, A., Panduro, M. A., Covarrubias, D. H. and Mendez, A., 2012).

By applying this rotation rule, only one optimization is required for beam steering in steps of $45°$ (in the whole azimuth plane) instead of one optimization for each beam steering direction. Then, the objective functions for this design case, of_1 and of_2, set to be minimized by the DEMO/parent algorithm are defined as follows:

$$of_1(n) = P_{energy}(\theta_{SLL}, \phi_{SLL}) \tag{56}$$

$$of_2(n) = BW(P_{energy}) \tag{57}$$

The proposed of_1 regards the maximum peak side lobe level represented by term $P_{energy}(\theta_{SLL}, \phi_{SLL})$, and proposed of_2 regards the beamwidth of the obtained energy pattern and it is represented by term $BW(P_{energy})$.

For this case of a steerable energy narrow-beam pattern, the main beam is steered in the azimuth plane $-180° \leq \phi_0 \leq 180°$ with an angular step of $45°$ in the cut of $\theta = \theta_0 = 90°$. Therefore, the number of elements for the circular antenna array is given by $N = 360°/45° = 8$, with an Euclidean spacing of $150mm$ among the antenna elements. According to (Chamaani et al., 2010) this spacing value can be enough to avoid important coupling effects. For generation of individuals, the maximum value of amplitudes excitation a_{max} was set to 10, and the maximum value of disturbing exciting time delay τ_{max} we have considered to $100ps$. For the parameters of the DEMO/parent algorithm, we have set the population size to 600. We consider a scaling factor $F = 0.5$ and a two

point crossover with a crossover probability of $p_c = 0.15$. The stopping criterion is 600 iterations.

5.4.1.1 Simulation Results

The DEMO/parent algorithm was implemented to optimize the time delays and amplitude excitations of TD circular antenna array. Figure 32 shows the nondominated front of both objective functions obtained by the DEMO/parent algorithm for the circular antenna array proposed. The result shown in Figure 32, illustrates that the DEMO/parent algorithm found nondominated solutions for the two objective functions. Furthermore, it is illustrated the selected design solution from the nondominated front.

To choose the selected solution it was necessary to find a region of best compromise between both objective function, of_1 and of_2. To determine this region, for this particular case, a summation of $of_1(n)$ and $of_2(n)$ is used as follows:

$$S_{of}(n) = of_1(n) + of_2(n) \tag{58}$$

where n is the evaluated solution from the nondominated front, and $S_{of}(n)$ is the summation of both objective functions. To determine our region of best compromise, since of_1 and of_2 were set to be minimized, we considered the solutions from the lowest value of S_{of}, let us called $S_{of_{min}}$, to the solutions with a S_{of} below a tolerance of 15% above $S_{of_{min}}$.

After defining the region of best compromise for this case, the decision to choose the selected solution was determined by taking the solution, inside this region, with the lowest $of_1(n)$. This is in order to have the best reduction of *SLL* without a significant growth of the main beam.

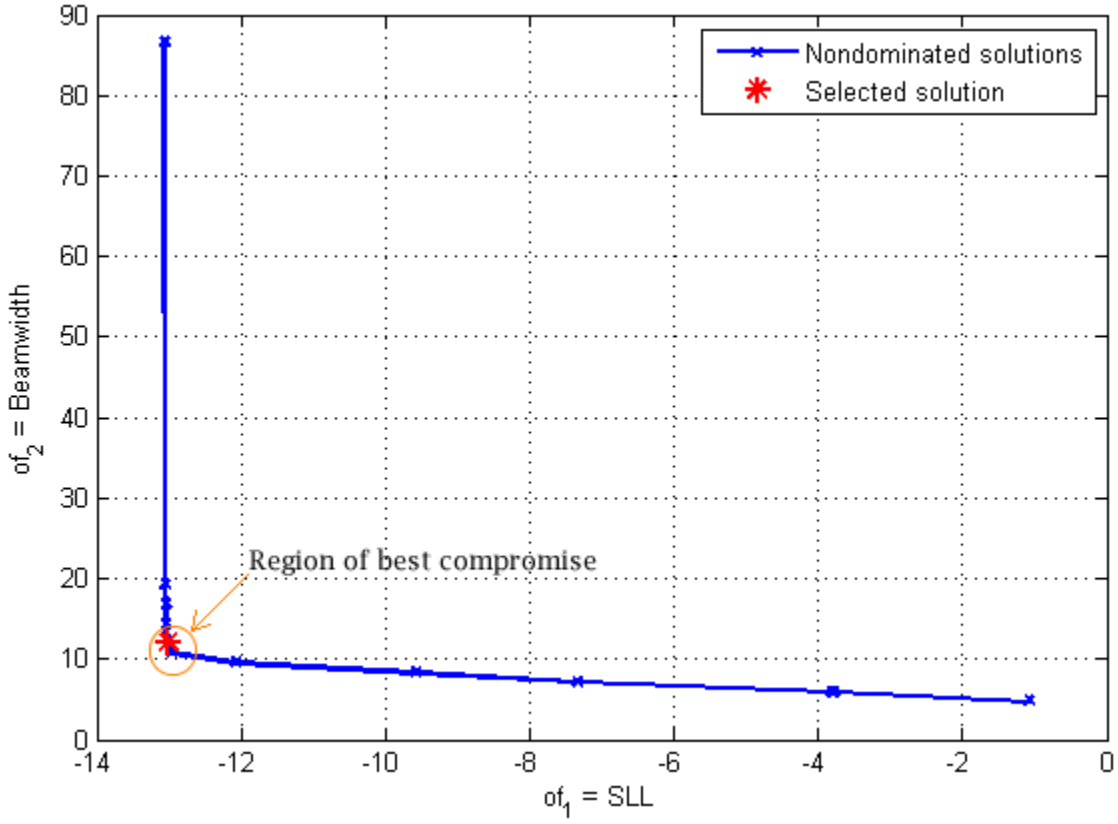

Figure 32. Nondominated front obtained by DEMO/parent algorithm and the selected solution for steerable energy pattern of a circular antenna array.

Figure 33 illustrates the selected set of amplitude excitations and disturbing exciting time delays optimized by DEMO/parent algorithm for the steerable energy patterns for the circular antenna array.

The sets of amplitudes and time delays provide the normalized energy pattern with a maximum $SLL \leq -12.7014\,dB$ and a maximum $BW \leq 11.52°$ for the beam steering directions of (a) $\phi_0 = -135°$; (b) $\phi_0 = -90°$; (c) $\phi_0 = -45°$; (d) $\phi_0 = 0°$; (e) $\phi_0 = 45°$; (f) $\phi_0 = 90°$; (g) $\phi_0 = 135°$; and (h) $\phi_0 = 180°$.

Each energy pattern is compared against a conventional progressive delay case of circular antenna array with uniform amplitude excitations and progressive delay excitation.

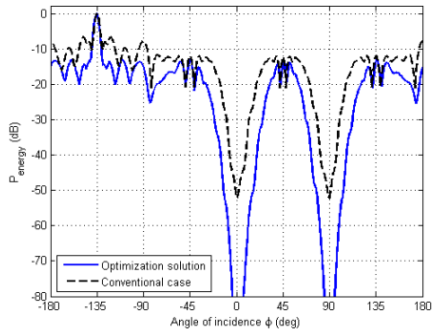

(a) $\phi_0 = -135°$.

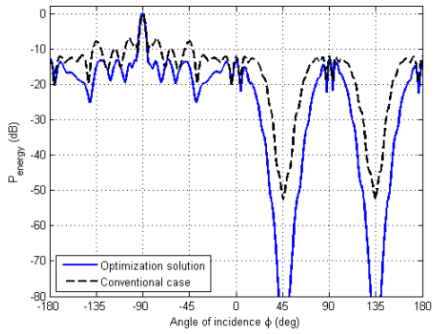

(b) $\phi_0 = -90°$.

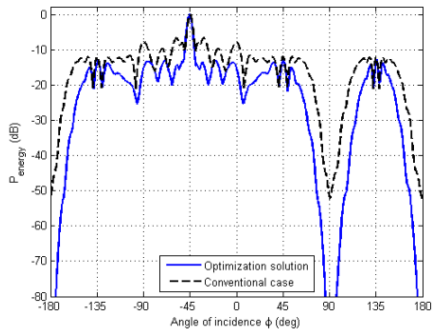

(c) $\phi_0 = -45°$.

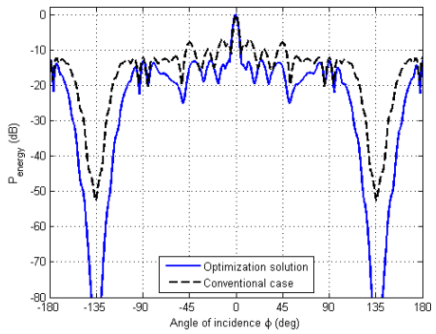

(d) $\phi_0 = 0°$.

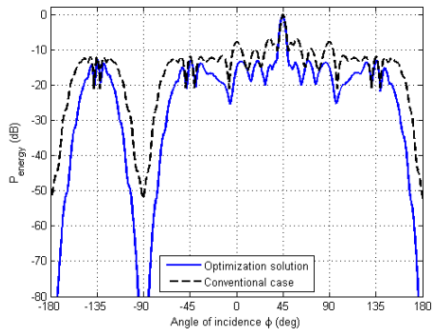

(e) $\phi_0 = 45°$.

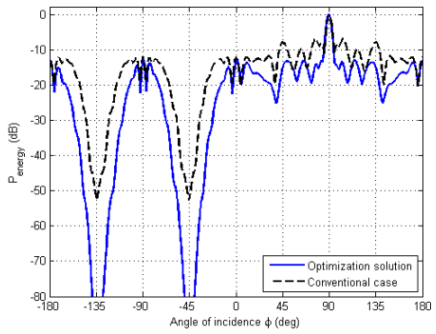

(f) $\phi_0 = 90°$.

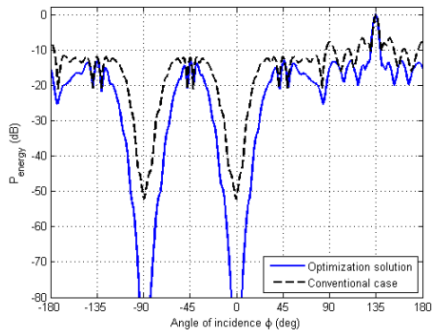

(g) $\phi_0 = 135°$.

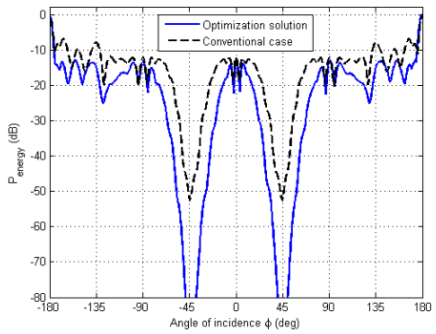

(h) $\phi_0 = 180°$.

Figure 33. Comparison of the energy patterns between conventional progressive delay case and optimized by DEMO/parent algorithm for (a) $\phi_0 = -135°$; (b) $\phi_0 = -90°$; (c) $\phi_0 = -45°$; (d) $\phi_0 = 0°$; (e) $\phi_0 = 45°$; (f) $\phi_0 = 90°$; (g) $\phi_0 = 135°$; and (h) $\phi_0 = 180°$.

From Figure 33, we can conclude that the DEMO algorithm obtained a reduction of the *SLL* and kept a beamwidth narrow for all beam steering directions. It is essential to mention that the obtained values of *SLL* and beamwidth for the optimized energy pattern are the same when the main beam is steered in the proposed directions, by rotating the optimized set of amplitude excitations and the time delays excitations in the circular antenna array.

The numerical values of the side lobe level and beamwidth for the optimized steerable energy pattern and its sets of amplitudes and time delays are presented in Table 7.

Table 7. Comparison of numerical values between the conventional progressive delay case and the optimized by DEMO/parent for the steerable energy pattern shown in the Figure 32 (amplitude and time delays values are for the case $\phi_0 = 0°$).

Design case	Max *SLL* (dB)	BW (degrees)	ϕ_n	a_n	τ_n (ps)
Conventional Progressive Delay case	-6.8731	9.6	0	1	0
			0.7854	1	0
			1.5708	1	0
			2.3562	1	0
			3.1416	1	0
			3.9270	1	0
			4.7124	1	0
			5.4978	1	0
Optimized solution	-12.7014	11.52	0	9.0309	69.7864
			0.7854	7.1734	77.1268
			1.5708	4.9271	87.0812
			2.3562	4.1092	84.9614
			3.1416	8.5237	87.8917
			3.9270	3.8870	72.6069
			4.7124	6.4498	75.0366
			5.4978	6.9596	73.3821

It is observed in Table 7 and Figure 33 that the DEMO algorithm could minimize the SLL and maintain a narrow beamwidth with respect to the conventional progressive delay case with only $1.92°$ of increment in the beamwidth, for this test case, this value of beamwidth is still considerated narrow-beam. Moreover, this table shows the amplitude excitations and disturbed exciting time delays required to generate the energy pattern for the direction of $\phi_0 = 0°$. It is important to mention that optimized solution and the conventional progressive delay case are nondominated solution with respect to each other, however, for this case, the most important design value for us is that the beamwidth have a little increase with respect the progressive delay case, and the side lobe level is minimized by

6 dB. Note that to generate the energy pattern in other directions; the rotation properties (mentioned previously for the circular array proposed) are applied.

Now, in order to observe the effect of the time-domain synthesis over the response in the frequency domain, we calculated the spectrum in frequency of the far–field waveform in time domain by using (54). Figure 34 shows the power patterns for all UWB frequency band of (a) optimized solution and (b) conventional progressive delay case, for $\phi_0 = 0$. Since there are no variations when the main beam is steered to the proposed directions, one case is enough to observe the effect of the time-domain synthesis over the response in the frequency domain.

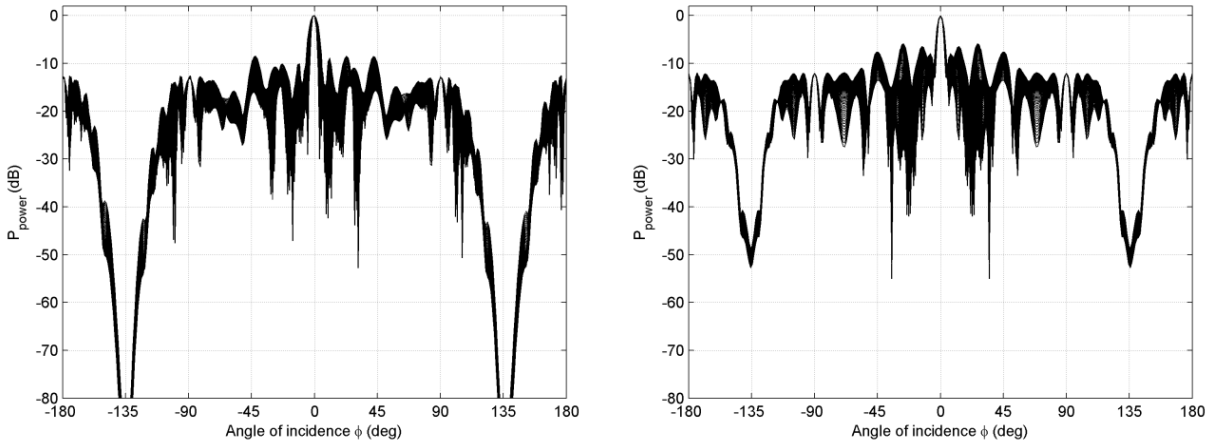

(a) Optimized solution (b) Conventional progressive delay case

Figure 34. Spectrum in frequency of (a) optimized solution, (b) conventional progressive delay case, for $\phi_0 = 0$.

Figure 34 illustrates that the different power patterns show variations in the *SLL*, with a maximum *SLL* of $-8.5134dB$ for the optimized solution and $-5.9157dB$ for the conventional progressive delay case; and the maximum beamwidth for the optimized solution was $15.6°$ and $12°$ for the conventional progressive delay case. These variations are due to the many frequencies in the UWB frequency band. Figure 35 presents the variations of the maximum *SLL* in the spectrum frequency of each case, as can be observed the optimization solution have lower *SLL* over the most part of the UWB frequency band. The variations of *SLL* are due to wavelength changes in each frequency, and the uniform spacing of the antenna elements in the array cause an increase in the *SLL*, especially near the boundaries of the spectrum frequency for the optimized solution.

Furthermore, Figure 36 illustrates the variations of the beamwidth along the frequency spectrum for each case; it is worth mentioning that the value of beamwidth decreases at higher frequency, with a difference (between its boundaries) of $7.2°$ for the optimized solution and $2.6°$ for the conventional progressive delay case. This difference is due to the non-uniform set of amplitude excitations and disturbed exciting time delays of the optimized solution.

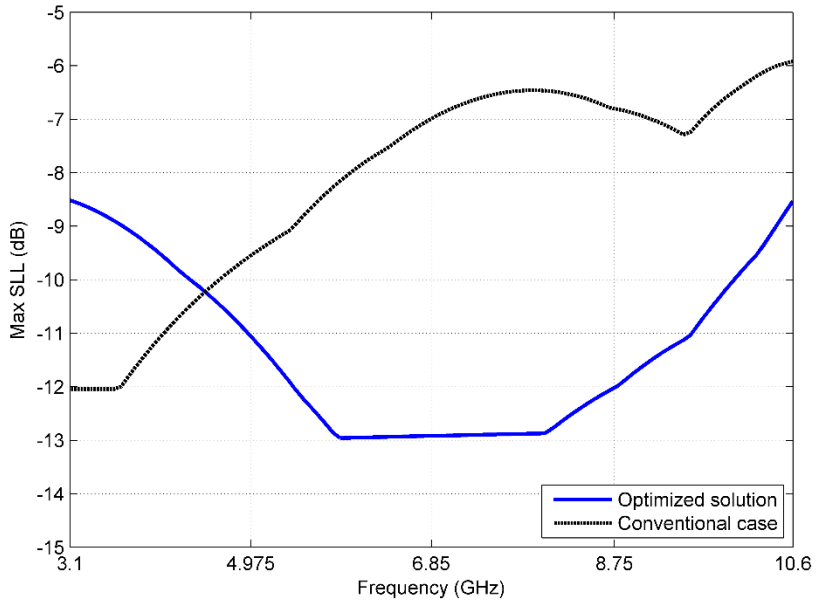

Figure 35. Comparison of the maximum *SLL* of the power pattern in each frequency in the UWB spectrum for the optimized solution and the conventional progressive delay case.

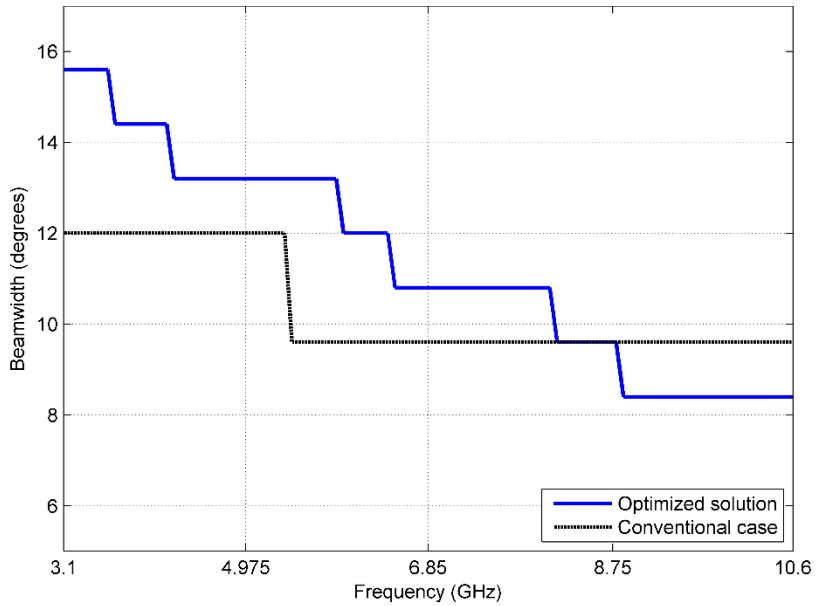

Figure 36. Comparison of the beamwidth of the power pattern in each frequency in the UWB spectrum for the optimized solution and the conventional progressive delay case.

5.4.2 Flat-Top Beam Pattern

The proposed synthesis process is to obtain an optimum flat-top energy pattern by optimizing the disturbed exciting time delays and amplitudes of a circular antenna array with low side lobe level. For this purpose, we have defined the next objective functions of_1 and of_2 to be minimized:

$$of_1(n) = \left| P_{energy}(\theta,\phi) - mask(\theta,\phi) \right| \tag{59}$$

$$of_2(n) = P_{energy}(\theta_{SLL},\phi_{SLL}) + BW(P_{energy}) \tag{60}$$

The proposed of_1 regards the error between optimized energy pattern $P_{energy}(\theta,\phi)$ and the flat-top mask $mask(\theta,\phi)$ in $\theta = 90°$ and ϕ in the interval of $[-15°, 15°]$, and regards the maximum peak side lobe level represented by term $P_{energy}(\theta_{SLL},\phi_{SLL})$ and we have added the beamwidth $BW(P_{energy})$ to of_2 to avoid a considerably increase of the beamwidth. In order to minimize the above objective functions, DEMO/parent algorithm was used to obtain a desired flat-top energy pattern.

5.4.2.1 Simulation Results

The DEMO/parent algorithm was implemented to optimize the amplitude excitations and disturbed exciting time delays of a circular antenna array for a flat-top energy pattern. The $P_{energy}(\theta,\phi)$ is evaluated in the azimuth plane $-180° \leq \phi \leq 180°$ in the cut of $\theta = 90°$. The number of antenna elements is $N = 8$ with a Euclidean spacing of $150mm$ among consecutive antenna elements.

For generation of individuals, the maximum value of amplitudes excitation I_{max} was set to 10, and the maximum value of time delay excitations τ_{max} we have considered to $100ps$. The parameters of DEMO/parent are configured with a scaling factor $F = 0.5$ and two point crossover with a crossover probability of $pc = 0.15$, the population size was set to 600 and the stopping criterion is to reach 600 iterations.

Figure 37, illustrates the nondominated front of both objective functions obtained by the DEMO/parent algorithm for the circular antenna array proposed. The result shown in Figure 37, shows that the DEMO/parent algorithm found nondominated solutions for the two objective functions. Furthermore, Figure 37 shows the selected design solution from the nondominated front. Since our principal objective is to obtain a flat-top energy pattern, we opted to select the nondominated solution with the lower error over the flat-top mask.

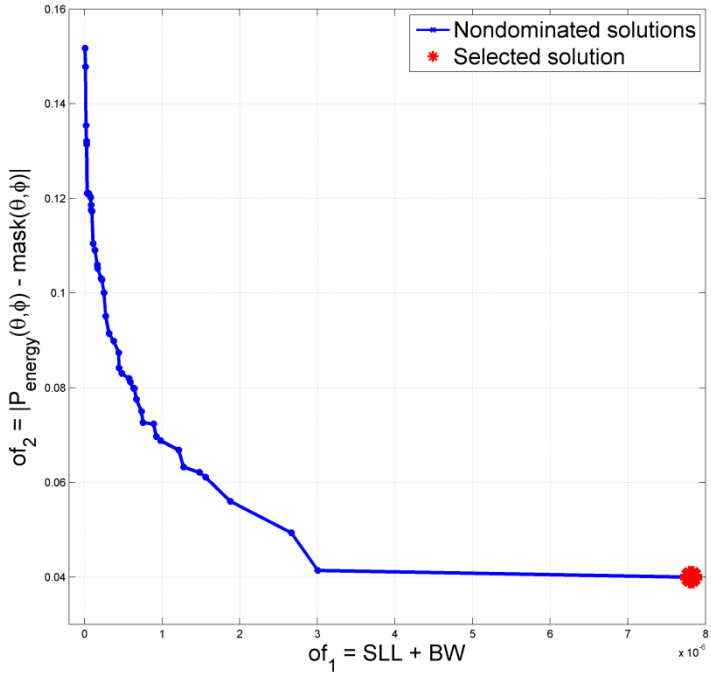

Figure 37. Nondominated front obtained by DEMO/parent algorithm and the selected solution for flat-top energy pattern of a circular antenna array.

The flat-top energy pattern of the selected solution from the nondominated front is illustrated in Figure 38. The synthesis in time domain of a circular antenna array provides a good performance of the flat-top shaped beam; also the optimized energy pattern presents a peak side lobe level under $-51dB$.

It is important to mention that simulations were tested using different numbers of antenna elements in the array. However, due to the large width of the flat-top mask, more number of antenna elements causes directive energy patterns, and these solutions are not desired for the optimization process.

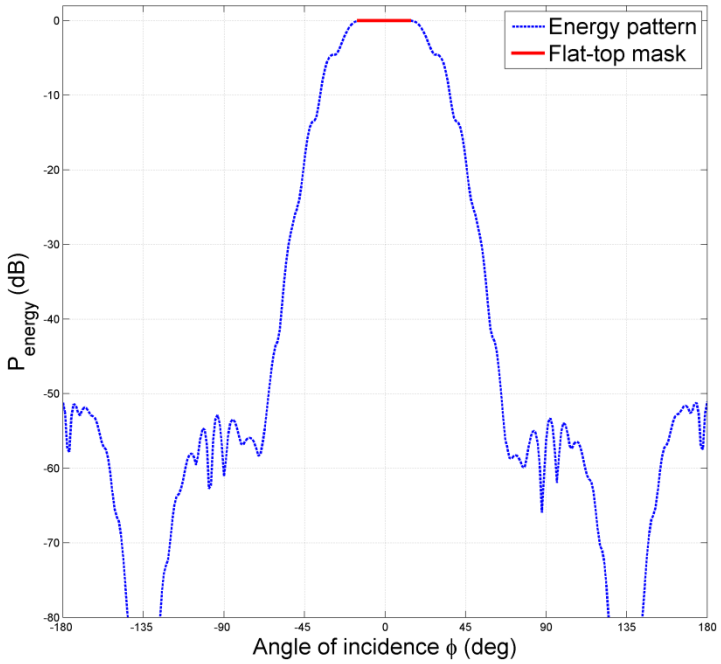

Figure 38. Flat-top energy pattern obtained by DEMO/parent algorithm for a circular antenna array.

Furthermore, in order to observe the behavior in the frequency domain after the time-domain synthesis, the power patterns are calculated by (54) for UWB spectrum frequency. Figure 39 shows the powers patterns of the far-field waveform in time domain of the circular antenna array.

As shown in Figure 39, low levels of peak side lobe prevail for all frequencies with a maximum variation of $5dB$. Power patterns shows a good behavior over the flat-top mask with a maximum variation of $1.97dB$ for frequencies near the UWB spectrum frequency boundaries $(3.1GHz, 10.GHz)$, this behavior (besides the oscillations along the power patterns) is because of the wavelength changes in each frequency. The proposed synthesis technique resulted in a good performance in the flat-top energy pattern for a circular antenna array and a good approximation for the power patterns in the frequency domain.

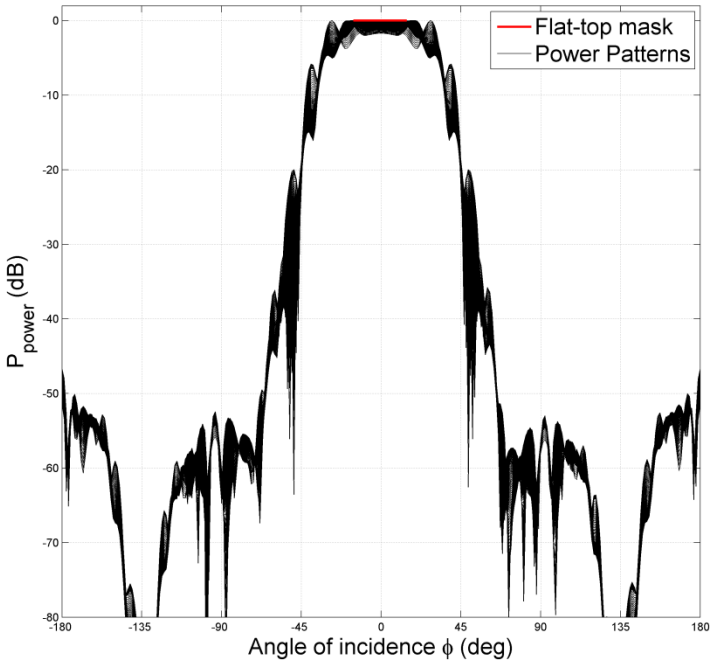

Figure 39. Flat-top energy pattern obtained by DEMO/parent algorithm for a circular antenna array.

Finally, Table 8 shows the antenna elements positions, optimum amplitude excitations and disturbed time delay excitations for the proposed circular antenna array. It is observed that the most contribution of amplitude excitation is in the antenna element located at the direction of maximum radiation $\phi = 0^{o}$.

Table 8. Numerical values of positions, amplitudes and time delays excitations for proposed time-domain circular antenna array.

ϕ_n	*Amplitudes*	*Time delays (ps)*
0	9.0804	74.6423
0.7854	0.0089	60.7872
1.5708	0.0206	1.2219
2.3562	0.0094	10.7868
3.1416	0.3160	0.8284
3.9270	0.0122	27.1707
4.7124	0.0201	0.8195
5.4978	0.0130	74.1508

5.5 Conclusions

This chapter has presented the synthesis of energy patterns for the design of TD circular antenna arrays by using the DEMO/parent algorithm to optimize the amplitude excitations and the disturbed exciting time delays. The study presented the synthesis process in the time domain for a steerable energy pattern and a flat-top energy pattern, and its effect in the UWB spectrum frequency.

The case of the steerable energy pattern low values of *SLL* and beamwidth were achieved and different beam steering angles were obtained by just one optimized solution due to rotation properties for circular antenna arrays. The optimized solution presents a reduction of *SLL* of 5.82dB with respect to the conventional progressive delay case. All patterns in the UWB frequency band resulted in a good performance of *SLL* and beamwidth.

In the case of the flat-top energy pattern, the DEMO/parent could find a solution that fulfilled the flat-top mask for the main beam with very low *SLL*. This behavior presented in the time-domain by the energy pattern is preserved in the frequency domain by the power patterns. Furthermore, very low SLL is maintained and the flat-top beam is with a maximum variation of *1.97d*B. This and the oscillations along the azimuth angle is because of the wavelength changes in each frequency, but the behavior is maintained.

Therefore, the presented optimization to design TD UWB circular antenna arrays is an excellent alternative to avoid individual beamforming for each frequency in the spectrum. Furthermore, with the presented methodology and results, the general objective of this thesis was fulfilled, and this approach represents an alternative for antenna arrays in order to operate for bandwidths extremely large, area that will be of main attention for future 5G wireless communication systems.

Moreover, the results presented were used to generate two papers, for an international journal and conference. These are presented in next chapter.

Chapter 6. Conclusions and Future Work

This chapter is focused on exposing the main contributions and conclusions presented in this research work, in addition to presenting some opportunity areas for future work.

The summary of contributions and conclusions is divided in two parts. In the first one, the main contributions of the synthesis of circular antenna arrays with sparseness characteristics (where the number of antenna elements is reduced) are exposed. Then, in the second last, main contributions of the methodology approach of UWB antenna arrays are presented.

6.1 Conclusions about circular antenna arrays with sparseness characteristics

The initial thematic, for the research process of this thesis, was to explore new synthesis solutions for circular antenna arrays in order to obtain sparseness characteristics, in other words, to reduce the number antenna elements, this is in order to support the green networks associated with LTE-A requirements exposed in Release 12 and beyond.

The most outstanding conclusions associated with this part of the thesis are summarized as follow:

- The synthesis of sparse antenna arrays represents a new approach that has gained high interest in the field of antenna array design, which allows to achieve significant reduction of number of elements in the antenna array, and therefore, this represents a reduction of cost, size, complexity, maintenance, and energy consumption of whole wireless communication system.

- The reduction factors above mentioned are key factors for the requirements of Release 12 and Beyond of 3GPP for LTE-A systems and their evolution. The benefits of reducing these factors are, first, the reduction supports the concept of green networks associated with evolution of LTE-A systems, and second, these

reduction benefits can be extended to the promising massive MIMO systems, which are provided to support higher requirements such as the use of high number of base station antennas on the present and future wireless communication systems (4G and 5G).

- After exploring the research pathway, the existing methodologies for the synthesis of antenna arrays with sparseness characteristics for linear and planar arrays, such the ones based on Matrix Pencil Method (MPM) and Bayesian Compressive Sensing (BCS), are not able to deal with the circular antenna array mathematical formulation. This is due to the non-orthogonality of the basis functions of the array factor for this kind of structure.

- The proposed synthesis procedure is based on the expansion in orthogonal basis function to represent a desired current distribution and the application of a density/amplitude tapering technique to obtain sparseness characteristics. In this sense, the proposed approach achieved a better performance in all test cases explored in terms of the reduction of antenna elements and the preservation of side lobe level and main beamwidth.

- The proposed synthesis approach yields a better fulfillment of the requirements with respect to a uniform sampled technique, in terms of *SLL* and beamwidth with a maximum error of 3 dB in a test case and 8° of beamwidth between the first nulls. The best behavior has presented in the case of the narrow-beam pattern, where our proposal does not exceed side lobe levels nor beamwidth.

- When the sparseness characteristic are achieved using the tapering function over the continuous current distribution for a circular array, it is necessary to avoid distortions over the current distribution when values of radius and number of harmonics are varied. This is due to that the reconstruction of the current distribution is highly sensible to this parameters.

- The orthogonal method applied to the synthesis of circular antenna arrays represents a suitable synthesis method to obtain sparseness characteristics. However, the optimum spatial distribution is not known and an additional method should be used to obtain optimum positions. However, our approach offers excitation currents and antenna element positions.

6.2 Conclusions about synthesis of UWB antenna arrays

The second part of this research work was focused on the design of UWB antenna arrays, a technology that will be integrated to present and future wireless communication technologies, such as LTE-A systems. This approach was essential to define the general objective of this research work.

The most outstanding conclusions associated with this part of the thesis, are listed as follow:

- The design of UWB antenna array has gained attention because the strategies associated at this technology will be exploded for future communications systems. This is due to the requirements provided by the future 5G technology, where the use of wideband of frequency will be necessary to cover higher requirements for new wireless communication systems,

- The large bandwidth of UWB frequency spectrum complicates the design of antenna arrays if a synthesis procedure analyzed from the frequency domain (as it is done in classical antenna array theory), is employed. This is because it causes an individual beamforming procedure for each frequency considered into the UWB spectrum. This option leads to a large number of solutions of excitation sets. Each set associated to a different radiation pattern for each frequency considered.

- Parameters for the design of UWB antenna arrays were identified. The main parameter in order to avoid major variations in the radiation pattern was the wave form used, and the 5^{th} derivative Gaussian pulse was found as the optimum wave

form because its power spectral density fulfill in the best way the FCC mask for UWB technology.

- The proposed time domain synthesis approach for UWB antenna arrays in a circular geometry, based on time domain pattern descriptors, avoided the individual beamforming problem given by the large UWB frequency spectrum. In this way, the proposed approach achieved an optimal performance in the whole UWB spectrum.

- The optimization process carried out by the Differential Evolution for Multiobjective Optimization (DEMO) algorithm, presented a good reduction of the side lobe level without a significant increase of the main beamwidth. Furthermore, because of the optimization was done in time domain by using the pattern descriptors, only one optimization process was needed for the whole UWB frequency spectrum, which simplify the optimization process.

- The rotation properties of monochromatic (one frequency) circular antenna array are also suitable for wideband circular antenna arrays. By using these rotation properties into the optimization process for the case of a steerable main beam lobe, it was able to rotate the main beam by just considering one set of optimized excitation currents, which represents having different beam direction by just one optimization process.

Before concluding with this sub-section, with the concatenation of these two thesis parts, the general and particular objectives defined in this thesis were fulfilled, which was focused on the design of antenna arrays considering the reduction of antenna elements and the large bandwidth associated to UWB technology.

6.3 Future research work

After completing the research activities, future lines of research have been identified, and listed as follows:

- As a first research topic, it is proposed to evaluate the radius of the proposed tapering technique by employing an optimization process, in order to find a better search algorithm to find a suitable radius value.

- In order to expand the sparse technique to a different geometry, such as concentric ring antenna array, it is proposed to concatenate the proposed tapering approach to the circular planar tapering techniques. This is in order to reduce the number of antenna elements in each ring. Besides, it is necessary to define new mathematical formulation to compute optimal sparse representation for a concentric ring antenna array.

- Another research topic proposed is to calculate the level of consumed energy over the antenna array with sparseness characteristics to quantize the energy between a filled array and a sparse array.

- As result of a concatenation of both research approaches in this thesis, a proposed line of research is the evaluation of the UWB antenna array under the concept of sparseness, in order to use a reduced number of antenna elements in the design. Furthermore, it is necessary to evaluate the behavior of the UWB antenna array to different number of antennas, since the behavior of a plane wave is completely different from a 5^{th} derivate Gaussian pulse.

- An important parameter that should be measured is the mutual coupling among the antenna elements in order to obtain a complete representation of the resultant antenna array for each proposed approach.

- Due to the large beamwidth associated to the UWB frequency spectrum, a proposed research topic in this scenario is the evaluation of the antenna array considering a particular antenna element in order to obtain a complete representation of the UWB antenna array.

- A proposal related to the future 5G mobile communication systems is the extension of the methodology used for the design of UWB antenna arrays, to the new frequency bands considering the lower frequencies of the millimeter band. Besides, it is necessary to identify the performance of the wave forms to different and higher.

List of References

4G Americas. (2015). Recomendations for 5G spectrum. White paper (Vol. XXXIII). Retrieved October 5 of 2015 from http://www.4gamericas.org/es/resources/white-papers/

Abbasi, Q. H., Khan, M. M., Alomainy, A., and Hao, Y. (2011). Radio channel characterisation and OFDM-based ultra wideband system modelling for body-centric wireless networks. Proceedings - 2011 International Conference on Body Sensor Networks, BSN 2011, 89–94.

Abdelmalek, N. N. (1971). Roundoff Error Analysis for Gram-Schmidt method and solution of linear least squares problems. Bit Numerical Mathematics, 11(4), 1345–1368.

Adamiuk, G., Heine, C., Wiesbeck, W., and Zwick, T. (2010). Antenna array system for UWB-monopulse-radar. Antenna Technology iWAT 2010 International Workshop on, 1–4.

Adamiuk, G., Zwick, T., and Wiesbeck, W. (2012). UWB antennas for communication systems. Proceedings of the IEEE, 100(7), 2308–2321.

Allen, B., Dohler, M., Okon, E., Malik, W., Brown, A., and Edwards, D. (2006). Ultra wideband antennas and propagation for communications, Radar and Imaging. John Wiley & Sons.

Angeletti, P., and Toso, G. (2009). Aperiodic Arrays for Space Applications : A combined amplitude / density synthesis approach. Antennas and Propagation, 2009. EuCAP 2009. 3rd European Conference on, 2026–2030.

Angeletti, P., Toso, G., and Ruggerini, G. (2014). Array antennas with jointly optimized elements positions and dimensions part II: planar circular arrays. IEEE Transactions on Antennas and Propagation, 62(4), 1627–1639.

Arce, A. (2012). Contributions to the design and application of beam-forming networks based on coherently radiating periodic structures. Centro de Investigación Científica y de Educación Superior de Ensenada.

Astely, D., Dahlman, E., Fodor, G., Parkvall, S., and Sachs, J. (2013). LTE release 12 and beyond. IEEE Communications Magazine, 51(7), 154–160.

Athukorala, L., Rabbi, K., Panagamuwa, C., Vardaxoglou, J. C., Philippakis, M., and Budimir, D. (2010). Optically reconfigurable microstrip UWB bandpass filters. 2010 Loughborough Antennas and Propagation Conference, LAPC 2010, (November), 617–620.

Balanis, C. A. (2005). Antenna theory: analysis and design (3rd ed.). John Wiley & Sons.

Barrett, T. W., and Vienna, V. A. (2001). Technical features, history of ultra wideband communications and radar: part I, UWB communications. Microwave Journal, 44(1), 22–56.

Björck, Å. (1994). Numerics of Gram-Schmidt orthogonalization. Linear Algebra and Its Applications, 197, 297–316.

Bucci, O. M., D'Urso, M., Isernia, T., Angeletti, P., and Toso, G. (2010). Deterministic synthesis of uniform amplitude sparse arrays via new density taper techniques. Antennas and Propagation, IEEE Transactions on, 58(6), 1949–1958.

Bucci, O. M., Isernia, T., and Morabito, A. F. (2013). An effective deterministic procedure for the synthesis of shaped beams by means of uniform-amplitude linear sparse arrays. Antennas and Propagation, IEEE Transactions on, 61(1), 169–175.

Bucci, O. M., Isernia, T., Morabito, A. F., Perna, S., and Pinchera, D. (2010). On the optimal synthesis of shaped beam sparse arrays having uniform amplitude excitations. Phased Array Systems and Technology ARRAY 2010 IEEE International Symposium on, 757–762.

Bucci, O. M., Isernia, T., Morabito, A. F., Perna, S., and Pinchera, D. (2012). Isophoric sparse arrays: A synthesis procedure for circularly symmetric shaped beams. 6th European Conference on Antennas and Propagation, EuCAP 2012, 832–836.

Bucci, O. M., and Perna, S. (2011). A deterministic two dimensional density taper approach for fast design of uniform amplitude pencil beams arrays. Antennas and Propagation, IEEE Transactions on, 59(8), 2852–2861.

Bucci, O. M., Perna, S., and Pinchera, D. (2012a). Advances in the deterministic synthesis of uniform amplitude pencil beam concentric ring arrays. IEEE Transactions on Antennas and Propagation, 60(7), 3504–3509.

Caratelli, D., and Viganó, M. C. (2011). A novel deterministic synthesis technique for constrained sparse array design problems. Antennas and Propagation, IEEE Transactions on, 59(11), 4085–4093.

Chamaani, S., Abrishamian, M. S., and Mirtaheri, S. A. (2010). Time-fomain fesign of UWB vivaldi antenna array using multiobjective particle swarm optimization. IEEE Antennas and Wireless Propagation Letters, 9, 666–669.

Chen, C., and Jensen, M. A. (2011). Secret key establishment using temporally and spatially correlated wireless channel coefficients. IEEE Transactions on Mobile Computing, 10(2), 205–215.

Chen, Z. (2007). UWB antennas: from hype, promise to reality. Loughborough Antennas and Propagation Conference, 2007, (April), 19–22.

Chen, Z. N., Wu, X. H., Li, H. F., Yang, N., and Chia, M. Y. W. (2004). Considerations for source pulses and antennas in UWB radio systems. IEEE Transactions on Antennas and Propagation, 52(7), 1739–1748.

Chong, C. C., Watanabe, F., and Inamura, H. (2006). Potential of UWB technology for the next generation wireless communications. 2006 IEEE Ninth International Symposium on Spread Spectrum Techniques and Applications, 422–429.

Ciattaglia, M., and Marrocco, G. (2008). Time domain synthesis of pulsed arrays. IEEE Transactions on Antennas and Propagation, 56(7), 1928–1938.

Di Benedetto, M.-G., Kaiser, T., Molisch, A. F., Politano, C., and Porcino, D. (2006). UWB communication systems: A comprehensive overview (Vol. 5). Hindawi Publishing Corporation.

Dumoulin, A., John, M., Ammann, M. J., and McEvoy, P. (2009). Performance evaluation of antennas for UWB radar and positioning systems. IET Irish Signals and Systems Conference (ISSC 2009), June 10-11, 1–6.

Ersoy, O. K. (1994). A comparative review of real and complex Fourier-related transforms. Proceedings of the IEEE, 82(3), 429–447.

Fang, D. G. (2009). Antenna theory and microstrip antennas. CRC Press.

FCC. (2002). Revision of part 15 of the commission's rules regarding ultra-wideband transmission systems. First Report and Order.

Foo, S., and Kashyap, S. (2003). Time-domain array factor for UWB antenna array. Electron Letters, 39(18), 1304–1305.

Galaviz, G. (2012). Diseño de algoritmos de despacho de recursos espectrales para sistemas LTE-avanzados con acumulación de portadoras. Centro de Investigación Científica y de Educación Superior de Ensenada.

Ghavami, M., Member, S., Amini, A., and Marvasti, F. (2008). Unified structure of basic UWB waveforms. IEEE Transactions on Circuits and Systems II: Express Briefs, 12(55), 1304–1308.

Griffiths, H. D., and Cullen, A. L. (2003). Sidelobe response of antennas to short pulse signals. Proceedings of the 2003 IEEE Radar Conference, May, 85–90.

Guo, L., Wang, S., Chen, X., and Parini, C. (2010). A Time domain study of a small quasi-self-complementary UWB antenna. Antenna Technology (iWAT), 2010 International Workshop on, March 1-3, 1–4.

Heidari, G. (2008). WiMedia UWB: Technology of choice for wireless USB and Bluetooth. John Wiley & Sons.

Huawei. (2015). 5G: New air interface and radio access virtualization. White Paper, (April). Retrieved October 5 of 2015 from http://www.huawei.com/minisite/ has2015/img/5g_radio_white paper.pdf

Immoreev, I. Y. (2010). Practical applications of UWB technology. IEEE Aerospace and Electronic Systems Magazine, 25(2), 36–42.

Ishimaru, A. (1962). Theory of unequally-spaced arrays. Antennas and Propagation, IRE Transactions on, 10(6), 691–702.

ITU. (2015). Handbook on national spectrum management. ITU-R. Retrieved from https://www.itu.int/pub/R-HDB-21

Jarmo Lundén, Visa Koivunen, and H. Vincent Poor. (2015). Spectrum exploration and exploitation for cognitive radio: Recent Advances. IEEE Signal Processing Magazine, 32(3), 123–140.

Jensen, M. A., and Wallace, J. W. (2004). A review of antennas and propagation for MIMO wireless communications. IEEE Transactions on Antennas and Propagation, 52(11), 2810–2824.

Jiang, Y., and Zhang, S. (2013). An Innovative strategy for synthesis of uniformly weighted circular aperture antenna array. Antennas and Wireless Propagation Letters, IEEE, 12, 725–728.

Johnson, S. G., and Frigo, M. (2007). A modified split-radix FFT with fewer arithmetic operations. IEEE Transactions on Signal Processing, 55(1), 111–119.

Josefsson, L., and Persson, P. (2006). Conformal array antenna theory and design (Vol.29 ed.). John Wiley & Sons.

Kaiser, T., Zheng, F., and Dimitrov, E. (2009). An overview of ultra-wide-band systems with MIMO. Proceedings of the IEEE, 97(2), 285–312.

Kantarovich, L. V., and Krylov, V. I. (1964). Approximate methods for higher analysis. (C. D. Benster, Ed.). New York: Interscience Publishers.

Kim, Y., and Joo, Y. (2005). Fifth-derivative gaussian pulse generator for UWB system. 2005 IEEE Radio Frequency Integrated Circuits Symposium, June, 671–674.

Leatherwood, D. A., Corey, L. E., Cotton, R. B., and Mitchell, B. S. (2000). Time-domain properties of phased array antennas. Proceedings 2000 IEEE International Conference on Phased Array Systems and Technology, 25–28.

Li, W. T., Shi, X. W., and Hei, Y. Q. (2009). Novel planar UWB monopole antenna with triple band-notched characteristics. IEEE Antennas and Wireless Propagation Letters, 8, 1094–1098.

Liao, C. H., Hsu, P., and Chang, D. C. (2011). Energy patterns of UWB antenna arrays with scan capability. IEEE Transactions on Antennas and Propagation, 59(4), 1140–1147.

Liu, Y., Liu, Q. H., and Nie, Z. (2010). Reducing the number of elements in the synthesis of shaped-beam patterns by the forward-backward matrix pencil method. Antennas and Propagation, IEEE Transactions on, 58(2), 604–608.

Liu, Y., Nie, Z., and Liu, Q. H. (2008). Reducing the number of elements in a linear antenna array by the matrix pencil method. IEEE Transactions on Antennas and Propagation, 56(9), 2955–2962.

Maffett, A. (1962). Array factors with nonuniform spacing parameter. IRE Transactions on Antennas and Propagation, 10(2), 131–136.

Malanchini, I., Cesana, M., and Gatti, N. (2009). On spectrum selection games in cognitive radio networks. Global Telecommunications Conference, 2009. GLOBECOM 2009. IEEE, November, 1–7.

Marrocco, G., and Galletta, G. (2010). Hermite-rodriguez UWB circular arrays. IEEE Transactions on Antennas and Propagation, 58(2), 381–390.

McLean, J. S., Foltz, H., and Sutton, R. (2005). Pattern descriptors for UWB antennas. IEEE Transactions on Antennas and Propagation, 53(1), 553–559.

Milligan, T. A. (2004). Space-tapered circular (ring) array. IEE Antennas and Propagation Magazine, 46(3), 70–73.

Oliveri, G., and Massa, A. (2011). Bayesian compressive sampling for pattern synthesis with maximally sparse non-uniform linear arrays. IEEE Transactions on Antennas and Propagation, 59(2), 467–481.

Panduro, M. A., Brizuela, C. A., Balderas, L. I., and Acosta, D. A. (2009). A comparison of genetic algorithms, particle swarm optimization and the differential evolution method for the design of scannable circular antenna arrays. Progress In Electromagnetics Research B, 13, 171–186.

Panduro, M. A., Brizuela, C. A., Garza, J., Hinojosa, S., and Reyna, A. (2013). A comparison of NSGA-II, DEMO, and EM-MOPSO for the multi-objective design of concentric rings antenna arrays. Journal of Electromagnetic Waves and Applications, 27(9), 1100–1113.

Panduro, M. A., and Foltz, H. (2013). Energy patterns of UWB antenna arrays with low side lobe level during beam-scanning. IEEE Antennas and Propagation Society, AP-S International Symposium (APSURSI), July, 17–18.

Prisco, G., and D'Urso, M. (2011). An effective approach for sparse arrays design with the minimum number of sensors. In Proceedings of the 5th European Conference on Antennas and Propagation (EUCAP) (pp. 1277–1278).

Qin, Y., Liao, C., and Wei, T. (2007). Application of micro genetic algorithm to optimization of time-domain ultra-wide band antenna array. In Proceedings of the International Conference on Microwave and Millimeter Wave Technology (ICMMT '07) (pp. 1–4). Builin, China.

Rahim, T. (1980). Directional pattern synthesis in circular arrays of directional antennas. Unversity College London.

Reyna, A., and Panduro, M. A. (2014). Unequally pulsed arrays for high resolution scanning and low side lobe level. In Antennas and Propagation Society International Symposium (APSURSI), 2014 IEEE (Vol. July, pp. 832–833).

Reyna, A., Panduro, M. A., Covarrubias, D. H., and Mendez, A. (2012). Design of steerable concentric rings array for low side lobe level. Scientia Iranica, 19(3), 727–732.

Reyna, A., Panduro, M. A., and Del-Rio Bocio, C. (2014a). Two-dimensional time-domain antenna arrays for optimum steerable energy pattern with low side lobe level. International Journal of Antennas and Propagation, 2014.

Reyna, A., Panduro, M. A., and Del-Rio Bocio, C. (2014b). Two-dimensional time-domain antenna arrays for steerable energy pattern with low side lobe level. In Antennas and Propagation (EuCAP), 2014 8th European Conference on, April, 1513–1517.

Ries, S., and Kaiser, T. (2006). Ultra wideband impulse beamforming: It is a different world. Signal Processing, 86(9), 2198–2207.

Robic, T., and Filipi, B. (2005). DEMO: differential evolution for multiobjective. In C. A. Coello Coello (Ed.), Evolutionary Multi-Criterion Optimization (pp. 520–533). Springer Berlin Heidelberg.

Sahalos, J. (1974). The orthogonal method of nonuniformly spaced arrays. Proceedings of the IEEE, 62(2), 281–282.

Sahalos, J. (2006). Orthogonal methods for array synthesis theory and the ORAMA computer tool. John Wiley & Sons.

SEMAFOUR. (2013). Self-managemement for unified heterogeneous radio access networks. Retrieved July 14, 2013, from: http://www.tno.nl/content.cfm?context=kennis&content=expertise_euproject&laag1=1&laag2=62&item_id=1882&Taal=2.

Sheng, H., Orlik, P., Haimovich, A. M., Cimini Jr., L. J., and Zhang, J. (2003). On the spectral and power requirements for ultra-wideband transmission. IEEE International Conference on Communications, 2003. ICC ’03., 1, 738–742.

Shlivinski, A., Heyman, E., and Kastner, R. (1997). Antenna characterization in the time domain. IEEE Transactions on Antennas and Propagation, 45(7), 1140–1149.

Shlivinski, A., Lager, I. E., and Heyman, E. (2013). Non-uniform array antennas – the time-domain perspective. In Antennas and Propagation (EuCAP), 2013 7th European Conference on (pp. 133–137).

Sierra, A., Choliz, J., Cluzeaud, P., and Slusanschi, E. (2011). UWB integration into heterogeneous access networks. In 2011 Future Network & Mobile Summit (pp. 1–9).

Sipal, V., Allen, B., Edwards, D., and Honary, B. (2012). Twenty years of ultrawideband: opportunities and challenges. IET Communications, 6(10), 1147–1162.

Sipal, V., Gelabert, J., Allen, B., Stevens, C., and Edwards, D. (2011). Frequency-selective fading of ultrawideband wireless channels in confined environments. IET Microwaves, Antennas & Propagation, 5(11), 1328–1335.

Skolnik, I. (1969). Nonuniform arrays. (Z. Collin, R. E., Ed.) Antenna Theory. McGraw-Hill.

Sorgel, W., Sturm, C., and Wiesbeck, W. (2005). Impulse responses of linear UWB antenna arrays and the application to beam steering. In 2005 IEEE International Conference on Ultra-Wideband (pp. 275–280).

Storn, R., and Price, K. (1997). Differential evolution–a simple and efficient heuristic for global optimization over continuous spaces. Journal of Global Optimization, 11(4), 341–359.

Taylor, T. T. (1960). Design of circular apertures for narrow beamwidth and low sidelobes. IRE Transactions on Antennas and Propagation, 8(1), 17–22.

Unz, H. (1960). Linear arrays with arbitrarily distributed elements. Antennas and Propagation, IRE Transactions on, 2(8), 222–223.

Unz, H. (1966). Nonuniformly spaced arrays: The orthogonal method. Proceedings of the IEEE, 54(1), 53–54.

Vigano, M. C., and Caratelli, D. (2010). Analytical synthesis technique for uniform-amplitude linear sparse arrays. In Antennas and Propagation Society International Symposium (APSURSI), 2010 IEEE (pp. 1–4).

Visser, H. J. (2005). Array and phased array antenna basics. John Wiley & Sons.

Vithanage, C. M., Sandell, M., Coon, J. P., Wang, Y., and Toshiba Research Europe Ltd. (2009). Precoding in OFDM-based multi-antenna ultra-wideband systems. IEEE Communications Magazine, 47(1), 41–47.

Weng, Y. F., Cheung, S. W., and Yuk, T. I. (2010). Triple band-notched UWB antenna using meandered ground stubs. In 2010 Loughborough Antennas and Propagation Conference, LAPC 2010 (pp. 341–344).

WiMedia Alliance. (n.d.). WiMedia Specifications. Retrieved from http://www.wimedia.org

Wu, X. H., Kishk, A. A., and Chen, Z. N. (2005). A linear antenna array for UWB applications. In 2005 IEEE Antennas and Propagation Society International Symposium (Vol. 1, pp. 594–597).

Yang, K., Zhao, Z., and Liu, Y. (2011). Synthesis of sparse planar arrays with matrix pencil method. In 2011 International Conference on Computational Problem-Solving, ICCP 2011 (pp. 82–85).

Yepes, L. (2014). Inter-cell interference management via coordinated multi-point transmission-reception (CoMP) associated with the LTE-Advanced systems. Centro de Investigación Científica y de Educación Superior de Ensenada.

Yepes, L. F., Covarrubias, D. H., Alonso, M. A, and Arceo, J. G. (2013). Synthesis of two-dimensional antenna array using independent compression regions. IEEE Transactions on Antennas and Propagation, 61(1), 449–453.

Yepes, L. F., Covarrubias, D. H., Alonso, M. A., and Ferrus, R. (2014). Hybrid sparse linear array synthesis applied to phased antenna arrays. IEEE Antennas and Wireless Propagation Letters, 13, 185–188.

Yuan, X. L., Zhang, G. F., Huang, J. J., and Yuan, N. C. (2008). Study of UWB time-domain antenna array scan. In 2008 International Conference on Microwave and Millimeter Wave Technology Proceedings, ICMMT (Vol. 3, pp. 1134–1136).

Appendix A

Mathematical formulation to obtain the parameter $\widehat{k}_{in}$

We have the inner product expression between the basis function $\varphi_n(\phi)$ and the orthonormalized function $\psi_i(\phi)$ as detailed in (Sahalos, J., 1974; Sahalos, J., 2006):

$$\int_{-\pi}^{\pi} \varphi_n(\phi)\, \psi_j^*(\phi)\, d(\phi) = \int_{-\pi}^{\pi} \exp(jkr\cos(\phi-\phi_n)) \times \sum_{i=1}^{m} C_i^{(m)} \exp(jkr\cos(\phi-\phi_i))\; d(\phi) = \sum_{i=1}^{m} C_i^{(m)}\, \hat{k}_{in} \tag{61}$$

The coefficient $\hat{k}_{in}$ can be written as:

$$\hat{k}_{in} = \int_{-\pi}^{\pi} \exp(jkr\cos(\phi-\phi_n))\; \exp(jkr\cos(\phi-\phi_i))\; d(\phi) \tag{62}$$

after using simple trigonometric identities, the expression above becomes as follows:

$$\hat{k}_{in} = \int_{-\pi}^{\pi} \exp\left(-2jkr\sin\left(\frac{\phi_n-\phi_i}{2}\right) \times \sin\left(\phi - \frac{\phi_n+\phi_i}{2}\right)\right)\; d(\phi) \tag{63}$$

then, by assuming:

$$\psi_{ni} = \frac{\phi_n-\phi_i}{2} \tag{64}$$

$$\hat{\psi}_{ni} = \frac{\phi_n+\phi_i}{2} \tag{65}$$

$$k = -2jkr \sin\left(\frac{\phi_n - \phi_i}{2}\right) \tag{66}$$

The expression (62) can be defined as:

$$\hat{k}_{in} = \int_{-\pi}^{\pi} \exp\left(jk \sin\left(\phi - \hat{\psi}_{ni}\right)\right) \tag{67}$$

Using the identity

$$\exp\left(jk \sin\left(\phi - \hat{\psi}_{ni}\right)\right) = \sum_{p=-\infty}^{\infty} J_p(k) \exp(jp \exp(\phi - \psi_{ni})) \tag{68}$$

Then, a new expression is obtained:

$$\hat{k}_{in} = \sum_{p=-\infty}^{\infty} 2\pi J_p(k) \exp\left(-jp \sin\left(\phi - \hat{\psi}_{ni}\right)\right) \frac{\sin(p\pi)}{p\pi} \tag{69}$$

And the, evaluating the resulting expression at $p = 0$, we obtain the new value of $\hat{k}_{in}$, as:

$$\hat{k}_{in} = 2\pi J_0(k) \tag{70}$$

With this expression of $\hat{k}_{in}$, the orthogonality for function $\psi_i(\phi)$ can be achieved.